



NAVAL POSTGRADUATE SCHOOL

MONTEREY, CALIFORNIA

DISSERTATION

**DEVELOPMENT OF A LOW-COST METHOD FOR
WHOLE-SPACECRAFT ISOLATION OF SMALL
SATELLITES**

by

Wenschel D. Lan

December 2015

Dissertation Supervisor:

James H. Newman

Approved for public release; distribution is unlimited

Reissued 10 Jan 2017 with corrected degree.

THIS PAGE INTENTIONALLY LEFT BLANK

REPORT DOCUMENTATION PAGE			Form Approved OMB No. 0704-0188	
Public reporting burden for this collection of information is estimated to average 1 hour per response, including the time for reviewing instruction, searching existing data sources, gathering and maintaining the data needed, and completing and reviewing the collection of information. Send comments regarding this burden estimate or any other aspect of this collection of information, including suggestions for reducing this burden to Washington headquarters Services, Directorate for Information Operations and Reports, 1215 Jefferson Davis Highway, Suite 1204, Arlington, VA 22202-4302, and to the Office of Management and Budget, Paperwork Reduction Project (0704-0188) Washington DC 20503.				
1. AGENCY USE ONLY (Leave Blank)		2. REPORT DATE December 2015		3. REPORT TYPE AND DATES COVERED Dissertation
4. TITLE AND SUBTITLE DEVELOPMENT OF A LOW-COST METHOD FOR WHOLE-SPACECRAFT ISOLATION OF SMALL SATELLITES			5. FUNDING NUMBERS	
6. AUTHOR(S) Wenschel D. Lan				
7. PERFORMING ORGANIZATION NAME(S) AND ADDRESS(ES) Naval Postgraduate School Monterey, CA 93943			8. PERFORMING ORGANIZATION REPORT NUMBER	
9. SPONSORING / MONITORING AGENCY NAME(S) AND ADDRESS(ES) N/A			10. SPONSORING / MONITORING AGENCY REPORT NUMBER	
11. SUPPLEMENTARY NOTES The views expressed in this document are those of the author and do not reflect the official policy or position of the Department of Defense or the U.S. Government. IRB Protocol Number: N/A.				
12a. DISTRIBUTION / AVAILABILITY STATEMENT Approved for public release; distribution is unlimited			12b. DISTRIBUTION CODE	
13. ABSTRACT (maximum 200 words) Force-limited vibration testing (FLVT) is effective in reducing the low-frequency vibration test environment for CubeSats on the Naval Postgraduate School CubeSat Launcher (NPSCuL); however, the CubeSats are still subjected to high-frequency amplifications above 500 Hz from the NPSCuL structure. The excessive, high-frequency vibration has caused test failures and forces CubeSat developers to focus more on surviving environmental testing instead of developing state-of-the-art technology. Whole-spacecraft isolation systems are often used to reduce these amplifications, but they currently exist only for large spacecraft and are too expensive to adapt for small satellites. These limitations motivated the combined use of FLVT and commercial-off-the-shelf (COTS) isolators on NPSCuL as a novel, practical, and low-cost method to reduce vibration levels for small satellites. This method significantly reduces the high-frequency amplification by up to 97%; the root-mean-square acceleration (G_{RMS}) over the entire test frequency range drops by up to 78%. These results should allow more sensitive and complex payloads to gain access to space on future NPSCuL missions and demonstrate how a worst-case environment on a small satellite can be improved. Implementing low-cost, COTS isolators on other small satellites and CubeSat launch applications could be useful as well.				
14. SUBJECT TERMS Force Limited Vibration Testing, Whole Spacecraft Isolation, CubeSat, ESPA, Small Satellites			15. NUMBER OF PAGES 199	
			16. PRICE CODE	
17. SECURITY CLASSIFICATION OF REPORT Unclassified	18. SECURITY CLASSIFICATION OF THIS PAGE Unclassified	19. SECURITY CLASSIFICATION OF ABSTRACT Unclassified	20. LIMITATION OF ABSTRACT UU	

NSN 7540-01-280-5500

Standard Form 298 (Rev. 2-89)
Prescribed by ANSI Std. Z39-18

THIS PAGE INTENTIONALLY LEFT BLANK

Approved for public release; distribution is unlimited

**DEVELOPMENT OF A LOW-COST METHOD FOR WHOLE-
SPACECRAFT ISOLATION OF SMALL SATELLITES**

Wenschel D. Lan

Civilian, Department of the Navy

B.S., M.S., California Polytechnic State University, San Luis Obispo, 2008

Submitted in partial fulfillment of the
requirements for the degree of

DOCTOR OF PHILOSOPHY IN ASTRONAUTICAL ENGINEERING

from the

NAVAL POSTGRADUATE SCHOOL

December 2015

Approved by:	James H. Newman Acting Provost and Academic Dean Professor of Space Systems Dissertation Supervisor	Young Kwon Distinguished Professor of Mechanical and Aerospace Engineering Dissertation Committee Chair
	Joshua H. Gordis Professor of Mechanical and Aerospace Engineering Co-Advisor	Isaac M. Ross Professor of Mechanical and Aerospace Engineering
	Rudolf Panholzer Chair and Professor of Space Systems	Francis Gulick Senior Tech Fellow United Launch Alliance
Approved by:	Garth Hobson Chair, Department of Mechanical and Aerospace Engineering	
Approved by:	O. Douglas Moses Vice Provost for Academic Affairs	

THIS PAGE INTENTIONALLY LEFT BLANK

ABSTRACT

Force-limited vibration testing (FLVT) is effective in reducing the low-frequency vibration test environment for CubeSats on the Naval Postgraduate School CubeSat Launcher (NPSCuL); however, the CubeSats are still subjected to high-frequency amplifications above 500 Hz from the NPSCuL structure. The excessive, high-frequency vibration has caused test failures and forces CubeSat developers to focus more on surviving environmental testing instead of developing state-of-the-art technology. Whole-spacecraft isolation systems are often used to reduce these amplifications, but they currently exist only for large spacecraft and are too expensive to adapt for small satellites. These limitations motivated the combined use of FLVT and commercial-off-the-shelf (COTS) isolators on NPSCuL as a novel, practical, and low-cost method to reduce vibration levels for small satellites. This method significantly reduces the high-frequency amplification by up to 97%; the root-mean-square acceleration (G_{RMS}) over the entire test frequency range drops by up to 78%. These results should allow more sensitive and complex payloads to gain access to space on future NPSCuL missions and demonstrate how a worst-case environment on a small satellite can be improved. Implementing low-cost, COTS isolators on other small satellites and CubeSat launch applications could be useful as well.

THIS PAGE INTENTIONALLY LEFT BLANK

Table of Contents

1	Introduction	1
1.1	Need for Reducing Vibration Levels	1
1.2	A Novel, Practical Method for Reducing Vibration Levels on Small Spacecraft	5
1.3	Background	5
1.4	Dissertation Summary	11
2	Evolution of Vibration Reduction Methods on NPSCuL	13
2.1	Force-Limited Vibration Testing	13
2.2	Isogrid NPSCuL	36
3	Incorporating Isolators on NPSCuL	41
3.1	Design Updates to NPSCuL	41
3.2	Test Set-Up and Configurations.	50
4	Experimental Results	59
4.1	Conical Isolator Results.	59
4.2	Cupmount Isolator Results	69
4.3	Combined Effects of FLVT and Isolation	88
4.4	Effects of Varying Random Vibration Inputs	90
4.5	Force Limit Example of Isolated NPSCuL	93
5	Finite Element Model and Analyses	95
5.1	Baseline NPSCuL FEM.	95
5.2	Baseline NPSCuL FEM with Conical Isolators	99
5.3	Isogrid NPSCuL FEM with Conical Isolators	103
5.4	Baseline NPSCuL FEM with Cupmount Isolators	105
5.5	Loads Analyses	107
6	Conclusion	111

6.1	Summary of Contributions	112
6.2	Recommendations for Future Work	113
Appendix A Shock and Acoustic Testing No-Test Rationale		115
A.1	Shock No-Test Rationale	115
A.2	Acoustic No-Test Rationale	115
Appendix B P-POD Response Comparison Plots		119
Appendix C Individual P-POD Responses, G_{RMS}		123
Appendix D MATLAB Code — Force Limit Validation		127
Appendix E MATLAB Code — Force Limit Calculation		139
Appendix F MATLAB Code — Data Processing		143
Appendix G MATLAB Code — Acoustic No-Test Rationale Calculation		157
Appendix H Random Vibration Analysis Example Verification		159
List of References		169
Initial Distribution List		173

List of Figures

Figure 1.1	ABC Input and P-POD Response Locations	2
Figure 1.2	ABC Input and P-POD Response Acceleration Profile Comparison	3
Figure 1.3	Whole-Spacecraft Isolation Systems	4
Figure 1.4	Common CubeSat Sizes	6
Figure 1.5	P-POD and Main Spring	7
Figure 1.6	Aft Bulkhead Carrier on Atlas V Centaur Aft Bulkhead	8
Figure 1.7	NPSCuL Baseline Design	9
Figure 1.8	OUTSat Mounted to ABC on Centaur Stage Aft End	9
Figure 1.9	FalconSat-3 and ESPA Payloads on STP-S26	10
Figure 2.1	Single-Channel Control	14
Figure 2.2	FLVT Set-Up of NPSCuL, X-Axis	15
Figure 2.3	Dual-Control Loop	16
Figure 2.4	Fixed Base Test Set-Up Represented as 1DOF Harmonic Oscillator Model with Prescribed Support Motion	17
Figure 2.5	FLVT Set-Up Represented as 2DOF Harmonic Oscillator Model with Prescribed Support Motion	17
Figure 2.6	Transmissibility of NPSCuL (SDOF Model) and ABC Plate (2DOF Model)	21
Figure 2.7	Predicted and Actual Force-Limited Acceleration Input	22
Figure 2.8	Normalized Force Spectral Limit from Simple TDFS Method	24
Figure 2.9	Complex TDFS Method Model	26
Figure 2.10	Force Limit Calculations for NPSCuL	32

Figure 2.11	Example Force Limit to 500 Hz, Z-Axis	33
Figure 2.12	Resulting Notch at Fundamental Mode in Acceleration Input, Z-Axis	34
Figure 2.13	X-Axis Response at P-POD #2 Interface (P2M2 Data at MPE +0 dB)	35
Figure 2.14	Isogrid NPSCuL Design	36
Figure 2.15	Unibase	37
Figure 2.16	X-Axis Notched Acceleration Control, Baseline and Isogrid NPSCuL at MPE -3 dB	38
Figure 2.17	X-Axis Random Vibration Response, Baseline and Isogrid NPSCuL at MPE -3 dB	39
Figure 3.1	Non-separating AP Envelope	43
Figure 3.2	ABC Interface	44
Figure 3.3	Aft Bulkhead Carrier (ABC) Vibration Requirement	45
Figure 3.4	Conical Isolator	47
Figure 3.5	Cupmount Isolator	47
Figure 3.6	Baseline NPSCuL Adapter Ring and Baseplate	48
Figure 3.7	Adapter Ring Designs	49
Figure 3.8	Isolators on Re-designed Adapter Rings	49
Figure 3.9	Modified Baseplate and Adapter Ring, Cupmount Isolators	50
Figure 3.10	FLVT Set-Up, Bare Fixture	51
Figure 3.11	Typical Qualification Test Set-Up	52
Figure 3.12	General Test Flow for Each Test Configuration	53
Figure 3.13	ABC and ORS Vibration Profiles	55
Figure 3.14	ABC, ESPA RUG, and GEVS Vibration Profiles	56

Figure 4.1	Apparent Mass, Conical Isolators on Baseline NPSCuL	61
Figure 4.2	Acceleration Responses at P-POD Interface Due to ABC Input with FLVT, Baseline NPSCuL with Conical Isolators	63
Figure 4.3	Reduction in High Frequency Content at P-POD Interface, Conical Isolators	65
Figure 4.4	Apparent Mass, Conical Isolators on Baseline NPSCuL	65
Figure 4.5	Apparent Mass, Fully Constrained Conical Isolators on Baseline NPSCuL	67
Figure 4.6	Apparent Mass, Conical Isolators on Baseline and Isogrid NPSCuL	68
Figure 4.7	Apparent Mass, Cupmount Isolators on Baseline NPSCuL	69
Figure 4.8	Apparent Mass, Conical and Cupmount Isolators on Baseline NPSCuL	71
Figure 4.9	Acceleration Responses at P-POD Interface Due to ABC Input with FLVT, Baseline NPSCuL with Cupmount Isolators	72
Figure 4.10	Acceleration Responses at P-POD Interface Due to ABC Input with FLVT, Baseline NPSCuL with Conical and Cupmount Isolators .	74
Figure 4.11	Reduction in High Frequency Content at P-POD Interface, Cup- mount Isolators	76
Figure 4.12	Z-Axis Test, Tension	77
Figure 4.13	Z-Axis Test, Compression	78
Figure 4.14	Lateral Test, Tension	78
Figure 4.15	Lateral Test, Compression	79
Figure 4.16	Lateral Random Vibe Test, Compression and Tension at MPE +0 dB	80
Figure 4.17	Lateral Random Vibe Test, Compression and Tension at MPE +0 dB	80
Figure 4.18	Pre- and Post-random Sine Sweep Comparison, Z-Axis Break-In Test	81
Figure 4.19	Damaged Isolators Due to Insufficient Torque	82

Figure 4.20	Isolator Designation	84
Figure 4.21	Thermocouple on Isolator 1	84
Figure 4.22	Isolator Temperatures — MPE +6 dB, Z	85
Figure 4.23	Isolator Temperatures — MPE +6 dB, X	86
Figure 4.24	Isolator Temperatures — MPE +6 dB, Y	86
Figure 4.25	Dynamic Modulus Variation of Silicone Due to Temperature . . .	88
Figure 4.26	Overall G_{RMS} Envelope at P-POD Interface, MPE +0 dB	89
Figure 4.27	Acceleration Response at P-POD Interface Due to ORS Input without FLVT, Baseline NPSCuL with and without Cupmount Isolators	91
Figure 4.28	Overall G_{RMS} Envelope at P-POD Interface, MPE -6 dB of ORS Vibration Profile, Unnotched	92
Figure 4.29	Overall G_{RMS} Envelope at P-POD Interface, MPE -6 dB of ORS Vibration Profile, FLVT	92
Figure 4.30	Transmissibility of Isolated NPSCuL (SDOF Model) and ABC Plate (2DOF Model)	93
Figure 4.31	Predicted and Actual Force-Limited Acceleration Input, Isolated NPSCuL	94
Figure 5.1	Baseline NPSCuL FEM	96
Figure 5.2	Baseline NPSCuL Fundamental Modes — Mode Shapes	99
Figure 5.3	Flat Ring and Conical Isolator FEM	100
Figure 5.4	Baseline NPSCuL with Conical Isolators — Fundamental Mode Shapes	102
Figure 5.5	Baseline NPSCuL with Conical Isolators — Secondary Mode Shapes	103
Figure 5.6	Isogrid NPSCuL FEM with Conical Isolators	104
Figure 5.7	Flat Ring and Conical Isolator FEM	106
Figure 5.8	Flat Ring FEM — Solid Brick Elements	109

Figure 5.9	Von Mises Stress Distribution Due to ABC Static Loads	110
Figure A.1	Atlas V Maximum Predicted Acoustic Levels	116
Figure B.1	Acceleration Response at P-POD Interface Due to ABC Profile, Configuration 1, with and without FLVT	119
Figure B.2	Acceleration Response at P-POD Interface Due to ABC Profile, Configuration 2, with and without FLVT	120
Figure B.3	Acceleration Response at P-POD Interface Due to ABC Profile, Configuration 3, with and without FLVT	121
Figure H.1	Mode Shapes of First Five Modes - Normalized Displacement . .	160
Figure H.2	Acceleration Response at L/4 and L/2	161

THIS PAGE INTENTIONALLY LEFT BLANK

List of Tables

Table 2.1	Force Limit Calculated Using Simple TDFS Method for NPSCuL	25
Table 2.2	Normalized Force Limit Spectrum for Complex TDFS with $Q = 20$	28
Table 2.3	Force Limit Calculated Using The Complex TDFS Method for NPSCuL	30
Table 2.4	P-POD 2 Response, with and without FLVT	35
Table 3.1	Test Configurations	53
Table 3.2	Sine Test Inputs for All Test Configurations	56
Table 3.3	Random Test Inputs for All Test Configurations	57
Table 4.1	Measured Frequencies from Apparent Mass, Conical Isolators on NPSCuL	62
Table 4.2	G_{RMS} Reduction at P-POD Interface, 20–2000 Hz — Conical Isolators	64
Table 4.3	G_{RMS} Reduction at P-POD Interface, 500–2000 Hz — Conical Isolators	64
Table 4.4	Measured Frequencies from Apparent Mass, Cupmount Isolators on NPSCuL	70
Table 4.5	G_{RMS} Reduction at P-POD Interface, 20–2000 Hz — Cupmount Isolators	75
Table 4.6	G_{RMS} Reduction at P-POD Interface, 500–2000 Hz - Cupmount Isolators	75
Table 4.7	Measured Fundamental Frequencies, Pre- and Post-random Sine Sweeps	87
Table 4.8	X-Axis G_{RMS} Envelope of P-POD Interface at MPE +0 dB, ABC Profile, Unnotched	89

Table 4.9	G_{RMS} Reduction at P-POD Interface, 20–2000 Hz — MPE -6 dB of ORS Input without Force Limiting	90
Table 4.10	G_{RMS} Reduction at P-POD Interface on Configuration 3, 20–2000 Hz — MPE -6 dB of ORS Input	90
Table 5.1	Material Properties	96
Table 5.2	Element Physical Properties	97
Table 5.3	Concentrated Mass Element Properties	97
Table 5.4	FEM Mass Properties Summary	98
Table 5.5	Baseline NPSCuL — Fundamental Frequencies	98
Table 5.6	Baseline NPSCuL with Conical Isolators — Fundamental Frequencies	101
Table 5.7	Isogrid NPSCuL with Conical Isolators — Fundamental Frequencies	104
Table 5.8	Frequencies of Baseline and Isogrid NPSCuL FEMs with Conical Isolators	105
Table 5.9	Baseline NPSCuL with Cupmount Isolators — Fundamental Frequencies	107
Table 5.10	Margins of Safety, Fastener Analysis — Cupmount Isolators on NPSCuL	108
Table 5.11	Torque Values For Baseline NPSCuL with Cupmount Isolators	108
Table 5.12	Margins of Safety, Stress Analysis — Cupmount Isolators on NPSCuL	109
Table 6.1	Launch Vehicle Requirements Summary	112
Table C.1	Configuration 1 P-POD Responses Due to ABC Input with FLVT	123
Table C.2	Configuration 1 P-POD Responses Due to ABC Input without FLVT	124
Table C.3	Configuration 2 P-POD Responses Due to ABC Input with FLVT	124
Table C.4	Configuration 2 P-POD Responses Due to ABC Input without FLVT	125

Table C.5	Configuration 3 P-POD Responses Due to ABC Input with FLVT	125
Table C.6	Configuration 3 P-POD Responses Due to ABC Input without FLVT	126
Table H.1	Frequency Comparison — MATLAB and NASTRAN FEMs . . .	159

THIS PAGE INTENTIONALLY LEFT BLANK

List of Acronyms and Abbreviations

ABC	Aft Bulkhead Carrier
AP	Auxiliary Payload
ASD	Acceleration Spectral Density
BTR	Broad-Temperature-Range
CG	Center of Gravity
CLA	Coupled Loads Analysis
COTS	Commercial-Off-The-Shelf
DOF	Degree of Freedom
EDU	Engineering Development Unit
EELV	Evolved Expendable Reusable Launch Vehicle
ELaNa	Educational Launch of Nanosatellites
ESPA	EELV Secondary Payload Adapter
FEM	Finite Element Model
FRF	Frequency Response Function
FLVT	Force-Limited Vibration Testing
FS	Factor of Safety
G_{RMS}	Root-Mean-Square Acceleration
GEMSat	Government Experimental Multi-satellite
GEVS	General Environmental Verification Standard
GRACE	Government Rideshare Advanced Concepts Experiment

GSE	Ground Support Equipment
ICD	Interface Control Document
JPL	Jet Propulsion Laboratory
LV	Launch Vehicle
MPA	Multiple Payload Adapter
MPE	Maximum Predicted Environment
MPF	Mode Participation Factor
MS	Margin of Safety
NASA	National Air and Space Administration
NEA	Non-Explosive Actuator
NLAS	Nanosatellite Launch Adapter System
NPS	Naval Postgraduate School
NPSCuL	Naval Postgraduate School CubeSat Launcher
OASPL	Overall Sound Pressure Level
ORS	Operationally Responsive Space
OUTSat	Operationally Unique Technologies Satellite
P/N	Part Number
P-POD	Poly-Picosatellite Orbital Deployer
P2M2	P-POD Mass Model
PSC	Planetary Systems Corporation
RSS	Root Sum Square

SAD	Splitter Auxiliary Device
SDOF	Single Degree-of-Freedom
SPL	Sound Pressure Level
TDFS	Two Degree-of-Freedom System
ULA	United Launch Alliance
ULTRASat	Unique Lightweight Technology and Research Auxiliary Satellite
VEM	Viso-Elastic Material

THIS PAGE INTENTIONALLY LEFT BLANK

Acknowledgments

First and foremost, I would like to thank Dr. Newman for giving me the opportunity to both work and get my degree at NPS. I have grown professionally while working on NPSCuL, and he is a great role model and an amazing advisor. I really appreciate how supportive he is in every way imaginable.

I owe my academic growth to all of my committee members, especially for their time, support, and guidance throughout my entire time at NPS. My sincere gratitude also goes to Fran Gulick for his invaluable feedback in this research.

I would like to acknowledge all of my colleagues in the Space Systems Academic Group for their continual support. In particular, Dr. Panholzer is always positive and encouraging, and he taught me to always have dessert first! Vidur Kaushish helped me talk through everything, from testing strategies to life's biggest questions. Without Dan Sakoda and David Rigmaiden keeping the vibe table and other facilities up and running, I would not have been able to collect all the data. I also appreciate Levi Owen's support in machining the various parts I needed for testing.

I would also like to thank my colleagues and good friends at the Office of Space Launch, United Launch Alliance, Cal Poly, Tyvak, and SRI for being a great group of people to work with; they definitely made carrying out this research an interesting and enjoyable experience.

Lastly, I would like to thank my family for their support. My parents continue to shape me into the person I am today, and my husband, Bryan, is always patient, accommodating, and supportive of everything I do. Getting to this point in my career would not have been possible without them.

THIS PAGE INTENTIONALLY LEFT BLANK

CHAPTER 1:

Introduction

In recent years, small satellites have become increasingly sophisticated due to the collaboration and innovation that occur within the small satellite community. This is particularly true for CubeSats, which are 10-cm-square picosatellites of varying lengths; while it was more common for these satellites to be simple and robust when they were first built in 1999, more CubeSats now have state-of-the-art technology. As a result, the CubeSat components are more sensitive, and the satellites require less harsh launch environments than what was acceptable in the past. Primary spacecraft, which are typically large and expensive, are mounted at the top of the launch vehicle and have a controlled launch environment in the fairing. However, secondary payloads, such as CubeSats, are often mounted in unique locations and orientations on the launch vehicle. The launch environment at these locations is not particularly well-controlled; the temperature range during flight is typically wider for a secondary payload compared to that of a primary payload, and the vibration environment is more harsh. One such mounting location for secondary payloads is on the aft end of the Centaur upper stage of the Atlas V launch vehicle. The Naval Postgraduate School CubeSat Launcher, or NPSCuL (pronounced NPS “cool”), carrying eight Poly-Picosatellite Orbital Deployers (P-PODs), is the most common secondary payload to fly in this location.

1.1 Need for Reducing Vibration Levels

As discussed in [1], the NPSCuL amplifies the response at the P-POD interface due to its cantilevered mounting configuration on the launch vehicle and thin-plate mounting walls, which results in a relatively high random vibration environment for the CubeSats flying on the Atlas V Aft Bulkhead Carrier (ABC) missions. While the ABC base input level of 7.6 G_{RMS} [2] is considered reasonable for satellites, the G_{RMS} levels at the P-POD interface can be double that of the input. This amplification occurs even with force-limiting, which is a method of reducing the conservatism during a fixed-base test. These relative locations are highlighted in the vibration test configuration shown in Figure 1.1.

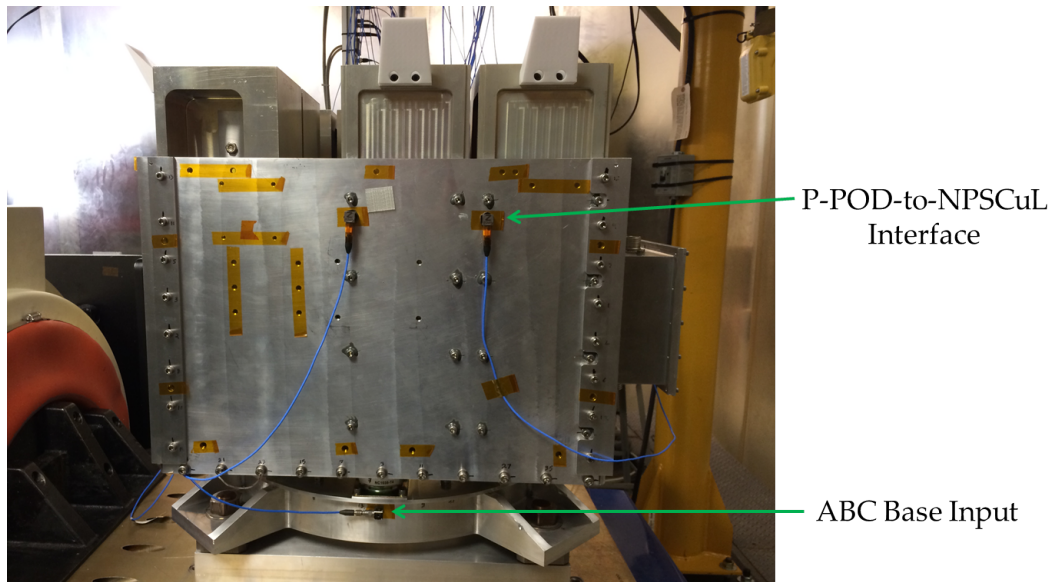


Figure 1.1: ABC Input and P-POD Response Locations

The resulting $15.1 G_{RMS}$ at the P-POD interface for a P-POD on NPSCuL is high compared to other P-POD launch interface environments, many of which are similar to NASA General Environmental Verification Standard (GEVS) vibration levels. In comparison, the GEVS levels are only $10.0 G_{RMS}$ [3] to satisfy the same test requirement. An acceleration spectral density (ASD) plot of a representative vibration profile on NPSCuL is shown in Figure 1.2, with the ABC input profile, indicating that there is a significant amount of energy across the entire test frequency range that needs to be reduced.

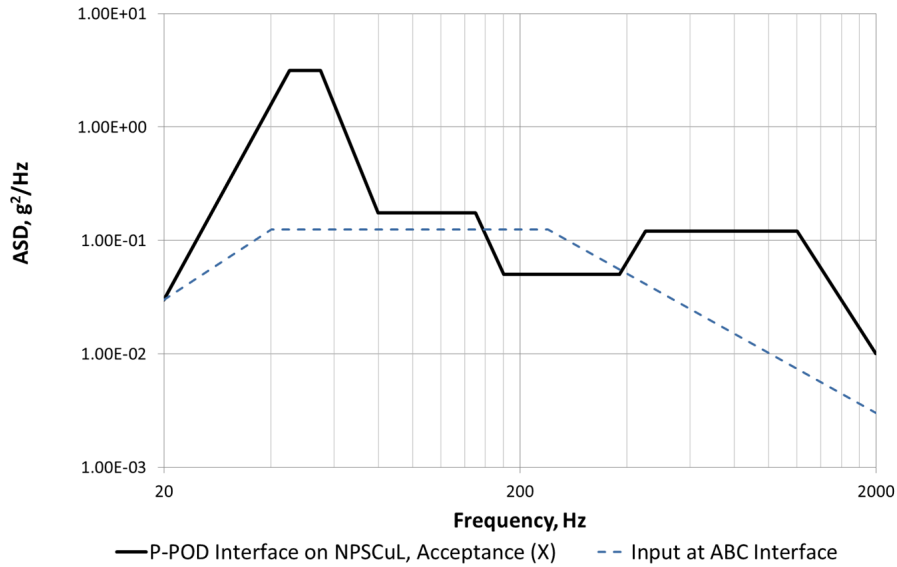


Figure 1.2: ABC Input and P-POD Response Acceleration Profile Comparison

Even though force-limited vibration testing has been used during ground testing for the past four missions, and is effective in lowering the low-frequency vibration test environment for CubeSats flying on NPSCuL, the high-frequency amplifications above 500 Hz were still problematic. The excessive, high-frequency vibration has caused test failures and has forced CubeSat developers to focus more on surviving environmental testing instead of optimizing satellite performance, thus motivating the need to reduce the vibration levels by re-designing NPSCuL, introducing isolators, or both [1].

1.1.1 Existing Spacecraft Isolation Systems

Whole-spacecraft isolation systems are often used to reduce these amplifications, but they currently only exist for large spacecraft and are too expensive to adapt for small satellites. Moog CSA Engineering is the leading developer of whole-spacecraft isolation systems for large spacecraft, including the Softride and Shock Ring systems [4]. These systems (shown in Figure 1.3) provide up to 50% attenuation of shock and vibration loads, but cost upward of \$200k. Additionally, the SoftRide systems are not easily adaptable for payloads such as NPSCuL. They are designed to maintain the existing load path between the LV

and the spacecraft, so there is one isolator per interface fastener. The Softride Uniflex and Omniflex systems are also tuned to the fundamental frequency of the primary spacecraft, resulting in recurring costs for each mission due to the analysis required, in addition to the manufacturing costs. This increase in complexity during the spacecraft mate process to the launch vehicle, as well as the high cost, is not desirable for an auxiliary payload [5], [6]. The Shock Ring was adapted for the ESPA interface, but it was priced at \$50k per ring, which is still relatively expensive for NPSCuL. Additionally, the attenuation was targeted for frequencies above 100 Hz, leaving any lower modes susceptible to amplification [7].

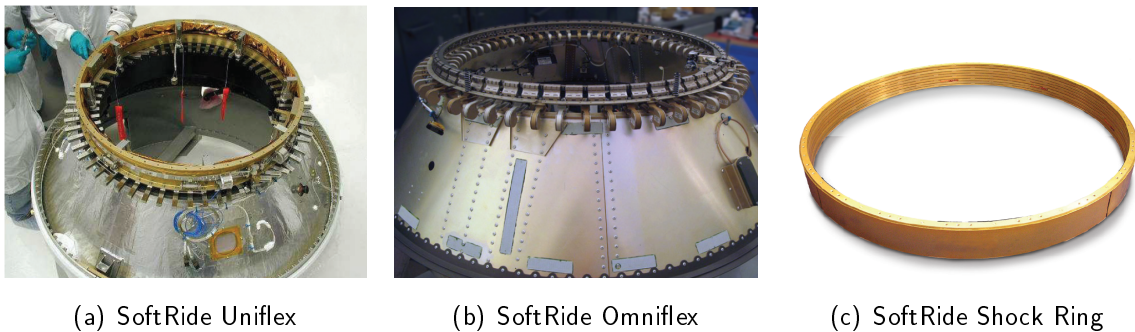


Figure 1.3: Whole-Spacecraft Isolation Systems.

Source: "SoftRide Brochure." [Online]. Available:
http://www.csaengineering.com/literature/Space_Defense/Vibration_Control/MoogCSA_SoftRide_brochure.pdf

Another limiting factor of adapting the Softride systems for small satellites is the survivability temperature range of the viscoelastic material (VEM) used. VEM is a common material used for vibration isolation; it has been incorporated in beam structures and other constrained-layer damping applications. [8], [9]. However, with a typical thermal operating range of 10–35 °C (50–95 °F) and a survivability range of 5–50 °C (41–122 °F) [10], VEMs are considered sensitive to temperature for auxiliary payloads, for which the launch environment temperature can range from -45–38 °C (-50–100 °F). Therefore, using VEMs with constrained-layer damping was not considered for NPSCuL.

1.2 A Novel, Practical Method for Reducing Vibration Levels on Small Spacecraft

Commercial-off-the-shelf (COTS) isolators are often used on launch vehicles and large spacecraft for avionics components and other sensitive equipment. However, these components usually weigh less than 22.7 kg (50 lbm) and are mounted using four isolators, one at each corner of the component or mounting plate [11]. These COTS isolators have not been previously used for spacecraft similar to the size of NPSCuL (approximately 90.7 kg, or 200 lbm) but are known to reduce high-frequency vibration. This dissertation discusses the combined use of FLVT and COTS isolators on NPSCuL and shows how a worst-case vibration environment can be reduced for small spacecraft in test and in flight. The resulting performance is better than that of whole-spacecraft isolation systems designed for large spacecraft and is achieved at a small fraction of the cost.

1.3 Background

The development of the CubeSats, the P-POD, and NPSCuL is provided as background information. Unlike the larger satellites that have a direct interface with the launch vehicle, CubeSats require a deployer to serve as the launch vehicle interface as well as provide a means of deployment. Various CubeSat deployers exist, but P-PODs are the most common deployers used for the ABC missions. To maximize the CubeSat capacity for this secondary payload launch opportunity, NPSCuL is the launch vehicle interface between the ABC and up to eight P-PODs. The vibration test requirements for this system, which consists of CubeSats, P-PODs, and NPSCuL, are defined by the Test Requirements for Launch, Upper-Stage and Space Vehicles (SMC-S-016) [12]. The associated test levels to satisfy these requirements are also provided.

1.3.1 The CubeSat Standard and P-PODs

The CubeSat standard was developed in 1999 using available COTS components as a joint collaboration between California Polytechnic State University, San Luis Obispo (Cal Poly) and Stanford University. CubeSats are nanosatellites and picosatellites that are defined by a 10-cm cube weighing up to 1.33 kg; these are the specifications for a "1U" in the CubeSat Design Specification [13]. The most common other CubeSat sizes are 1.5U, 2U, and

3U, as shown in Figure 1.4. The original objective was to provide an educational platform for students to develop and launch satellites rapidly with low costs; the small size of these satellites allows for an entire mission life cycle to be completed within two years, or the average length of a master's program [14]. Due to the small size and low cost of these satellites, CubeSats are considered secondary payloads. While universities are still provided the opportunity to participate in this unique educational experience, mainly through NASA's Educational Launch of Nanosatellites (ELaNa) program, there is an increasing number of CubeSats that are developed by government organizations and private companies.

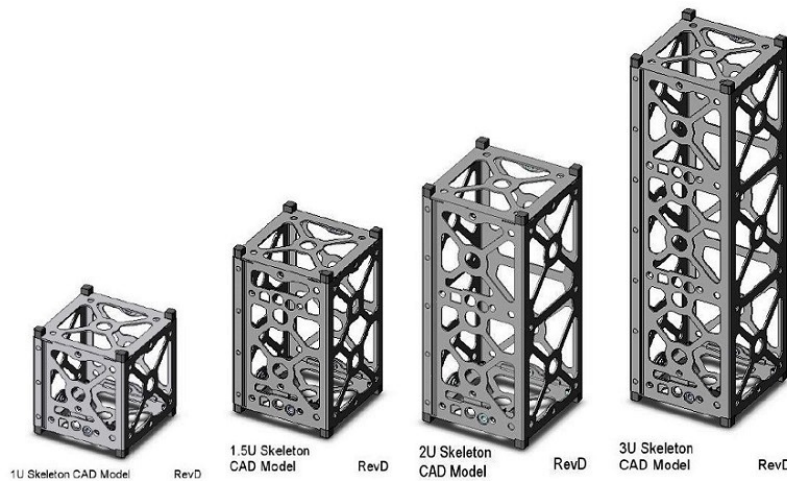


Figure 1.4: Common CubeSat Sizes.

Source: S. Naik, "CubeSat Constellation around Mars," Dec. 2013. [Online]. Available: http://ccar.colorado.edu/asen5050/projects/projects_2013/Naik_Siddhesh/Cubesats.html

The P-POD was developed by Cal Poly and is the most commonly-used, standardized CubeSat deployment system in the world today. Shown in Figure 1.5, the P-POD is a non-separating, rectangular box made of aluminum, carrying any combination adding up to 3Us' worth of CubeSats. The most common combinations are a single 3U or three 1U CubeSats. The P-POD's spring-loaded door is released by a non-explosive actuator (NEA), and the CubeSats are subsequently deployed by the main spring [13].

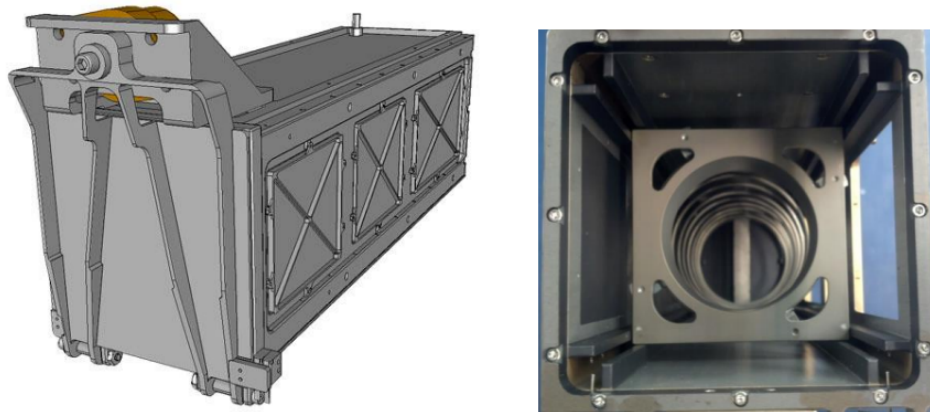


Figure 1.5: P-POD and Main Spring.
Source: CubeSat Design Specification, CubeSat Program, Cal Poly SLO Std., Feb. 2014.

1.3.2 NPSCuL Overview

The concept of clustering P-PODs in the NPSCuL was first published in 2007 in response to the increasing need for U.S.-based launch opportunities [15]. The objective was to improve rideshare opportunities for the CubeSat community as a standard bus for interfacing multiple P-PODs to a launch vehicle. The standard bus was designed to be either a primary or secondary payload because late-stage manifesting was also considered in the event that a primary or secondary payload could not meet a milestone during the launch vehicle integration flow [16]. The original NPSCuL was designed to maximize the space and mass available for an Evolved Expendable Launch Vehicle (EELV) Secondary Payload Adapter (ESPA) payload, which resulted in the D-advanced structure. This original design accommodated 10 5U P-PODs, carrying up to 50 1U CubeSats [17].

In late 2008, NPSCuL was redesigned for the United Launch Alliance (ULA) ABC concept, which has a smaller envelope and mass allowable than the ESPA payload specification [18]. The ABC concept, shown in Figure 1.6, was conceived when ULA determined that one of the helium bottles on the aft end of the Centaur upper stage of the Atlas V vehicle was no longer necessary; this allowed for a secondary payload to take up the volume and mass. The ESPA 15-inch bolt-hole pattern is the standard interface on the ABC plate.

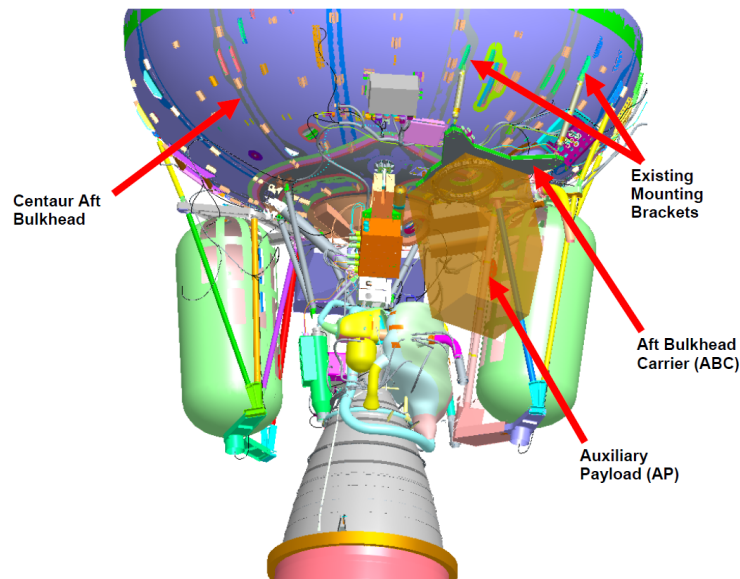


Figure 1.6: Aft Bulkhead Carrier on Atlas V Centaur Aft Bulkhead.
Source: Aft Bulkhead Carrier Auxiliary Payload User's Guide, United Launch Alliance Std., May 2014.

As shown in Figure 1.7, the resulting re-design of NPSCuL became the baseline NPSCuL design [19]. This design can accommodate eight P-PODs, four 6U dispensers, or various combinations of 3U and 6U dispensers. The 6U is a larger CubeSat form factor that is starting to be used; NPSCuL is compatible with both the dispensers built by Tyvak Nano-Satellite Systems, Inc. and Planetary Systems Corporation (PSC). The 6U dispenser built by Tyvak is derived from the Nanosatellite Launch Adapter System (NLAS) [20]. NPSCuL is an ESPA-compatible, five-sided aluminum structure with a non-separating adapter ring. The Splitter Auxiliary Device (SAD), an electrical interface box between the launch vehicle (LV) and the deployers, is also considered to be part of NPSCuL. Eight years after the NPSCuL concept was published, it has flown four times as part of the Operationally Unique Technologies Satellite (OUTSat), the Government Experimental Multi-Satellite (GEMSat), the Unique Lightweight Technology and Research Auxiliary Satellite (ULTRASat), and the Government Rideshare Advanced Concepts Experiment (GRACE) missions. These missions were launched in 2012, 2013, and 2015, and a total of 46 CubeSats were successfully deployed. A fully-integrated payload is shown mounted to the ABC on the aft end of the

Atlas V Centaur stage in Figure 1.8.

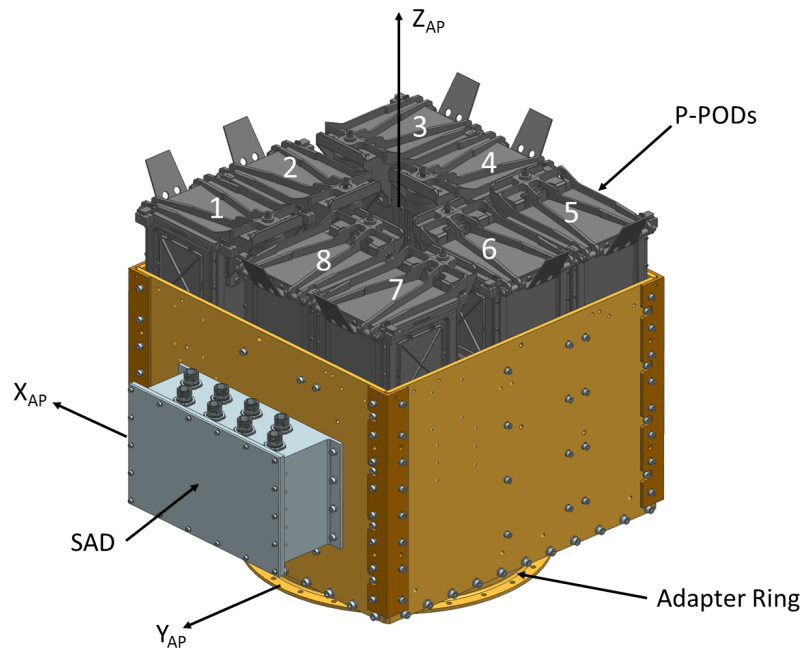


Figure 1.7: NPSCuL Baseline Design

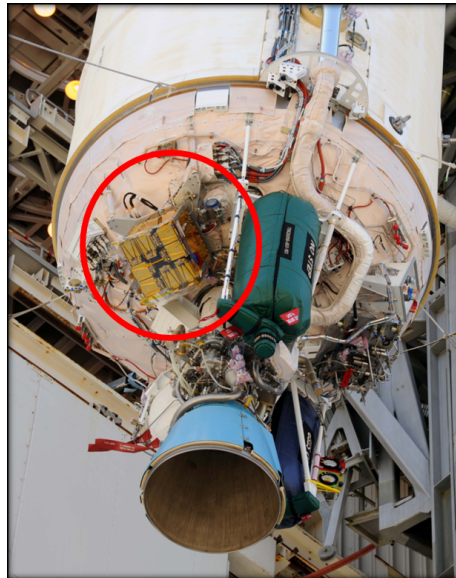


Figure 1.8: OUTSat Mounted to ABC on Centaur Stage Aft End

1.3.2.1 Use of NPSCuL

The NPSCuL geometry and interface to the LV is not unique for Evolved Expendable Reusable Launch Vehicle (EELV) Secondary Payload Adapter (ESPA) payloads. A ring-to-box structure is common for many nanosatellites due to the ESPA standard, and the NPSCuL mass of approximately 90.7 kg (200 lbm) is at the low end of the typical range of 90.7 to 227 kg (200 to 500 lbs) for an ESPA payload. FalconSat-3, mounted to one port of the ESPA ring, and the four ESPA payloads from the STP-S26 mission mounted to the Multiple Payload Adapter (MPA) at the forward end of the Minotaur IV launch vehicle are shown in Figure 1.9. These payloads did not have any reported vibration test issues, and the STP-S26 test environments were much less harsh due to their primary payload status, but they are examples of other ESPA payloads with similar geometry and boundary conditions between the launch vehicle and components mounted to the primary spacecraft structure.

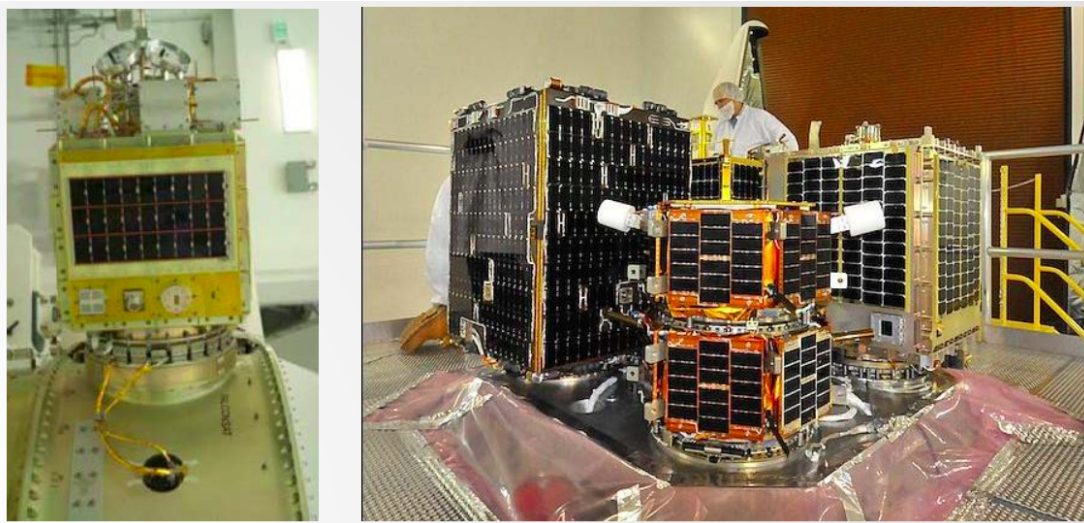


Figure 1.9: FalconSat-3 (left) and ESPA Payloads on STP-S26 (right).

Sources: "Falconsat-3," 2002. [Online]. Available: <https://directory.eoportal.org/web/eoportal/satellite-missions/f/falconsat-3>; "Stp-s26," 2002. [Online]. Available: <https://directory.eoportal.org/web/eoportal/satellite-missions/s/stp-s26>

1.3.3 Definition of Test Levels

Satellite vibration test requirements can come from various sources and often depends on the responsible organization. As a result, the definition of test levels can also vary. The maximum predicted environment (MPE) at the ABC is the base input shown in Figure 1.2; the MPE is also considered the acceptance level for vibration testing. Following the guidelines in [12], protoqualification and qualification levels, defined as MPE +3 dB and MPE +6 dB, respectively, are used for different reasons throughout the spacecraft development cycle. Typically, the qualification levels are used on an engineering development unit (EDU) to show that the design has adequate margins for surviving launch loads. The acceptance levels are used for testing performed on the flight unit in its final configuration after a flight-like EDU has been tested to qualification levels; these levels are meant to show that the unit has been properly built, which also demonstrates process control for multiple flight units. The protoqualification levels, which are performed on a flight unit, are used on a case-by-case basis when there is no EDU available or when the risk of testing an EDU to qual is higher than testing a flight unit with extra margin to gain confidence in its structural integrity. With this approach, the flight unit must also be subjected to an acceptance test. In both the qualification and protoqualification test approaches, subsequent flight units can then be tested to acceptance levels [12]. It is noted that the protoqualification approach is not the same as the protoflight approach, even though the terms are sometimes used interchangeably. In the protoflight testing strategy, the flight unit is only subjected to the protoqualification test levels, and it is not re-tested at the acceptance level. This approach is often used to reduce hardware cost, but it carries schedule and technical risk [21].

1.4 Dissertation Summary

The progression of methods used to reduce the vibration environment on NPSCuL, which include the benefits and shortcomings of using FLVT and the isgorid design, are presented in Chapter 2. In Chapter 3, the driving design requirements, the isolator selection, and the associated re-design of NPSCuL to accommodate each isolator are discussed along with a summary of the test configurations, test inputs, and test set-up. The test results are presented and discussed in Chapter 4, as well as the performance assessment of both isolators. Chapter 5 describes the finite element models that were constructed and used for analysis for each test configuration, as well as the loads analyses that were performed

on the configuration that is the most likely to fly on a future ABC mission. Concluding remarks, the summary of contributions, and future work are provided in Chapter 6.

CHAPTER 2:

Evolution of Vibration Reduction Methods on NPSCuL

Changing the test set-up, the structure itself, and the test levels from the LV provider were considered as methods to reduce the vibration levels on NPSCuL. Only changes to the test set-up and the NPSCuL design will be discussed; at this time, ULA is performing a study to reduce the test levels, but updated test levels are not available. [1].

2.1 Force-Limited Vibration Testing

The qualification and acceptance random vibration tests performed at the system level for the four NPSCuL missions to date all used force-limited vibration testing (FLVT) [19]. It is based on the concept that due to the vibration absorber effect, there is a physical limit on the force at the base of the test article that is often exceeded at the test article's resonant frequencies with a fixed-base test set-up. Similar to the acceleration input, the force limit represents the envelope of the total expected force at an interface during flight [22]. The resonances at the NPSCuL fundamental frequencies are effectively reduced with the force-limited test set-up, resulting in a notched acceleration input that is less conservative than the prescribed acceleration input in [2] but still satisfies the ULA vibration test requirements. Traditionally, the test article is mounted directly to the shaker adapter plate for a fixed-base, random-vibration test. The input is only controlled with respect to acceleration. This type of single-channel control is shown in Figure 2.1.

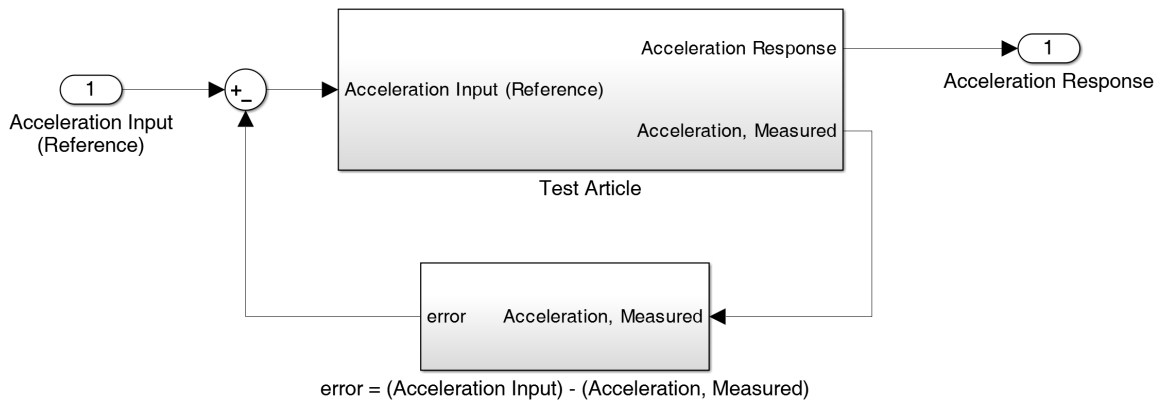


Figure 2.1: Single-Channel Control

In an FLVT set-up, such as the one used for NPSCuL shown in Figure 2.2, dual control is used; both the acceleration input and the force limit are the control channels. The force measured between the shaker and the base of the test article is compared to the force limit while the acceleration input is compared to the reference input; both are done simultaneously by the shaker controller software. The software nominally controls the shaker using the acceleration input, but when the force limit is met or exceeded, the control switches to the force limit, which is set as a watchdog. At these frequencies where the force is being controlled, the resulting acceleration is only being measured. A top-level depiction of the dual-control loop used in an FLVT set-up is shown in Figure 2.3.

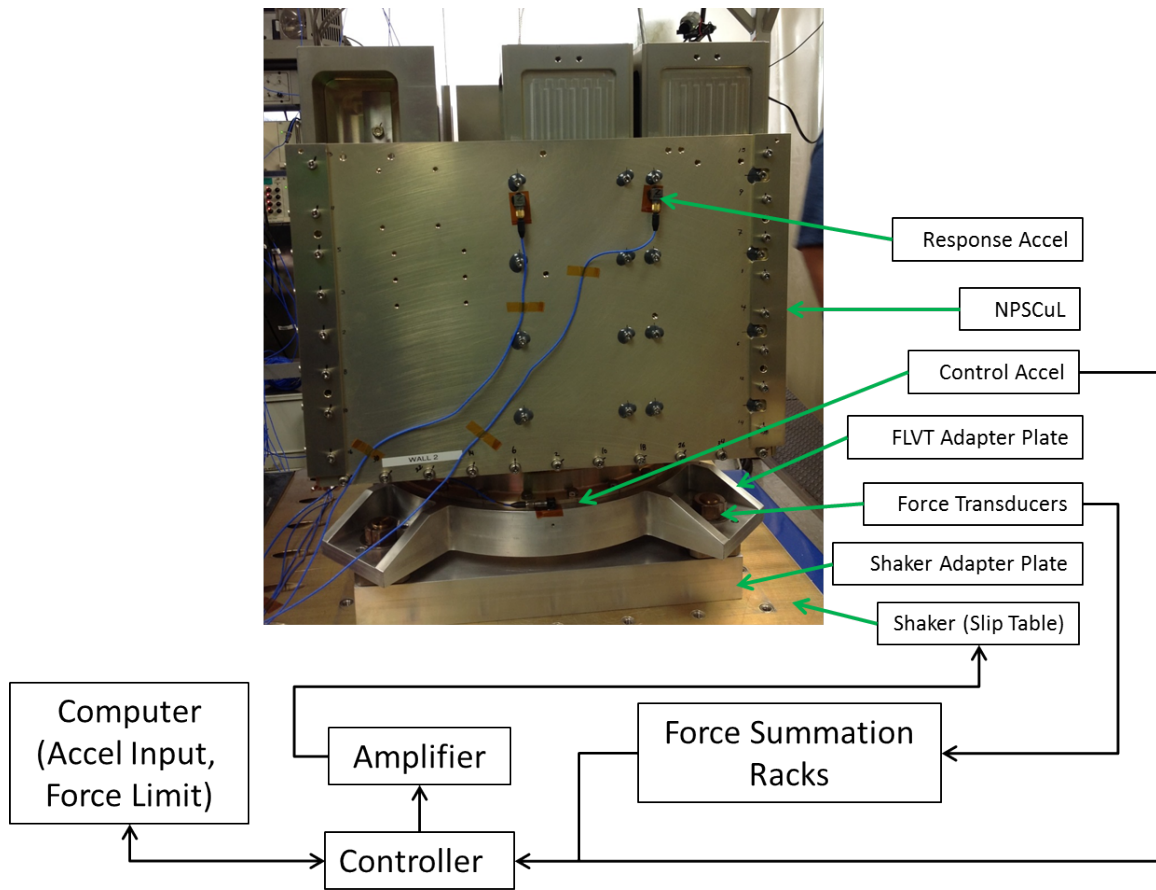


Figure 2.2: FLVT Set-Up of NPSCuL, X-Axis

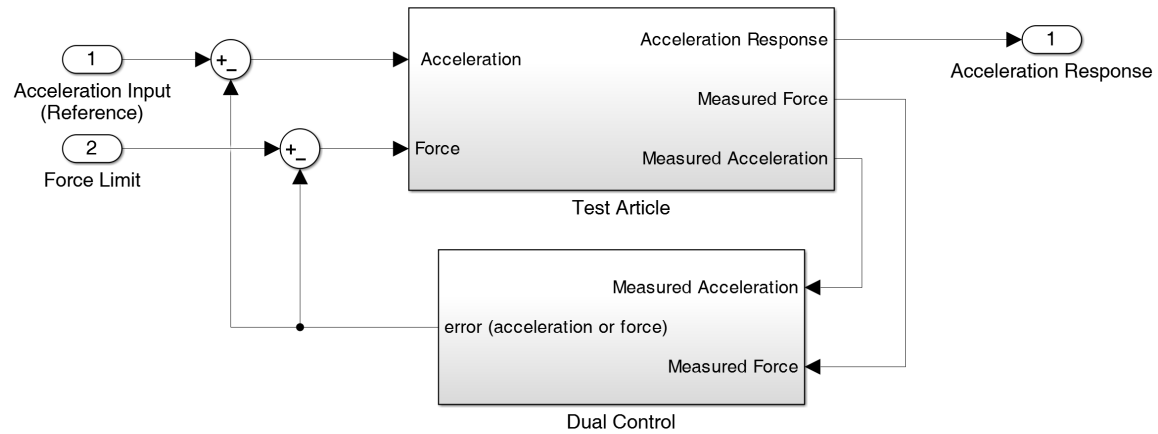


Figure 2.3: Dual-Control Loop

2.1.1 FLVT Background

FLVT was developed at the Jet Propulsion Laboratory (JPL) for large spacecraft and Space Shuttle payloads as a way to reduce over-test resulting from a traditional, acceleration-controlled, fixed-base vibration input [23]. It is well known that the rigid fixed-base boundary condition is conservative and not representative of the flight condition, but the margin associated with vibration testing is also widely accepted by the aerospace industry. This type of set-up can be represented as shown in Figure 2.4.

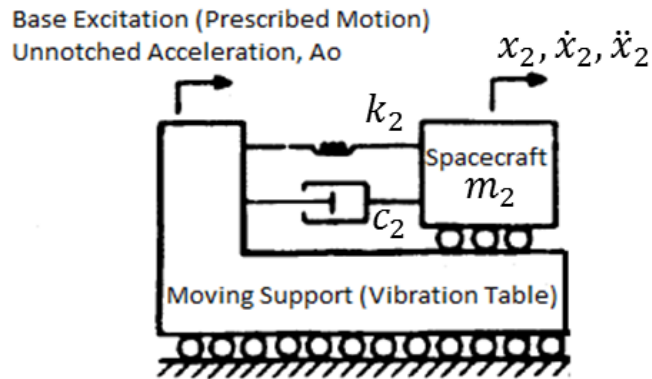


Figure 2.4: Fixed Base Test Set-Up Represented as 1 DOF Harmonic Oscillator Model with Prescribed Support Motion.

Adapted from NASA-HDBK-7004B - Force Limited Vibration Testing, NASA Std., Jan. 2003.

In flight, however, the spacecraft is mounted to a flexible structure, not a rigidly fixed structure; therefore, the system can be simplified to a two degree-of-freedom (2DOF) harmonic oscillator model with prescribed motion, as shown in Figure 2.5.

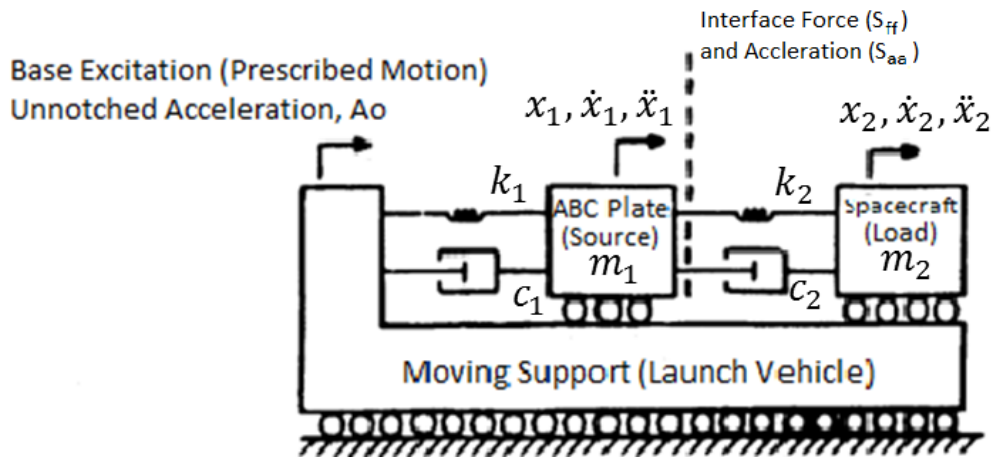


Figure 2.5: FLVT Set-Up Represented as 2DOF Harmonic Oscillator Model with Prescribed Support Motion.

Adapted from NASA-HDBK-7004B - Force Limited Vibration Testing, NASA Std., Jan. 2003.

This set-up results in the vibration absorber effect, in which the second mass, or the load (m_2), acts as a tuned absorber such that the anti-resonance frequency of the first mass, or the source (m_1), is at the fundamental frequency of the load. The anti-resonance is a frequency at which the response of the excited mass is zero for an undamped system, or small for a damped system. The drop in magnitude of the source acceleration, at the fixed-base fundamental frequency of the load, is the theory behind the resulting notch in the acceleration control input when using a force limit. The transmissibility equations used to show this effect using NPSCuL in Section 2.1.1.3 are derived as follows.

2.1.1.1 Transmissibility Equation - Forced Excitation of SDOF System Due to Support Motion

The transmissibility equation for the SDOF mass due support motion is derived from the equation of motion for a mass-spring-damper system with prescribed support motion using absolute coordinates, where x is the coordinate of the lumped mass, ζ is the damping ratio, and ω_n is the natural frequency of the system.

$$\ddot{x} + 2\zeta\omega_n\dot{x} + \omega_n^2x = \omega_n^2y + 2\zeta\omega_n\dot{y} \quad (2.1)$$

The prescribed motion, y , is a function of time, where Ω is the excitation frequency.

$$y(t) = Y\sin(\Omega t) \quad (2.2)$$

To solve the ordinary differential equation, the particular solution for $x(t)$ and $y(t)$ are assumed to be as follows, where X and Y are the amplitudes of displacement of the lumped mass and the support motion, respectively.

$$x(t) = Xe^{j\Omega t} \quad (2.3a)$$

$$y(t) = Ye^{j\Omega t} \quad (2.3b)$$

Substituting Equation 2.3 into Equation 2.1 and solving for the ratio between X and Y yields the non-dimensionalized transmissibility equation shown in Equation 2.4.

$$TR = \frac{X}{Y} = \sqrt{\frac{1 + (2\zeta \frac{\Omega}{\omega_n})^2}{(1 - (\frac{\Omega}{\omega_n})^2)^2 + (2\zeta \frac{\Omega}{\omega_n})^2}} \quad (2.4)$$

2.1.1.2 Transmissibility Equation - Forced Excitation of 2DOF System Due to Support Motion

The transmissibility equations for each of the masses with prescribed base motion can be derived starting with the equations of motion for the 2DOF system in matrix form are shown in Equation 2.5, assuming c_1 is zero [24]).

$$\begin{bmatrix} m_1 & 0 \\ 0 & m_2 \end{bmatrix} \begin{bmatrix} \ddot{x}_1 \\ \ddot{x}_2 \end{bmatrix} + \begin{bmatrix} c_2 & -c_2 \\ -c_2 & c_2 \end{bmatrix} \begin{bmatrix} \dot{x}_1 \\ \dot{x}_2 \end{bmatrix} + \begin{bmatrix} k_1 + k_2 & -k_2 \\ -k_2 & k_2 \end{bmatrix} \begin{bmatrix} x_1 \\ x_2 \end{bmatrix} = \begin{bmatrix} \omega_n^2 y \\ 0 \end{bmatrix} \quad (2.5)$$

Similar to the SDOF case, the prescribed motion is defined in Equation 2.2. The frequency response functions (FRF) between the base and each mass, H_1 and H_2 , can be calculated by taking the inverse of the impedance matrix, which is defined in Equation 2.6.

$$[Z(\Omega)] = [K - \Omega^2 M + j\Omega C] \quad (2.6)$$

The resulting FRFs, calculated using Matlab (see Appendix D), are shown in Equation 2.7.

$$H_1 = \frac{j(m_2\Omega^2 - k_2) + c\Omega}{j(-k_1k_2 + k_1m_2\Omega^2 + k_2m_1\Omega^2 + k_2m_2\Omega^2 - m_1m_2\Omega^4) + (c_2k_1\Omega + c_2m_1\Omega^3 + c_2m_2\Omega^3)} \quad (2.7a)$$

$$H_2 = \frac{k_2 + jc_2\Omega}{(k_1k_2 - k_1m_2\Omega^2 - k_2m_1\Omega^2 - k_2m_2\Omega^2 + m_1m_2\Omega^4) + j(c_2k_1\Omega - c_2m_1\Omega^3 - c_2m_2\Omega^3)} \quad (2.7b)$$

Equation 2.7 is now in the form [25]

$$H_i = \frac{A + jB}{C + jD} \quad (2.8)$$

and can be transformed into the form shown in Equation 2.9.

$$H_i = \sqrt{\frac{A^2 + B^2}{C^2 + D^2}} \quad (2.9)$$

Non-dimensionalizing Equation 2.7 in the form of Equation 2.9 yields

$$A_1 = \sqrt{\frac{(2\zeta r_1 q)^2 + (r_1^2 - q^2)^2}{(r_1^4 - (1 + (1 + \mu)q^2)r_1^2 + q^2)^2 + (2\zeta r_1 q)^2(1 - r_1^2(1 + \mu))^2}} \quad (2.10a)$$

$$A_2 = \sqrt{\frac{q^4 + (2\zeta q)^2}{(r_1^4 - (1 + (1 + \mu)q^2)r_1^2 + q^2)^2 + (2\zeta r_1 q)^2(1 - r_1^2(1 + \mu))^2}} \quad (2.10b)$$

using the ratios shown in Equation 2.11 [24].

$$r_1 = \frac{\Omega}{\omega_1} \quad (2.11a)$$

$$r_2 = \frac{\Omega}{\omega_2} \quad (2.11b)$$

$$\mu = \frac{m_2}{m_1} \quad (2.11c)$$

$$q = \frac{\omega_2}{\omega_1} \quad (2.11d)$$

Equations 2.10a and 2.10b are the transmissibility equations for the 2DOF system, similar to Equation 2.4 for the SDOF system.

2.1.1.3 Force Limit Example with NPSCuL as a Single Degree-of-Freedom

If NPSCuL is assumed to be a simple lumped mass weighing 85.7 kg (189 lbm), the fixed base set-up can be modeled using the mass of NPSCuL and an assumed stiffness. In this

example, the stiffness is chosen such that the fundamental frequency of NPSCuL in the SDOF model is 117 Hz, as shown in Figure 2.6. This fundamental frequency corresponds to the first mode of NPSCuL in the axial (Z) direction. When the test set-up is modeled as a 2DOF system, the anti-resonance of the ABC plate is at 117 Hz, which is a result of the vibration absorber effect.

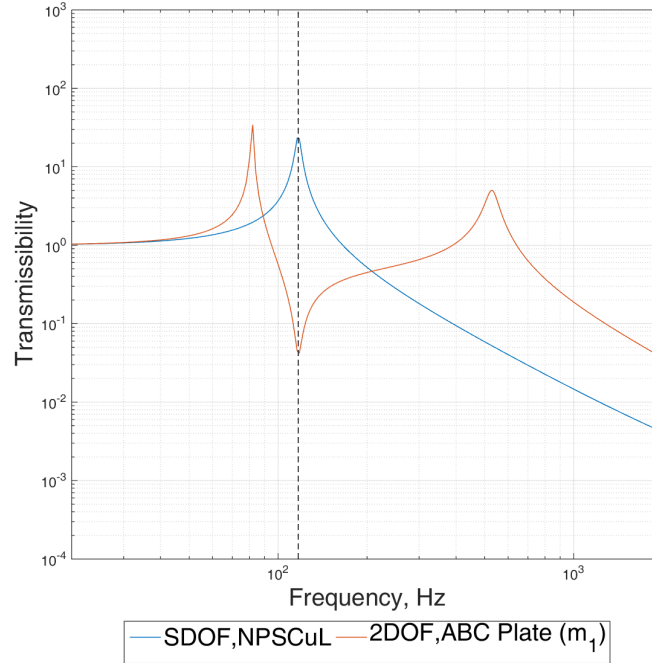


Figure 2.6: Transmissibility of NPSCuL (SDOF Model) and ABC Plate (2DOF Model)

The more realistic acceleration input corresponding to the acceleration of the ABC plate (m_1), near the fundamental frequency of NPSCuL, is then predicted using the transmissibility of the ABC plate in the 2DOF model. The mass of the ABC plate is estimated to be 9.07 kg (20 lbm). The transmissibility of the ABC plate is then multiplied by the un-notched acceleration input (corresponding to the support motion, A_o , in Figure 2.5) to obtain the predicted notched acceleration input. In this example, the random vibration environment defined at the ABC interface, shown in Figure 1.2, is used as the un-notched acceleration input.

As shown in Figure 2.7, the actual acceleration input used during test compares well with the notch predicted in the 2DOF model. The two peaks in the predicted acceleration input are irrelevant; force limiting is only intended to reduce the input at the fundamental frequency of the system, so the 2DOF model is only used to validate the resulting notch in the FLVT test set-up. Additionally, the force limit has been shown to be conservative compared to actual flight data [23].

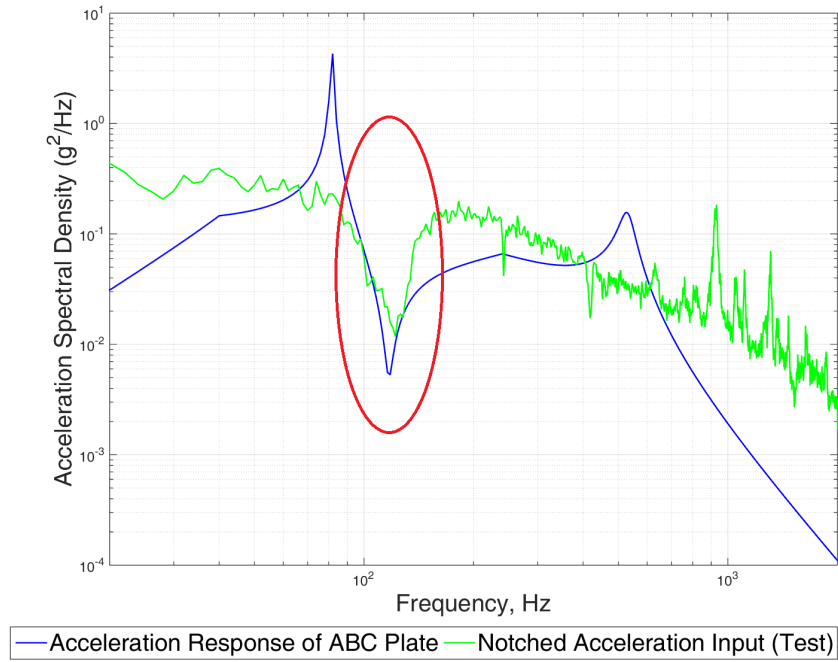


Figure 2.7: Predicted and Actual Force-Limited Acceleration Input

2.1.2 Force Limit Derivation Methods

The force limit can be determined using one of two analytical derivation methods, the simple and complex two-degree-of-system (TDFS) methods, or the semi-empirical method. The analytical methods require more knowledge of the system and have been shown to be more conservative than the semi-empirical method. All three methods will be described, but due to the unavailability of residual and modal masses of the launch vehicle interface and the trend that the analytical methods are typically more conservative, the semi-empirical method was used for NPSCuL. An example of how the force limit is calculated using the

simple and complex TDFS methods can be found in [23] and is demonstrated for NPSCuL here for all three methods.

2.1.2.1 Simple Two Degree-of-Freedom System Method

The simple TDFS method of deriving force limits is also referred to as the frequency shift method of predicting maximum force [26]. In this method, the following equation for a single-output, single-input force spectral density, is likened to $F=ma$, where S_{ff} is the force spectral density, \mathbf{M}_2 is the load apparent mass, and S_{aa} is the acceleration spectral density [27]].

$$S_{ff}(\Omega) = |\mathbf{M}_2(\Omega)|^2 S_{aa}(\Omega) \quad (2.12)$$

The apparent mass is an FRF between the force and acceleration, and all three quantities are functions of frequency. The force and acceleration spectral densities are defined at the interface between the source and the load (see Figure 2.5). The dynamic amplification equation for the force spectral density, otherwise known as the normalized force limit, is simply the square of the right-hand side of Equation 2.4, where ζ is replaced with $Q = \frac{1}{2\zeta}$ [27].

$$\frac{S_{ff}(\Omega)}{M_2^2 S_{aa}(\Omega)} = \frac{1 + \left(\frac{\Omega}{\omega_n}\right)^2}{\left(1 - \left(\frac{\Omega}{\omega_n}\right)^2\right)^2 + \left(\frac{\Omega}{Q}\right)^2} \quad (2.13)$$

Q is also known as the quality factor and corresponds to the transmissibility at resonance for an SDOF system [21]. Note that M_2 is the scalar load mass, which is not the same as the apparent mass in Equation 2.12. For a classical undamped absorber, the squared ratio between the excitation frequency and the natural frequency of the system is shown in Equation 2.14, where μ is the mass ratio, $\frac{m_2}{m_1}$ [25].

$$\left(\frac{\Omega}{\omega}\right)^2 = 1 + \frac{1}{2}\mu \pm \sqrt{\mu + \frac{1}{4}\mu^2} \quad (2.14)$$

Equation 2.14 is substituted into Equation 2.13 to generate Figure 2.8. This plot is used to determine the maximum normalized force spectral density for varying mass ratios. These normalized values also correspond to the C^2 value in the semi-empirical method.

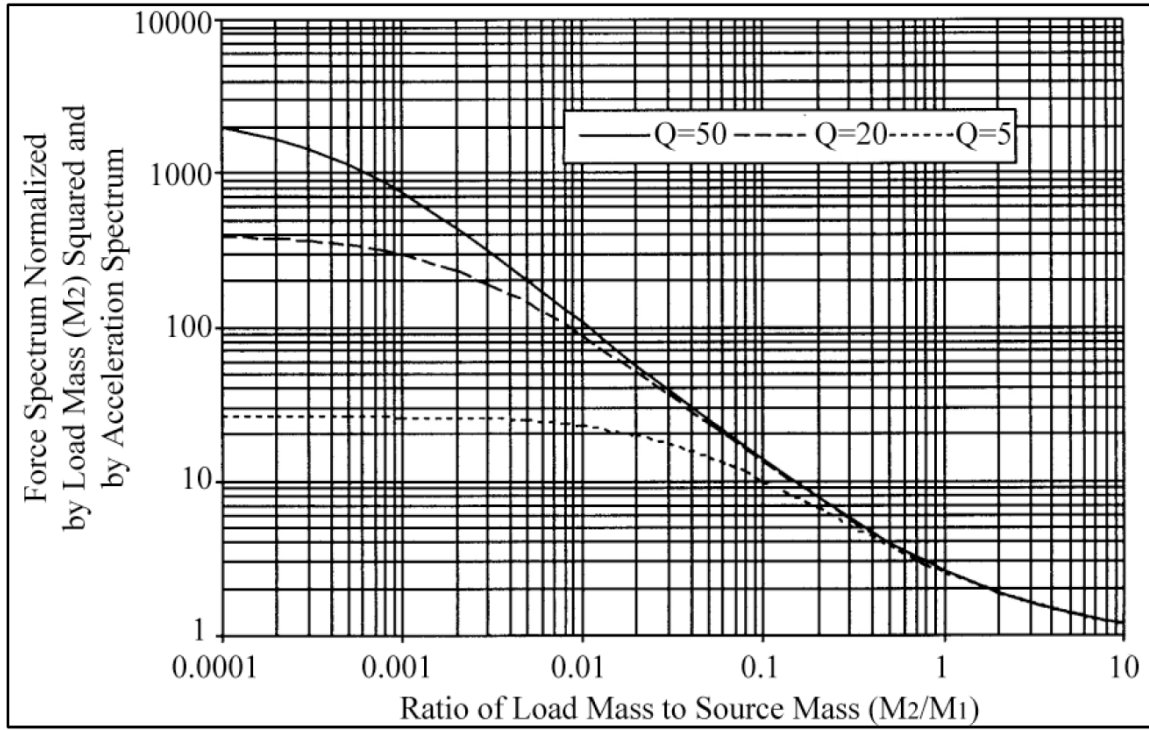


Figure 2.8: Normalized Force Spectral Limit from Simple TDFS Method.
Source: NASA-HDBK-7004C - Force Limited Vibration Testing, NASA Std., Nov. 2012.

The actual force limit is determined by multiplying the normalized value by the acceleration spectral density value; this is done at frequencies throughout the force-limited frequency range. It is recommended to determine the ratio of load to source masses using the asymptotic apparent masses [28]. It is also recommended that the force-limited frequency range be split into one-third octave bands, which can be calculated as shown in Equation 2.15 [29].

$$\frac{f_{n+1}}{f_n} = 2^k \quad (2.15)$$

Using the masses of NPSCuL and the ABC plate, the mass ratio is approximately 10. Therefore, the maximum normalized force spectral density is approximately 1.4 from Figure 2.8. The one-third frequency bands, the ASD values from the ABC levels at MPE corresponding to the center frequencies, and the resulting force limit values are shown in Table 2.1.

Table 2.1: Force Limit Calculated Using Simple TDFS Method for NPSCuL

Frequency Range Split Into 1/3 Octave Bands			Acceleration	Force
Low Frequency, Hz	Center Frequency, Hz	High Frequency, Hz	Spectral Density, $S_{aa} (g^2/Hz)$	Spectral Density, $S_{ff} (N^2/Hz) [lbf^2/Hz]$
19.8	25	31.5	0.0515	1.16E+04 [1.52E + 03]
31.7	40	50.4	0.125	2.81E+04 [2.60E + 03]
50.8	64	80.6	0.125	2.48E+04 [6.31E + 03]
81.0	102	128.5	0.125	1.31E+04 [5.57E + 03]
128.6	162	204.1	0.125	1.31E+04 [2.95E + 03]
204.8	258	325.1	0.1101	1.15E+04 [2.95E + 03]
325.4	410	516.6	0.0487	5.10E+03 [2.59E + 03]
396.9	500	630.0	0.003	3.14E+02 [1.15E + 03]

2.1.2.2 Complex Two Degree-of-Freedom System Method

The expansion of the simple TDFS model to account for the modal (m_n) and residual (M_n) masses, for both the source (ABC plate, m_1 and M_1) and the load (NPSCuL, m_2 and M_2), is shown in Figure 2.9. The modal mass refers to the effective mass of a fundamental mode, and the residual mass refers to the sum of the effective masses that are above the fundamental mode; these values are usually obtained from a finite element model (FEM).

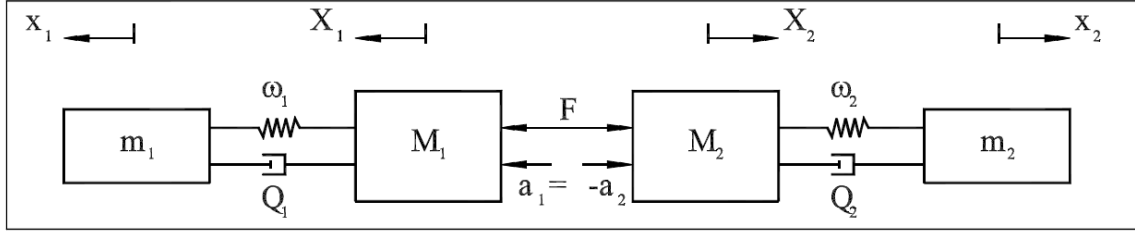


Figure 2.9: Complex TDFS Method Model.

Source: Y. Soucy, V. Dharanipathi, and R. Sedaghati, "Comparison of methods for force limited vibration testing," in Proceedings of the IMAC XXIII Conference, vol. 31. 31 January3 February 2005, Orlando Fla. Society for Experimental Mechanics, Bethel, Connecticut, Paper No. 295, 2005. [Online]. Available: <http://sem-proceedings.com/23i/sem.org-IMAC-XXIII-Conf-s03p02-Application-Operating-Data-Scaling-Techniques-Using-Multiple.pdf>

In the complex TDFS method, the modal and residual masses are accounted for in the $H_2(\Omega)$ term of Equation 2.12, as shown in Equation 2.16.

$$|H_2(\Omega)|^2 = \frac{((1 - \beta_2^2) + \alpha_2)^2 + \beta_2^2(1 + \alpha_2)^2/Q_2^2}{(1 - \beta_2^2)^2 + \beta_2^2/Q_2^2} \quad (2.16)$$

The variables in Equation 2.16 are defined in Equation 2.17.

$$\beta_2^2 = -\frac{1}{2}B \pm \frac{1}{2}\sqrt{B^2 - 4C} \quad (2.17)$$

$$B = \frac{(1 + \mu + \alpha_1)/(\omega_2/\omega_1)^2 + (1 + \mu + \mu\alpha_2)}{1 + \mu} \quad (2.18)$$

$$C = \frac{1 + \mu + \alpha_1 + \mu\alpha_2}{(1 + \mu)(\omega_2/\omega_1)^2} \quad (2.19)$$

$$\alpha_1 = m_1/M_1 \quad (2.20)$$

$$\alpha_2 = m_2/M_2 \quad (2.21)$$

$$\mu = M_2/M_1 \quad (2.22)$$

However, the peak acceleration and peak force cannot be assumed to occur at the same frequency; therefore, the acceleration peak ratio between a_1 to the external acceleration of

the residual mass, A_1 , must be calculated to appropriately scale $H_2(\Omega)$, where $H_1(\Omega)$ is the FRF between the source and the drive point. [26]:

$$\left| \frac{a_1}{A_1} \right|^2 = \left| \frac{H_1}{H_1 + H_2} \right|^2 \quad (2.23)$$

Both the load and source are accounted for in this model, so the ratio of the resonance frequencies between them is also a variable in this force limit derivation method. Therefore, the normalized maximum force limit values are tuned to ensure that the maximum value was found for all mass and damping combinations considered [26]. Due to the greater number of ratios involved in the complex TDFS method, the normalized force spectral limit is tabulated in terms of α_1 , α_2 , and μ . These values, for a Q of 20, are shown in Table 2.2 [28].

Table 2.2: Normalized Force Limit Spectrum for Complex TDFS with $Q = 20$.

Source: NASA-HDBK-7004C - Force Limited Vibration Testing, NASA Std., Nov. 2012.

Ratio of modal to residual mass $m_1/M_1, m_2/M_2$	Residual mass ratio, M_2/M_1								
	0.001	0.003	0.01	0.03	0.1	0.3	1	3	10
8.0, 8.0	932	933	936	948	1001	1180	1240	1234	1238
8.0, 4.0	233	233	233	235	239	256	294	265	250
8.0, 2.0	58	58	58	58	59	60	68	73	68
8.0, 1.0	15	15	15	15	15	15	17	23	22
8.0, 0.5	4	4	4	4	4	4	4	7	6
8.0, 0.25	1	1	1	1	1	1	1	2	5
8.0, 0.125	1	1	1	1	1	1	1	1	3
8.0, 0.0	1	1	1	1	1	1	1	1	1
4.0, 8.0	871	867	858	849	904	1042	1067	1110	1229
4.0, 4.0	218	218	217	216	220	250	254	250	252
4.0, 2.0	55	55	55	55	56	61	72	68	67
4.0, 1.0	14	14	14	14	14	16	21	23	22
4.0, 0.5	3	3	4	4	4	4	6	10	10
4.0, 0.25	1	1	1	1	1	1	2	5	5
4.0, 0.125	1	1	1	1	1	1	1	3	3
4.0, 0.0	1	1	1	1	1	1	1	1	1
2.0, 8.0	1586	1478	1260	1061	990	946	982	1099	1201
2.0, 4.0	406	391	355	305	272	259	238	236	254
2.0, 2.0	103	101	97	88	79	82	70	65	62
2.0, 1.0	26	26	26	25	24	25	25	23	22
2.0, 0.5	7	7	7	7	7	9	10	10	10
2.0, 0.25	2	2	2	2	2	3	5	5	6
2.0, 0.125	1	1	1	1	1	1	3	3	4
2.0, 0.0	1	1	1	1	1	1	1	1	1
1.0, 8.0	11041	5731	2714	1486	967	901	984	1095	1181
1.0, 4.0	3869	2206	1105	567	332	247	233	238	248
1.0, 2.0	1228	826	432	226	125	83	71	66	64
1.0, 1.0	359	283	166	100	50	34	26	23	23
1.0, 0.5	100	89	63	42	24	15	12	11	11
1.0, 0.25	28	27	23	17	11	8	6	6	6
1.0, 0.125	8	8	8	7	5	5	4	4	4
1.0, 0.0	1	1	1	1	1	1	1	1	1
0.5, 8.0	13889	7720	3501	1726	1023	880	974	1093	1171
0.5, 4.0	4516	2895	1417	695	357	247	225	240	244
0.5, 2.0	1346	1003	561	283	136	89	70	64	65
0.5, 1.0	377	319	211	117	59	39	27	24	22
0.5, 0.5	102	95	74	48	27	17	12	11	10
0.5, 0.25	28	27	25	19	13	8	7	6	6
0.5, 0.125	8	8	8	8	6	5	4	4	4
0.5, 0.0	1	1	1	1	1	1	1	1	1
0.25, 8.0	17378	9978	4092	1944	1017	833	936	1092	1166
0.25, 4.0	5194	3725	1805	812	380	249	225	241	242
0.25, 2.0	1455	1205	741	359	173	93	71	66	65
0.25, 1.0	391	354	269	160	74	43	28	23	22
0.25, 0.5	103	99	86	63	38	22	14	12	11
0.25, 0.25	28	28	27	23	16	10	8	7	7
0.25, 0.125	8	8	8	8	7	5	5	4	4
0.25, 0.0	1	1	1	1	1	1	1	1	1
0.125, 8.0	19966	12425	5389	2331	1048	849	918	1092	1163
0.125, 4.0	5748	4417	2241	1080	400	266	228	242	241
0.125, 2.0	1533	1368	901	429	184	102	72	66	65
0.125, 1.0	400	380	312	192	91	45	29	24	22
0.125, 0.5	104	102	95	75	42	24	14	12	11
0.125, 0.25	27	28	27	26	20	13	8	7	6
0.125, 0.125	8	8	8	8	8	7	5	4	4
0.125, 0.0	1	1	1	1	1	1	1	1	1
0.0, 8.0	25114	21284	10111	2700	1125	867	900	1091	1161
0.0, 4.0	6394	6108	4156	1560	454	256	231	240	240
0.0, 2.0	1608	1590	1409	757	257	109	68	67	66
0.0, 1.0	404	403	390	310	148	52	30	25	22
0.0, 0.5	102	102	101	95	60	30	16	12	11
0.0, 0.25	27	27	27	26	22	17	9	7	6
0.0, 0.125	8	8	8	7	7	6	6	5	4
0.0, 0.0	1	1	1	1	1	1	1	1	1

When calculating the force limit using the complex TDFS method for NPSCuL, the modal and residual masses of NPSCuL were obtained from the FEM. The modal and residual masses of the ABC plate are unknown, so these values were estimated. These masses, the resulting ratios, the corresponding normalized force spectral density from Table 2.2, and the actual force spectral density for each one-third octave band are summarized in Table 2.3. The same octave bands and corresponding ASD values used in the simple TDFS method are used for this calculation as well; therefore, only the center frequencies of each band are shown here for reference.

Table 2.3: Force Limit Calculated Using The Complex TDFS Method for NPSCuL

Center Freq.,Hz	Modal Masses, kg [lbm]		Residual Masses, kg [lbm]		Mass Ratios		Normalized Force Spectral Density	Force Spectral Density (S_{ff}), N^2/Hz [$lb f^2/Hz$]
	m_1	m_2	M_1	M_2	α_1	α_2		
20	0.00 [0.00]	0.00 [0.00]	9.08 [20.0]	85.8 [189]	0.00	0.00	1	4.77E+03 [1.52E + 03]
25	0.00 [0.00]	0.00 [0.00]	9.08 [20.0]	85.8 [189]	0.00	0.00	1	8.18E+03 [2.60E + 03]
40	2.27 [5.00]	0.03 [0.07]	6.81 [15.0]	85.78 [189]	0.25	0.00	1	1.98E+04 [6.31E + 03]
64	6.72 [14.8]	5.18 [11.4]	0.09 [0.20]	80.60 [178]	0.74	0.06	4	7.02E+04 [5.57E + 03]
102	0.00 [0.00]	22.00 [48.5]	0.09 [0.20]	58.6 [129]	0.00	0.26	6	6.59E+04 [2.95E + 03]
162	0.00 [0.00]	0.00 [0.01]	0.09 [0.20]	58.6 [129]	0.00	0.00	1	1.99E+04 [2.95E + 03]
258	0.00 [0.00]	0.00 [0.00]	0.09 [0.20]	58.6 [129]	0.00	0.00	1	1.75E+04 [2.59E + 03]
410	0.00 [0.00]	0.04 [0.09]	0.09 [0.20]	58.6 [129]	0.00	0.00	1	7.73E+03 [1.15E + 03]
500	0.00 [0.00]	0.00 [0.00]	0.09 [0.20]	58.6 [129]	0.00	0.00	1	4.77E+02 [7.06E + 01]

It is noted that if the analytical approach is used, the force limit should be calculated using both the simple and complex TDFS methods, and the force limit should consist of the max values [23]. Also, modal and residual mass values of the launch vehicle are not typically available.

2.1.2.3 Semi-Empirical Method

The semi-empirical method is based on the extrapolation of interface force data measured during flight on various launch vehicles and mounting structures. The random vibration equations used in the semi-empirical method to calculate the force spectral limit are similar to 2.12 and are shown in Equation 2.24, where S_{ff} is the force spectral density, Ω is the driving frequency, M_2 is the total mass of the load, S_{aa} is the acceleration spectral density, ω_0 is the fundamental frequency of the load, and n is a positive constant.

$$S_{ff}(\Omega) = C^2 M_2^2 S_{aa}(\Omega) \quad \Omega \leq \omega_0 \quad (2.24)$$

$$S_{ff}(\Omega) = C^2 M_2^2 S_{aa}(\Omega) / (\omega_0 / \Omega)^n \quad \Omega > \omega_0 \quad (2.25)$$

n is usually 2, but can be adjusted to fit experimental measurements of the payload apparent mass, which is the FRF between the measured force and acceleration. The C^2 term can be obtained from Figure 2.8, but using a C^2 value of 2 has also been shown to envelope the interface force data. Additionally, C is usually no higher than 1.4 due to the vibration absorber effect [27]. The decrease in payload residual mass as a function of frequency is accounted for in the f/f_0 term [23], [28].

The force limit calculated using the semi-empirical method for NPSCuL is shown in Figure 2.10, along with the force limits calculated using the simple and complex TDFS methods. For the semi-empirical method, M_2 is the mass of NPSCuL, and ω_0 is 117 Hz.

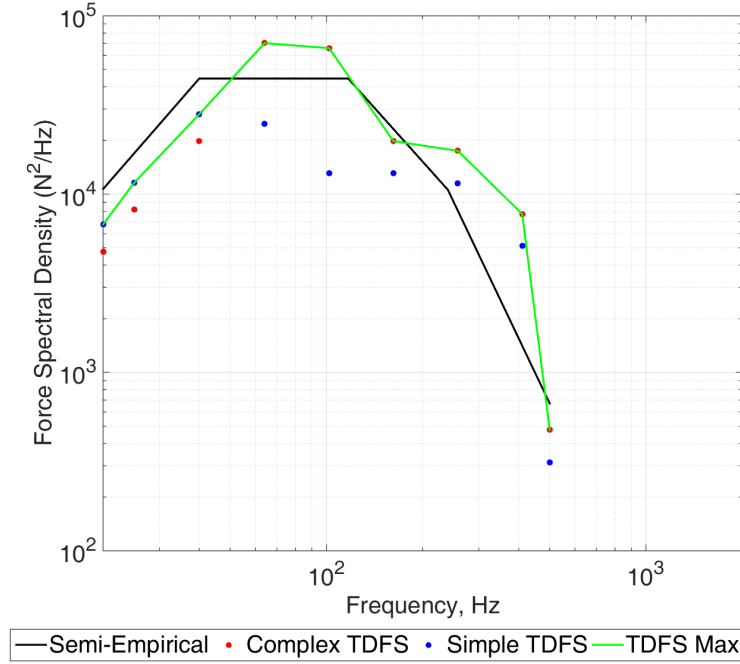


Figure 2.10: Force Limit Calculations for NPSCuL

Consistent with the force limits calculated for various spacecraft and spacecraft components in [23], [28], the force limit calculated using the analytical methods (max values of both simple and complex TDFS methods) is generally more conservative than the semi-empirical method.

2.1.3 Implementation of Force Limiting on NPSCuL

Examples of a force limit for NPSCuL, derived using the semi-empirical method, and the resulting acceleration input at the base of NPSCuL are shown in Figure 2.11 and Figure 2.12. In Figure 2.11, the measured force is expected to hit the force limit near the fundamental frequencies; it is not expected to hit the limit at other frequencies because of the absence of resonances. Because the modal and residual masses of the source are not typically readily available, the semi-empirical method is used to derive the force limit [23].

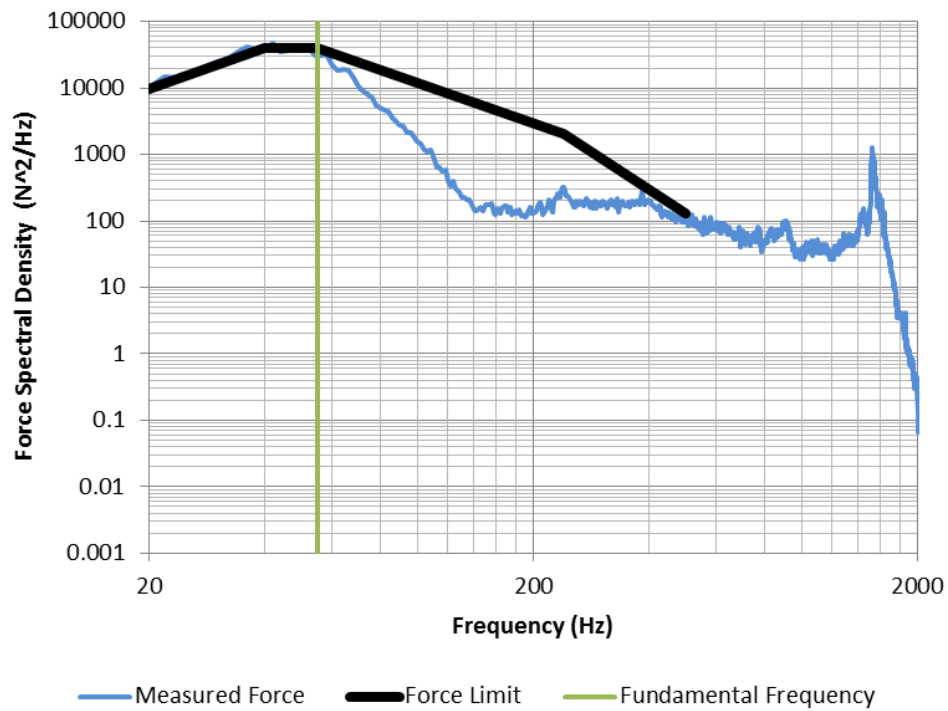


Figure 2.11: Example Force Limit to 500 Hz, Z-Axis

The notches in the acceleration input, shown in Figure 2.12, are near the frequencies at which the measured force does hit the force limit because the acceleration input has been adjusted according to the differences in the measured forces and the force limit at those frequencies. At all other frequencies (i.e., where the measured force does not meet the force limit) it is expected that the force-limited input is the same as the unnotched input.

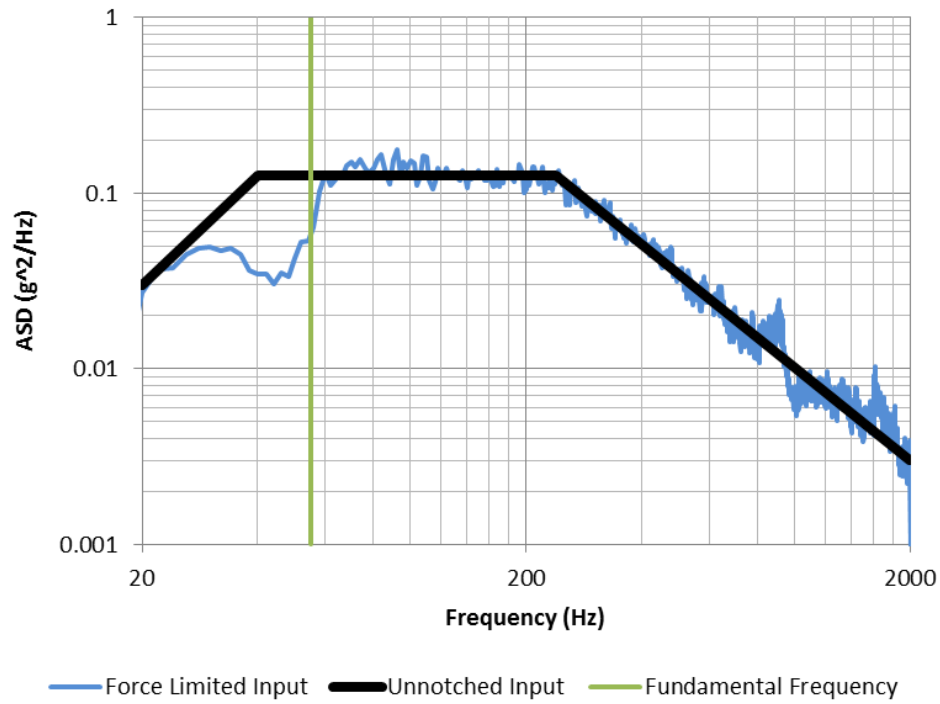


Figure 2.12: Resulting Notch at Fundamental Mode in Acceleration Input, Z-Axis

The X-axis response at the P-POD #2 interface shown in Figure 2.13 and the corresponding G_{RMS} values shown in Table 2.4 highlight both the effectiveness of force-limiting and the inadequacies that still exist without further modifications to NPSCuL. The overall G_{RMS} is reduced by 56%, but the responses, shown in the frequency domain, are a representative case of the amount of high-frequency content that is present, even if an FLVT set-up is used.

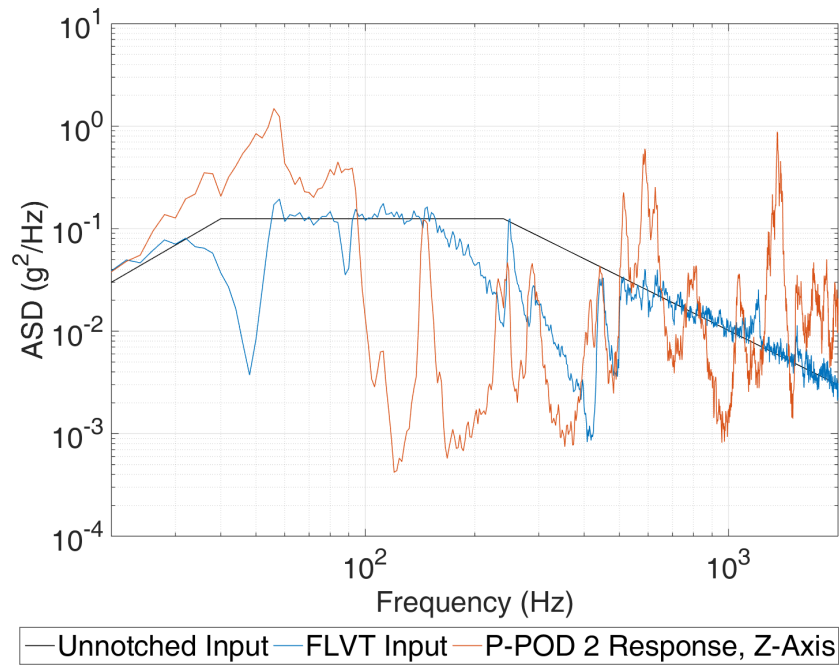


Figure 2.13: X-Axis Response at P-POD #2 Interface (P2M2 Data at MPE +0 dB)

Table 2.4: P-POD 2 Response, with and without FLVT

Level	Base Input G_{RMS}	P-POD Interface G_{RMS}
With Force Limiting	6.18	11.8
Without Force Limiting	7.6	26.7

It is noted that there is no relief past the force-limited range; however, test data shows that there is a significant amount of energy above 500 Hz at the P-POD interface, which is the frequency range of concern to many CubeSats. However, force limiting is only intended to reduce the input at the fundamental frequency of the system; it is not meant to change the properties of the system.

2.2 Isogrid NPSCuL

FLVT is intended to change the test set-up by reducing the acceleration input at the fundamental frequency, and it is very effective for that purpose on NPSCuL. However, FLVT is not intended to be a mechanism for changing the resonant properties of a system, so it was recognized that NPSCuL had to be modified to reduce the vibration environment at the P-POD interface. The main intent of the design changes were to stiffen the structure so that the displacement, and energy required to excite the resonant modes, would decrease. For a system subjected to a static force, the displacement decreases when the stiffness increases; in a dynamic environment, more energy is required to excite higher modes. The baseplate and wall thicknesses were increased, and an isogrid design was implemented to keep the primary structure mass to a minimum. Additionally, the baseplate and adapter ring were combined into a single part, called the unibase. The resulting re-designed isogrid NPSCuL structure is shown in Figure 2.14 and Figure 2.15 [19].

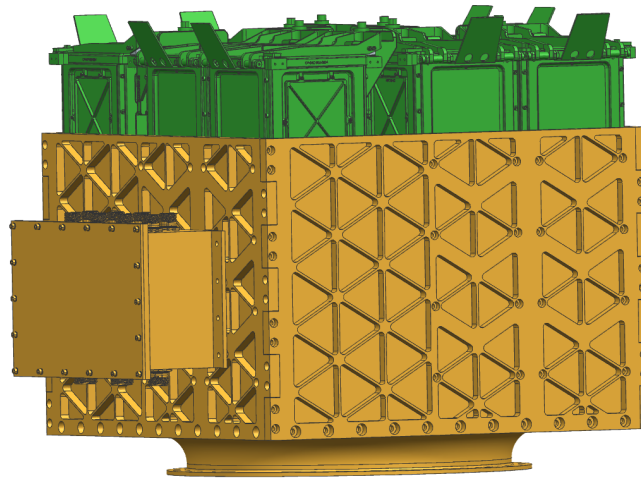


Figure 2.14: Isogrid NPSCuL Design.

Source: V. Kaushish, "Force limited vibration testing and subsequent re-design of the naval postgraduate school CubeSat launcher," Master's thesis, Monterey, California: Naval Postgraduate School, 2014. [Online]. Available: <http://calhoun.nps.edu/handle/10945/42656>.

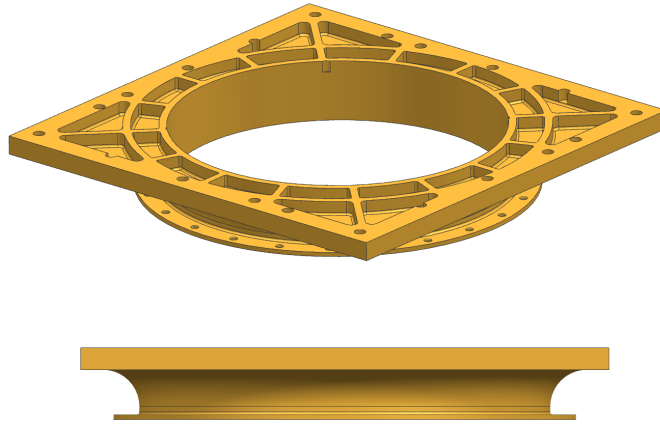


Figure 2.15: Unibase.

Source: V. Kaushish, "Force limited vibration testing and subsequent re-design of the naval postgraduate school CubeSat launcher," Master's thesis, Monterey, California: Naval Postgraduate School, 2014. [Online]. Available: <http://calhoun.nps.edu/handle/10945/42656>.

The isogrid NPSCuL design was built and tested, and test results were compared with the baseline NPSCuL vibration test results. It was found that, although the first fundamental frequencies of the isogrid NPSCuL design are higher than the baseline NPSCuL fundamental frequencies, FLVT is less effective on the isogrid NPSCuL structure. This is because the force roll-off frequency associated with FLVT, which coincides with the fundamental frequency of the system, begins at a lower frequency when testing the baseline, less-stiff NPSCuL, allowing for a broader roll-off frequency range and slightly deeper notches. This is depicted in Figure 2.16, where the notch at 45 Hz, the fundamental frequency of the baseline NPSCuL, is deeper than the notch around 60 Hz, which coincides with the fundamental frequency of the isogrid NPSCuL in the X-axis.

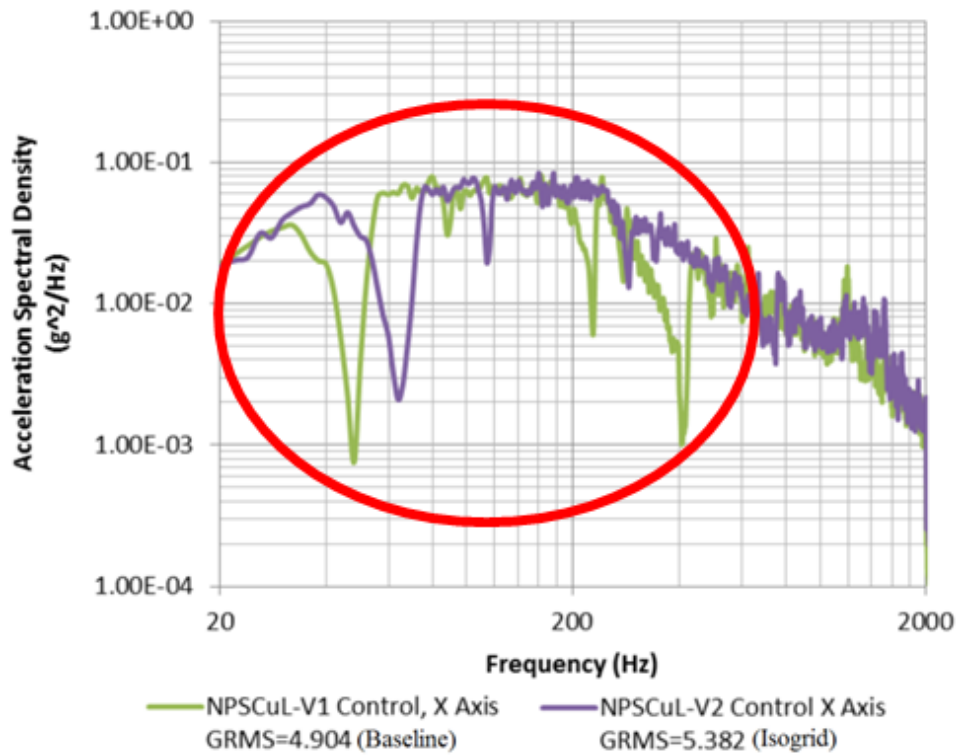


Figure 2.16: X-Axis Notched Acceleration Control, Baseline and Isogrid NPSCuL at MPE -3 dB.

Source: V. Kaushish, "Force limited vibration testing and subsequent re-design of the naval postgraduate school CubeSat launcher," Master's thesis, Monterey, California: Naval Postgraduate School, 2014. [Online]. Available: <http://calhoun.nps.edu/handle/10945/42656>.

The resulting overall G_{RMS} levels measured at the P-POD-to-NPSCuL interface are higher for the stiffer isogrid structure, even when utilizing FLVT. This is shown in Figure 2.17, which contains the X-axis data taken at P-POD #2 for both the baseline and isogrid NPSCuL designs.

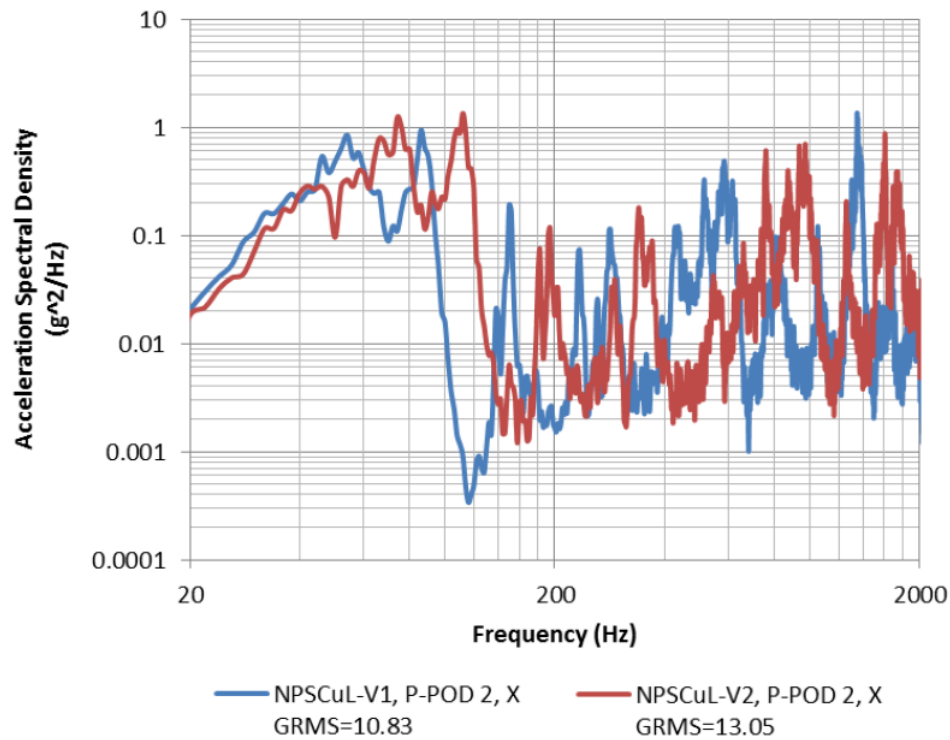


Figure 2.17: X-Axis Random Vibration Response, Baseline and Isogrid NPSCuL at MPE -3 dB.

Source: V. Kaushish, "Force limited vibration testing and subsequent re-design of the naval postgraduate school CubeSat launcher," Master's thesis, Monterey, California: Naval Postgraduate School, 2014. [Online]. Available: <http://calhoun.nps.edu/handle/10945/42656>.

The results of the isogrid NPSCuL testing show that stiffening a structure may not reduce vibration test levels when utilizing FLVT. Additionally, there is no relief in amplitude at the P-POD interface, especially above 500 Hz. It was determined that either introduction of damping or utilization of vibration isolation techniques would probably be required to achieve better vibration environments [1], [19].

THIS PAGE INTENTIONALLY LEFT BLANK

CHAPTER 3:

Incorporating Isolators on NPSCuL

Stiffening the structure did not produce favorable results even when combined with FLVT, so incorporating isolators on NPSCuL was investigated as a way of reducing the stiffness to improve the vibration environment. The lower stiffness would potentially result in a lower roll-off frequency, thus providing more relief in the force-limited frequency range. Additionally, by lowering the fundamental frequencies of the fully-integrated system, isolators reduce the transmissibility to the components, whose resonant modes are subsequently in the isolation region. It is also known that softer springs, or reducing the stiffness, are more effective in the isolation region. The expected increase in damping from the isolators was also desired to minimize the peak response at the fundamental frequencies. Therefore, the NPSCuL designs were updated to accommodate two different isolators, and vibration tests were performed with and without FLVT on the various configurations to demonstrate the combined use of FLVT and COTS isolators as a feasible vibration reduction method for small satellites.

3.1 Design Updates to NPSCuL

The isogrid NPSCuL test results showed that changes to the adapter-ring-to-baseplate interface were the most effective in changing the fundamental frequencies of the system; therefore, NPSCuL was re-designed to incorporate isolators at the joint between the adapter ring and baseplate. Both this joint and the interface between the P-PODs and the NPSCuL wall were considered. However, incorporating isolators at this joint was thought to be the most global solution for other ESPA payloads, and existing isolation systems for larger spacecraft are implemented at similar locations.

3.1.1 Design Requirements

The design changes for incorporating isolators on NPSCuL were driven by the Atlas V launch vehicle requirements because it is the most likely launch vehicle that will fly an NPSCuL in the future. The pertinent requirements for this design change are as follows [2]:

- AP static envelope must be within the auxiliary payload (AP) volume
- AP mechanical interface must be compatible with the ABC plate
- AP mass properties must be within the interface control document (ICD) range
- AP must be able to withstand thermal, static loads, and random vibration environments
- AP fundamental frequency must be above 35 Hz
- Mission-specific coupled loads analyses (CLAs) performed by ULA must show no negative impacts to the LV and the primary spacecraft

Other general design considerations included ease of assembly and access to the ABC interface fasteners. The following requirements are taken from the ABC User's Guide and do not necessarily reflect the mission-specific requirements for past NPSCuL missions.

3.1.1.1 Static Envelope

The non-separating AP envelope for the ABC secondary payload launch system, shown in Figure 3.1, had to be maintained for any changes made to NPSCuL. The envelope was defined with a tight tolerance (within 2.54 cm, or 1") on the outer dimensions of an NPSCuL integrated with eight P-PODs, so there was not much room for expansion in any given direction.

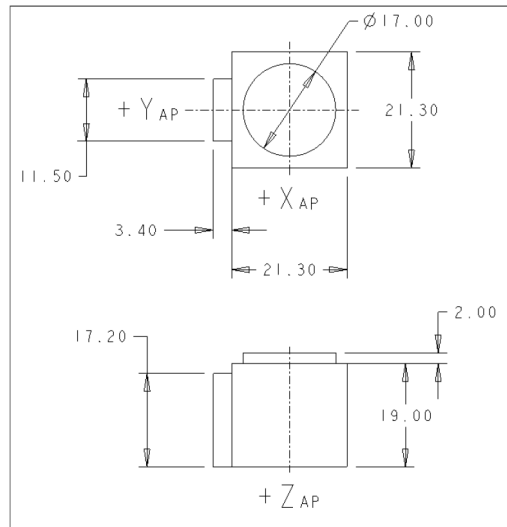


Figure 3.1: Non-separating AP Envelope.

Source: Aft Bulkhead Carrier Auxiliary Payload User's Guide, United Launch Alliance Std., May 2014.

3.1.1.2 Mechanical Interface to Launch Vehicle

The ABC plate is mounted to the aft end of the Centaur stage with struts (see Figure 1.6). The ABC plate interface, shown in Figure 3.2, consists of 24 fasteners on a 38.1 cm (15") diameter circle. This is derived from the ESPA standard.

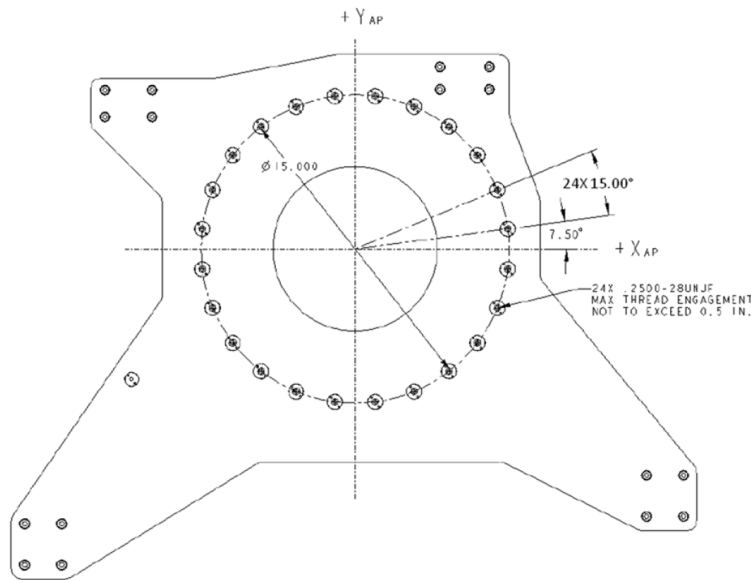


Figure 3.2: ABC Interface.

Source: Aft Bulkhead Carrier Auxiliary Payload User's Guide, United Launch Alliance Std., May 2014.

3.1.1.3 Mass Properties

The mass properties requirements are provided as a range for both the mass and center of gravity (CG). The mass requirement is $65.8 \text{ kg} \pm 11.4 \text{ kg}$ ($145 \pm 25 \text{ lbm}$), the Z CG location must be $24.4 \text{ cm} \pm 1.91 \text{ cm}$ ($9.6" \pm 0.75"$), and the X and Y CG offsets must be $0 \text{ cm} \pm 1.27 \text{ cm}$ ($0" \pm 0.5"$) [2]. However, the mass requirement is often mission-specific because it depends on the mass budget and loads analyses results.

3.1.1.4 Launch Environments

3.1.1.4.1 Thermal Environment Between the pre-launch and flight thermal environments, the minimum and maximum expected temperature range is between $-46 \text{ }^{\circ}\text{C}$ and $38 \text{ }^{\circ}\text{C}$ (-50 and $100 \text{ }^{\circ}\text{F}$). However, the thermal vacuum qualification test range from of -34 to $71 \text{ }^{\circ}\text{C}$ (-29 to $160 \text{ }^{\circ}\text{F}$) were used as a more conservative design requirement to cover any extreme temperatures that may occur during flight [2], [12].

3.1.1.4.2 Static Loads The launch vehicle design load factors are specified to be 7 Gs and 5 Gs in the axial and lateral directions, respectively, and are to be applied at the CG of the AP simultaneously. It is noted that unlike most primary spacecraft that are subjected to an axial load that is mainly in compression, the axial static load is mainly in tension due to the orientation of the AP on the ABC plate.

3.1.1.4.3 Random Vibration The random vibration environment defined at the ABC interface is shown in Figure 3.3; this is the maximum predicted environment (MPE) by the launch vehicle provider for this location.

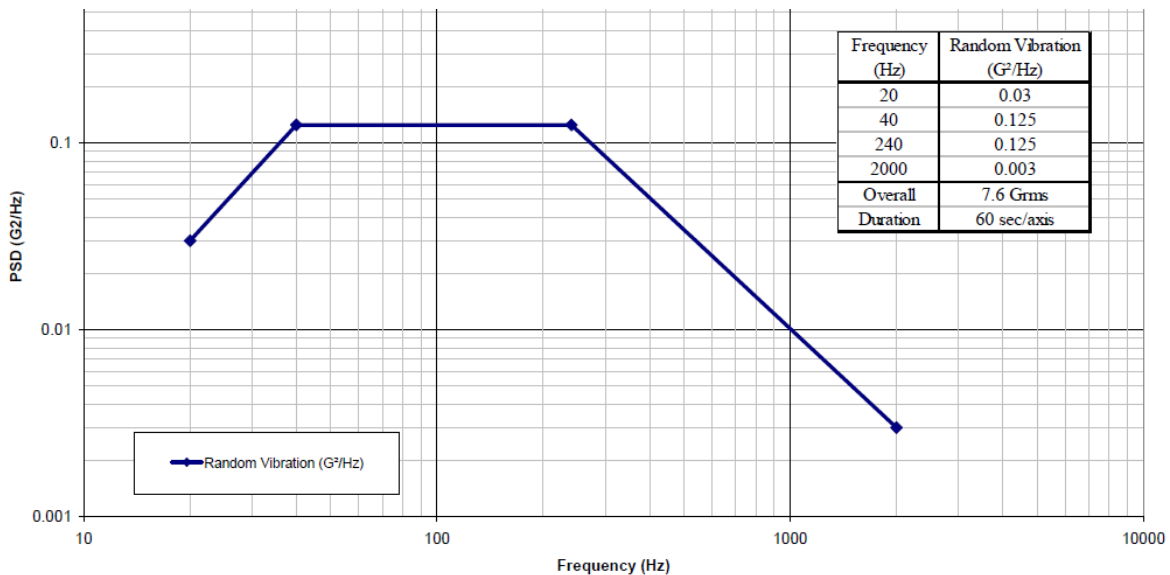


Figure 3.3: Aft Bulkhead Carrier (ABC) Vibration Requirement.
Source: Aft Bulkhead Carrier Auxiliary Payload User's Guide, United Launch Alliance Std., May 2014.

3.1.1.5 Fundamental Frequency

The launch vehicle also commonly requires that the fundamental frequency of the AP be above 35 Hz; however, this general guideline was relaxed for the purposes of choosing an isolator, and the impacts of having an isolated AP will require further evaluation by ULA. Isolators typically lower the fundamental frequencies of the system, but an effort was made

to choose isolators that had higher fundamental frequencies to mitigate the risk of coupling between NPSCuL and the Centaur aft bulkhead components.

3.1.1.6 Mission-Specific CLA

The CLAs are performed on the entire launch vehicle model, which includes the primary spacecraft and AP models, to assess potential impacts to the LV and the primary spacecraft for different launch events [2]. The CLAs also confirm that the design load factors are adequate. A finite element model of the AP is delivered to ULA for these analyses; this has been done for all previous missions and will also be done for any future flights that include isolators on NPSCuL.

3.1.2 Isolator Selection

The two isolators that were chosen for feasibility testing were the LORD conical broad-temperature-range (BTR) silicone isolators (P/N AM-009-14) and the Barry cupmount hi-damp silicone elastomer isolators (P/N NC-1035-T4). Due to the size and static load ratings of the isolators, it was determined that eight isolators were sufficient for both types.

3.1.2.1 Conical Isolator Description

The conical isolator shown in Figure 3.4 was initially chosen for feasibility testing due to its low profile of 1.80 cm (0.71"), low mass of 81.6 g (0.180 lbm), and wide operating temperature range of -56 to 149 °C (-65 to 300 ° F). It had the highest maximum static load per mount of 111 N (25.0 lbf) and the highest axial natural frequency of 42 Hz compared to other similar isolators. Additionally, it was capable of handling the random vibration environment shown in Figure 3.3. However, it is generally recommended for use in compression only; its use in tension is to be assessed on a case-by-case basis. This type of isolator is also not fail-safe, meaning that if the elastomer fails, there is no other retention mechanism to prevent the isolator from falling apart [30].

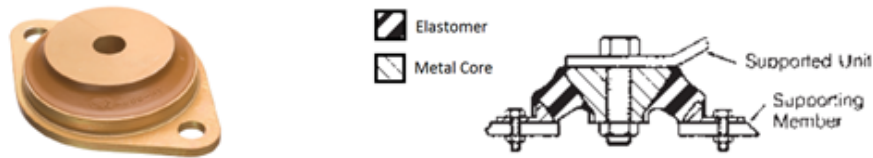


Figure 3.4: Conical Isolator.

Source: "LORD aero catalog," 2011. [Online]. Available: <http://www.lord.com/productsand-solutions/vibration-and-motion-control/aerospace-catalog.xml>

3.1.2.2 Cupmount Isolator Description

The cupmount isolator shown in Figure 3.5 was chosen for its fail-safe and all-attitude features. Not only does it have a retention mechanism if the elastomer fails, the isolator can support static weight in any direction or orientation; it is not restricted to use in compression only [31]. Similar to the conical isolator, the axial natural frequency is 40 Hz, it has a broad operating temperature range of -55 to 149 °C (-67 to 300 ° F), and it can support up to 311 N (70 lbf) of static load in vibration or 107 to 169 N (24 to 38 lbf) shock. The cupmount isolator weighs 170 g (0.375 lbm) and is heavier than the conical isolator [32].

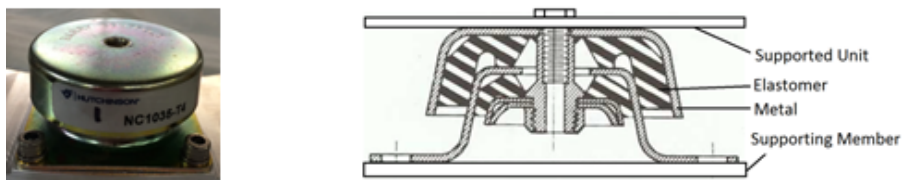


Figure 3.5: Cupmount Isolator.

Source: "Barry Controls - Core Spin," June 2015. [Online]. Available: <http://www.hutchinsonai.com/uploads/tech/Core%20spin.pdf>

Due to its fail-safe and all-attitude features, the cupmount isolator is more suitable for NPSCuL on the ABC plate; however, both isolators will be discussed due their potential use in other applications that may not have the tension-loading requirement.

3.1.3 Design Change to NPSCuL

The adapter ring and baseplate, shown in Figure 3.6, were modified to accommodate isolators on NPSCuL and to keep the overall dimensions within the static envelope.

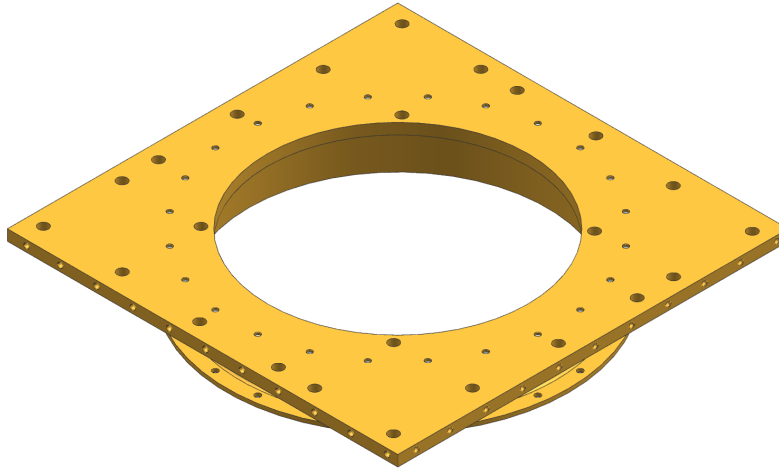


Figure 3.6: Baseline NPSCuL Adapter Ring and Baseplate

The adapter ring was re-designed to be a flat ring with two different thicknesses. The thinner portions of the ring were kept at a 0.432 cm (0.170") thickness, the same thickness of the -Z flange of the baseline adapter ring, to maintain the same thread engagement length of the interface fasteners between the ring and the ABC plate. The thicker portions of the ring were adjusted to accommodate an adequate amount of thread engagement for the fasteners holding the isolators to the ring, as well as any nuts or fasteners that needed to be installed on the underside of the isolator. The inner and outer diameters of the re-designed ring were also adjusted to accommodate the footprint of the isolator. A separate ring was designed for each isolator; the three designs are shown in Figure 3.7. The re-designed adapter rings, with the isolators installed, are shown in Figure 3.8. In both adapter ring designs, only eight of the 24 available ABC interface fasteners are used.

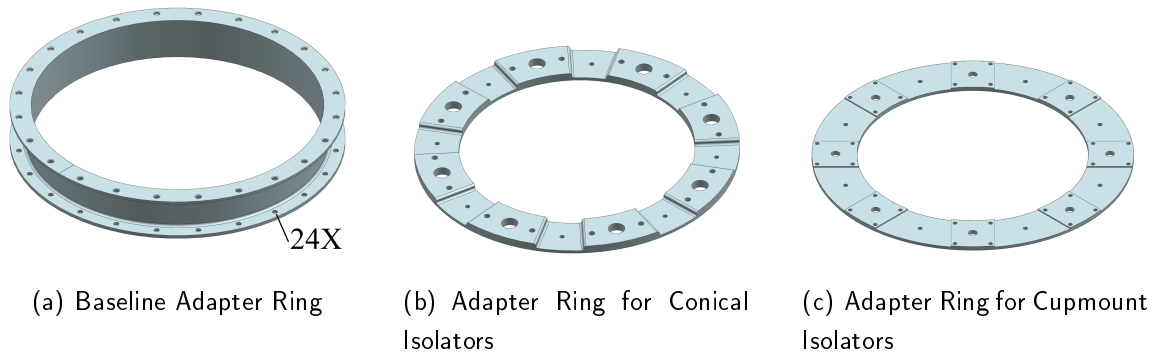


Figure 3.7: Adapter Ring Designs

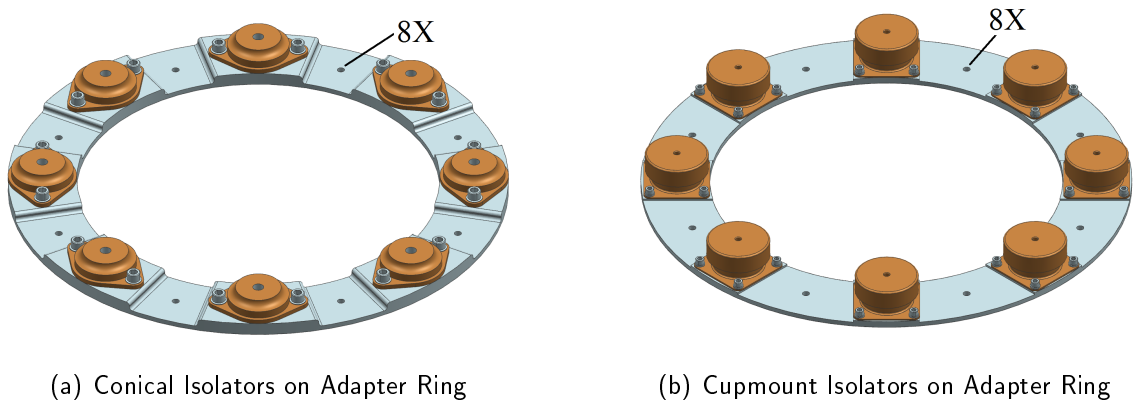


Figure 3.8: Isolators on Re-designed Adapter Rings

The 24 threaded holes in the baseplate for the ring-to-baseplate fasteners were replaced with eight counterbore holes; the size of the counterbore was dependent on the size of the isolator-to-baseplate fasteners; the conical isolators required 9.525-mm-diameter (3/8") fasteners, and the cupmount isolators required 6.35-mm-diameter (1/4") fasteners. The modified baseplate is shown in Figure 3.9.

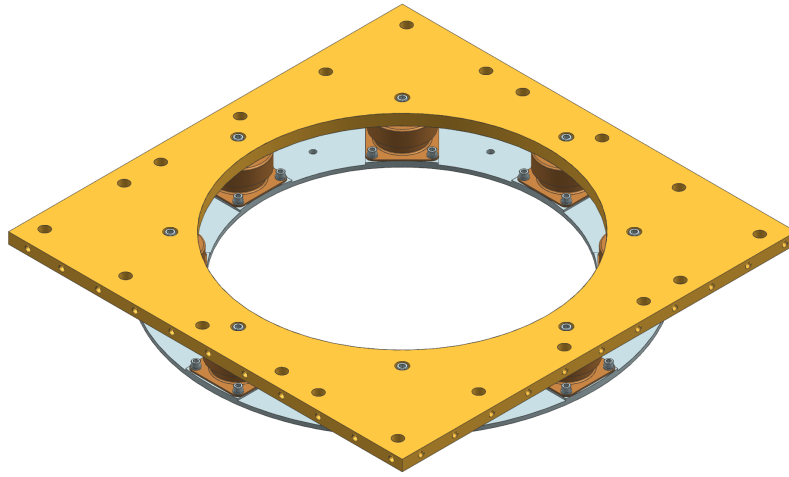


Figure 3.9: Modified Baseplate and Adapter Ring, Cupmount Isolators

The resulting reductions in overall height are 2.29 cm (0.9") and 1.78 cm (0.7") with the conical and cupmount isolators. The adapter ring masses for the conical and cupmount isolators are 1.66 and 1.04 kg (3.67 and 2.30 lbm), respectively. Although the re-designed adapter rings are about the same mass or lighter than the baseline adapter ring (weighing 1.54 kg, or 3.40 lbs), the combined mass with the isolators increased the overall mass of the NPSCuL structure by 1.04 and 2.27 kg (2.3 and 2.5 lbm) with the conical and cupmount isolators, respectively.

3.2 Test Set-Up and Configurations

3.2.1 FLVT Test Set-Up

The FLVT set-up shown in Figure 3.10 depicts four force transducers are sandwiched between the shaker adapter plate and a second plate, or the FLVT adapter plate, that interfaces with the test article. As recommended in [23], the mass of the FLVT adapter plate was designed to be no more than 10% of the test article mass, or 8.62 kg (19 lbm). This set-up allows the force transducers, which must be pre-loaded [33], to measure the force at the mounting interface. The force-limited set-up was used in all test configurations (with and without force-limiting) and for all sine and random test inputs; this was done to maintain a consistent test boundary condition.

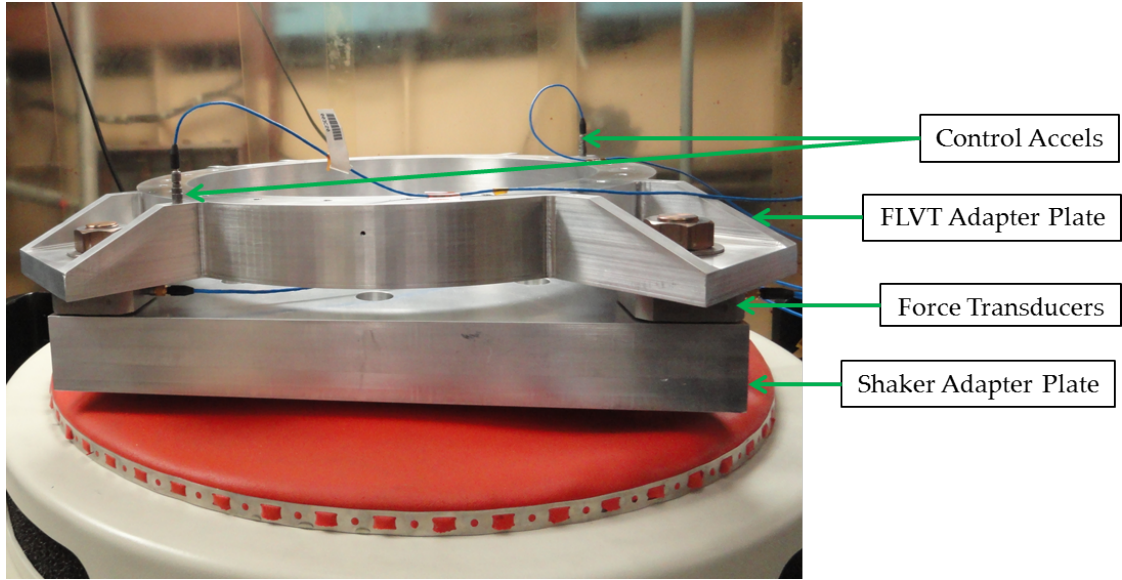


Figure 3.10: FLVT Set-Up, Bare Fixture

3.2.1.1 Force Limit Parameters

When using the semi-empirical method, the physical total mass (M_0), the acceleration spectral density (S_{aa}), and the roll-off (fundamental) frequency (f_0) are either pre-defined or properties of the system. S_{aa} is a given mission requirement, M_0 is measured before the test, and f_0 is also measured from the sine sweeps performed before each random test. The C^2 term and the cut-off frequency, f , are determined by recommendations in [23] or rules of thumb based on existing data. For NPSCuL, the recommended C^2 value of 2 and cut-off frequency of 500 Hz were used in calculating the force limit [23]. It is also recommended that the maximum roll-off slope should not exceed 9 dB/Oct, but this recommendation was not followed for NPSCuL because the resulting notched ABC acceleration input was determined to be conservative compared to the flight environment, despite a steeper roll-off slope. The Matlab code used for the force limit calculation can be found in Appendix E.

3.2.2 Test Article Description

For all test configurations, eight P-POD mass models (P2M2s) and the SAD EDU were installed on the main NPSCuL structure; this is the typical NPSCuL qualification test con-

figuration and is shown in Figure 3.11. Although using P-PODs would have been a more flight-like representation of the system, the P2M2s are simple structures that can be easily modeled and have predictable dynamic behavior; the P-PODs are much more complex with variable behavior above 500 Hz due to the internal constraints on the CubeSats and the variation in CubeSat dynamic properties. Past data also shows that the acceleration measured at the P-POD to NPSCuL interface using P2M2s results in a worst-case response; this response was measured just below the upper-left fastener for each P-POD location.

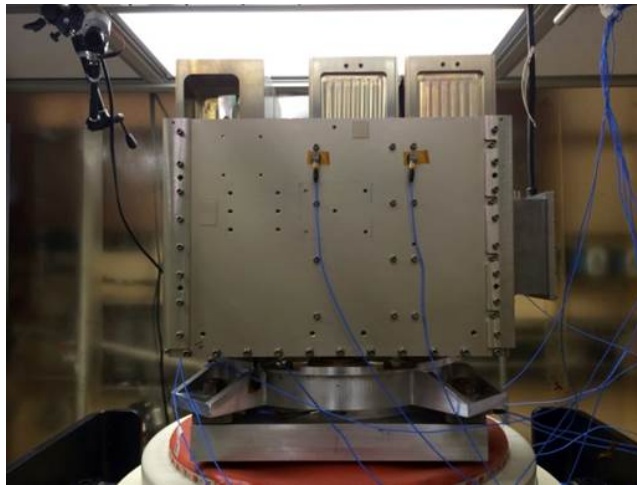


Figure 3.11: Typical Qualification Test Set-Up

The test configurations are summarized in Table 3.1. The conical isolators and modified adapter ring were installed on both the baseline and isogrid NPSCuL structures (Configurations 2 and 5) for the initial round of feasibility testing. This testing was repeated with the cupmount isolators installed on the baseline structure (Configuration 3), and the qual test was only performed on this configuration because the cupmount isolator is more suitable for NPSCuL on the ABC plate and had the most favorable results observed during feasibility testing. The cupmount isolators were not tested with the isogrid structure due to behavior observed during the feasibility testing performed with the conical isolators. The unmodified baseline and isogrid NPSCuL designs (Configuration 1 and 4) were subjected to the same inputs as the other configurations to serve as the comparison point for the isolated designs. The baseline NPSCuL was successfully qualification-tested for previous missions in June 2011 and September 2012.

Table 3.1: Test Configurations

Configuration	NPSCuL Structure	Isolators	Feasibility Testing	Qual Test
1	Baseline	N/A	Y	Y
2	Baseline	Conical	Y	N
3	Baseline	Cupmount	Y	Y
4	Isogrid	N/A	Y	N
5	Isogrid	Conical	Y	N

3.2.3 Sine and Random Inputs

Each test configuration was subjected to sine sweeps before and after each random test; this cycle of tests was repeated for several random inputs in each axis. The general test flow is shown in Figure 3.12.

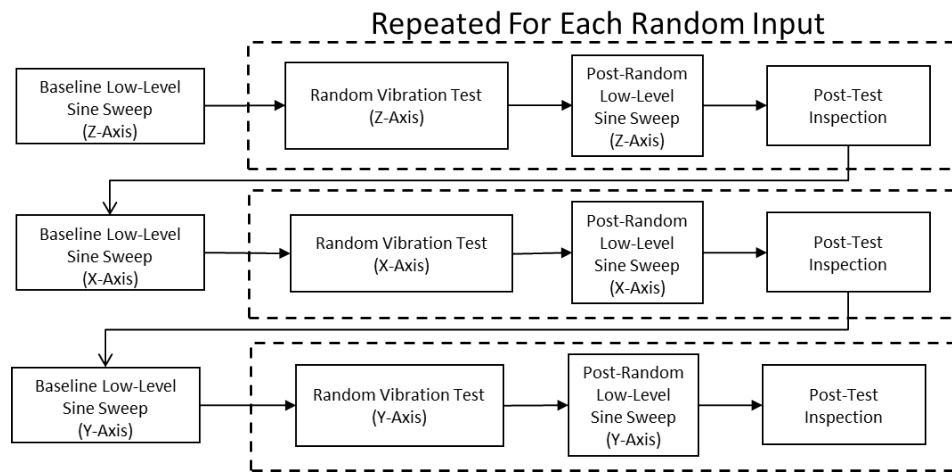


Figure 3.12: General Test Flow for Each Test Configuration

The sine sweeps were performed at 0.25 or 0.50 G from 20–2000 Hz. In some cases, the starting frequency was adjusted down to 5 or 10 Hz to capture lower modes. The pre- and post-random sine sweep data were compared at each accelerometer location and the force measurement to check for frequency and amplitude shifts of the fundamental modes, which are typical indicators of a major change to the system. The sine sweep data was also used to experimentally determine the frequency and damping of each fundamental mode, and to calculate the apparent mass as a function of frequency. The apparent mass is used as

an indication of the transmissibility of the system; in the rigid-body region, it is used as a sanity check to ensure that the force transducers have not lost any pre-load [33]. The apparent mass is calculated by dividing the measured force by the acceleration control at each frequency:

$$m(\omega) = \frac{F(\omega)}{a(\omega)} \quad (3.1)$$

The damping was determined using the half-power bandwidth method [34]:

$$\zeta = \frac{\Delta f}{2f_n} \quad (3.2)$$

where ζ is the damping ratio, f_n is the natural frequency of interest, and Δf is the frequency bandwidth between the -3 dB points, or half-power points, on the FRF.

The ABC and Operationally Responsive Space (ORS) random inputs, shown in Figure 3.13, were used in the feasibility testing to investigate the effects of FLVT on the isolated and un-isolated spacecraft; the test configurations were subjected to these random inputs with and without force limiting. The results from the random vibration tests for the ABC profile with force limiting were used for the isolator performance assessment because it was a driving requirement for the re-design of NPSCuL. The responses from the random vibration tests for the ABC profile without force limiting were used to assess the isolators' effect on NPSCuL without the expected benefit of FLVT. The ORS random vibration profile was used to investigate the effects of the isolators and FLVT for a random vibration input that has vast differences in frequency content compared to the ABC profile. However, it is defined at the LV to P-POD interface and is not realistic for a spacecraft such as NPSCuL; the profile was only used due to its high-frequency content. Additionally, the target level was adjusted to MPE -6 dB for the ORS profile to avoid over-driving the shaker above 400 Hz, where there is a significant amount of energy required to achieve the levels for a 90.7 kg (200 lbm) spacecraft instead of the intended 9.07 kg (20 lbm) spacecraft. The ABC profile was representative of other vibration profiles for similar spacecraft, so no other profiles were used; this comparison is shown in Figure 3.14. The summary of inputs,

in order of when each configuration was tested, is shown in Table 3.2 and Table 3.3. The sine and random vibration tests were performed for each configuration using the test flow shown in Figure 3.12. The random input levels used are listed in relative magnitude to the maximum predicted environment (MPE) of each vibration profile.

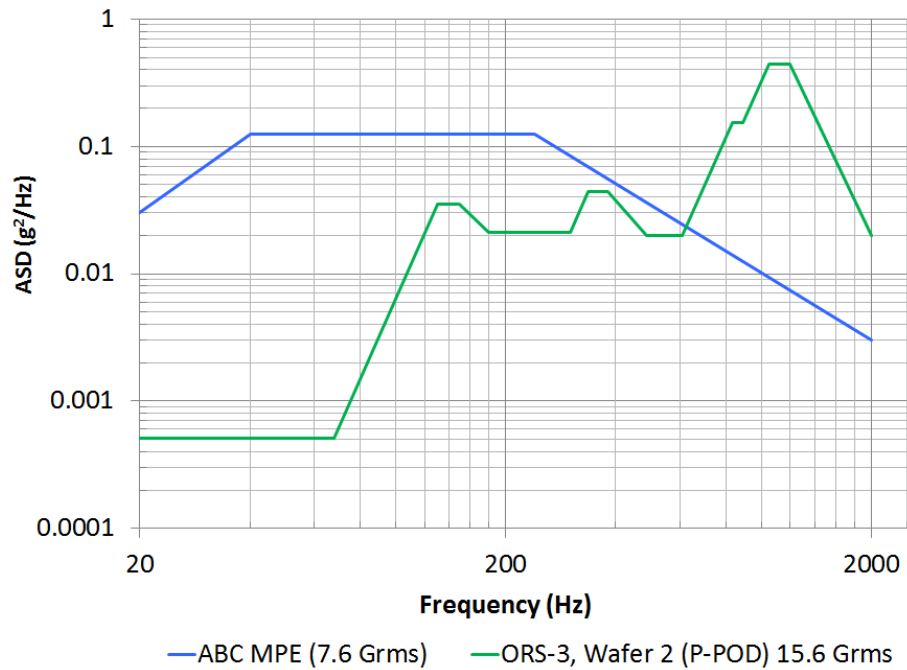


Figure 3.13: ABC and ORS Vibration Profiles.
Adapted from Aft Bulkhead Carrier Auxiliary Payload User's Guide, United Launch Alliance Std., May 2014 and "Operationally Responsive Space CubeSat-to-P-POD Interface Control Document," Apr. 2013.

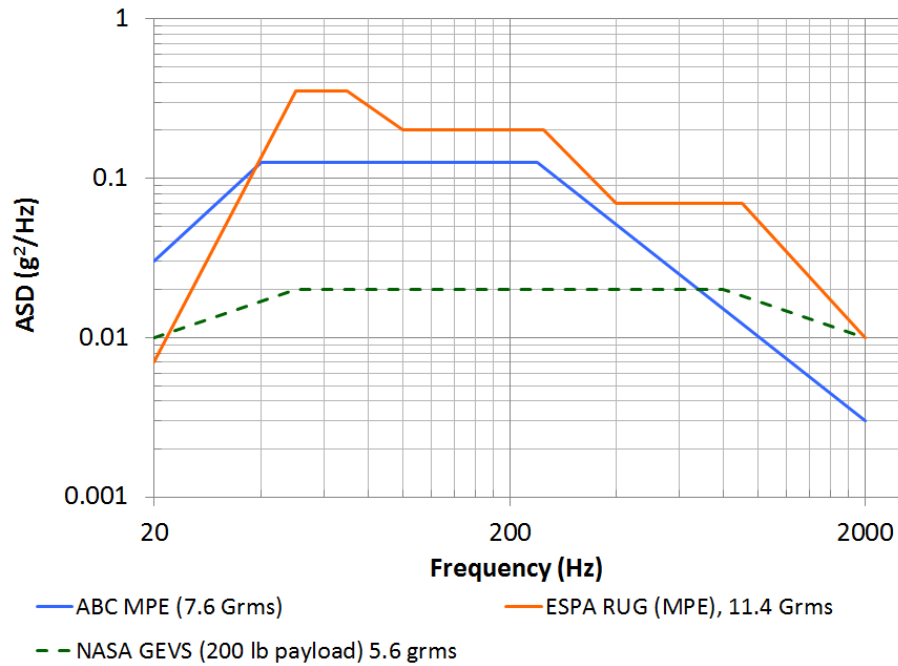


Figure 3.14: ABC, ESPA RUG, and GEVS Vibration Profiles.
Adapted from Aft Bulkhead Carrier Auxiliary Payload User's Guide, United Launch Alliance Std., May 2014; Evolved Expendable Launch Vehicle Secondary Payload Adapter Rideshare Users Guide (ESPA RUG), DoD Space Test Program Std., May 2010; and General Environments Verification Standard (GEVS), NASA Goddard Space Flight Center Std., Apr. 2013.

Table 3.2: Sine Test Inputs for All Test Configurations

Configuration	NPSCuL Structure	Isolators	Sine Sweep Frequency Range
1	Baseline	N/A	0.5 G, 20–2000 Hz
4	Isogrid		
2	Baseline	Conical	
5	Isogrid		
3	Baseline	Cupmount	0.25 G, 10-2000 Hz (Z) 5-2000 Hz (X, Y)

Table 3.3: Random Test Inputs for All Test Configurations

Configuration	NPSCuL Structure	Isolators	ABC Levels		ORS Levels	
			Unnotched	FLVT	Unnotched	FLVT
1	Baseline	N/A	MPE +0 dB, 20 sec	MPE +0 dB, 20 sec	MPE -6 dB, 20 sec	N/A
4	Isogrid					
2	Baseline	Conical				
5	Isogrid					
3	Baseline	Cupmount		MPE +6 dB, 3 min		MPE -6 dB, 20 sec

THIS PAGE INTENTIONALLY LEFT BLANK

CHAPTER 4:

Experimental Results

The results from the baseline and isogrid NPSCuL test configurations (Configurations 1 and 4) were used as comparison point for evaluating the effectiveness of the isolators and force limiting. These two configurations had been previously subjected to the ABC input with force limiting [19], but the additional testing performed using the remaining three random vibration profiles allow for consistent comparisons between the isolated and unisolated configurations. Although the cupmount isolator configuration was subjected to the higher, qualification-level random vibration test, the responses measured during MPE +0 dB for all configurations were used for comparison and performance evaluation purposes.

The evaluation metrics were the apparent mass measured at the base of NPSCuL, the enveloped acceleration response at the P-POD interface, and the corresponding G_{RMS} . The apparent mass was used to determine the measured dynamic properties as well as an indication of the response at the P-POD interface. The FRF is inversely proportional to the impedance (Eqn. 2.6), so a lower apparent mass indicates that the impedance is high, thus resulting in a lower response at the P-POD interface. The enveloped acceleration data are the max ASD values of every instrumented P-POD location in the specified axis; it includes the cross-axis response as well. For example, the X-axis envelope would be the maximum ASD values measured in the X-axis, at the interface of all eight P-PODs, during the X, Y, and Z-axis tests. Enveloping the response by axis is the most straight-forward method of assessing the isolators' performance and is independent of the individual P-PODs' orientations on NPSCuL. The data for the individual P-POD responses (in G_{RMS}) can be found in Appendix C.

4.1 Conical Isolator Results

4.1.1 Conical Isolators on Baseline NPSCuL

The apparent mass plots of the baseline NPSCuL with and without conical isolators (Configurations 1 and 2) are shown in Figure 4.1, and the fundamental frequencies measured

from these sine sweeps are shown in Table 4.1. With the isolators (Configuration 2), there are two distinct modes in each lateral axis (X and Y) that are much lower in amplitude compared to the fundamental mode in the baseline NPSCuL. These modes correspond to the rocking and shear modes in the lateral directions. This is typical behavior for base-mounted isolators on a box-like structure; many isolated avionics boxes on launch vehicles exhibit similar dynamic behavior [35]. In the axial direction (Z), there are decreases in both the frequency and the amplitude of the fundamental mode. The decrease in frequency, which was expected, is due to the stiffness properties of the isolators. The reduction in amplitude of all of the fundamental modes can be attributed to the increased damping provided by the isolators. As expected, the isolation region in each axis starts at approximately $\sqrt{2}\omega_n$, where ω_n is the second fundamental frequency in the X and Y axes and the first fundamental frequency in the Z axis. In general, the apparent mass above 500 Hz is very low, indicating that the response at the P-POD interface will be lower as well. The peak at 1560 Hz in the Z-axis corresponds to an FLVT plate mode that is excited in the axial direction.

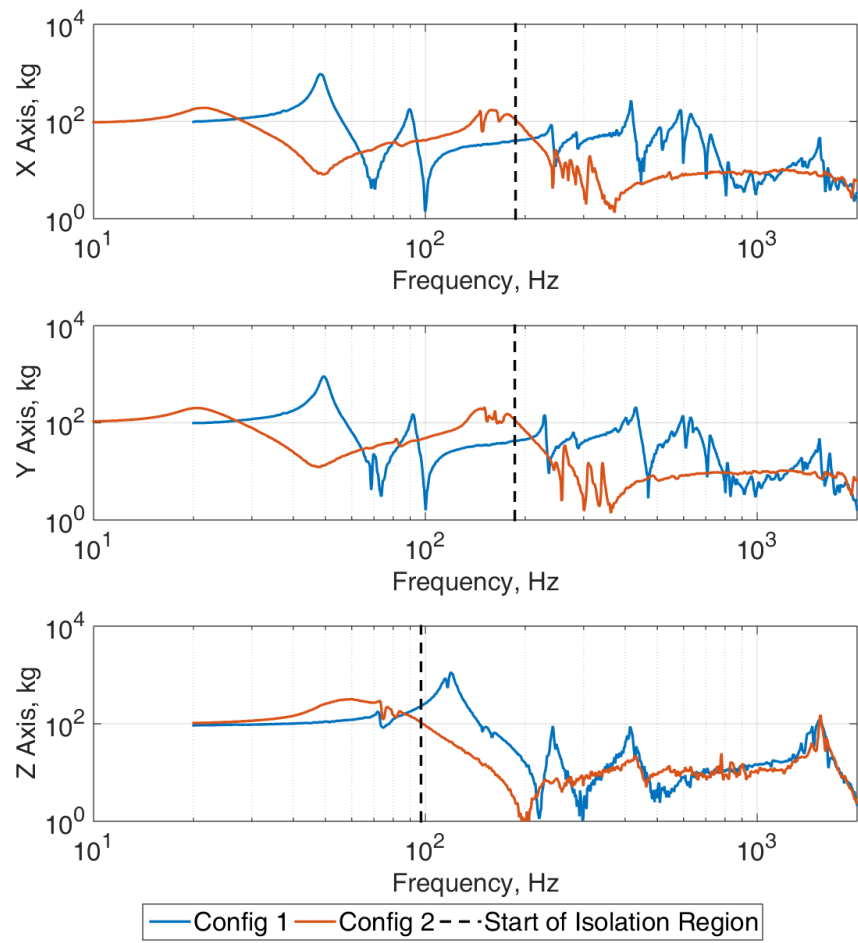


Figure 4.1: Apparent Mass, Conical Isolators on Baseline NPSCuL

Table 4.1: Measured Frequencies from Apparent Mass, Conical Isolators on NPSCuL

Mode	Measured Frequencies (Hz)	
	Configuration 1	Configuration 2
1 (Rocking, Y)	49.7	19.8
2 (Rocking, X)	48.5	20.4
3 (Axial, Z)	117.0	56.3

The enveloped acceleration responses at the P-POD interface in each test axis for both configurations are shown in Figure 4.2; these responses were measured during the random vibration test for the ABC profile with force limiting. The amplitudes of the responses up to 200 Hz are comparable in all axes, and the peaks are shifted due to the differences in fundamental frequencies. However, the shift in frequency above 200 Hz is negligible, and the response consistently drops by two orders of magnitude in all axes. This indicates that COTS isolators are effective in reducing the P-POD response response above 500 Hz, which provides the most benefit to the CubeSats.

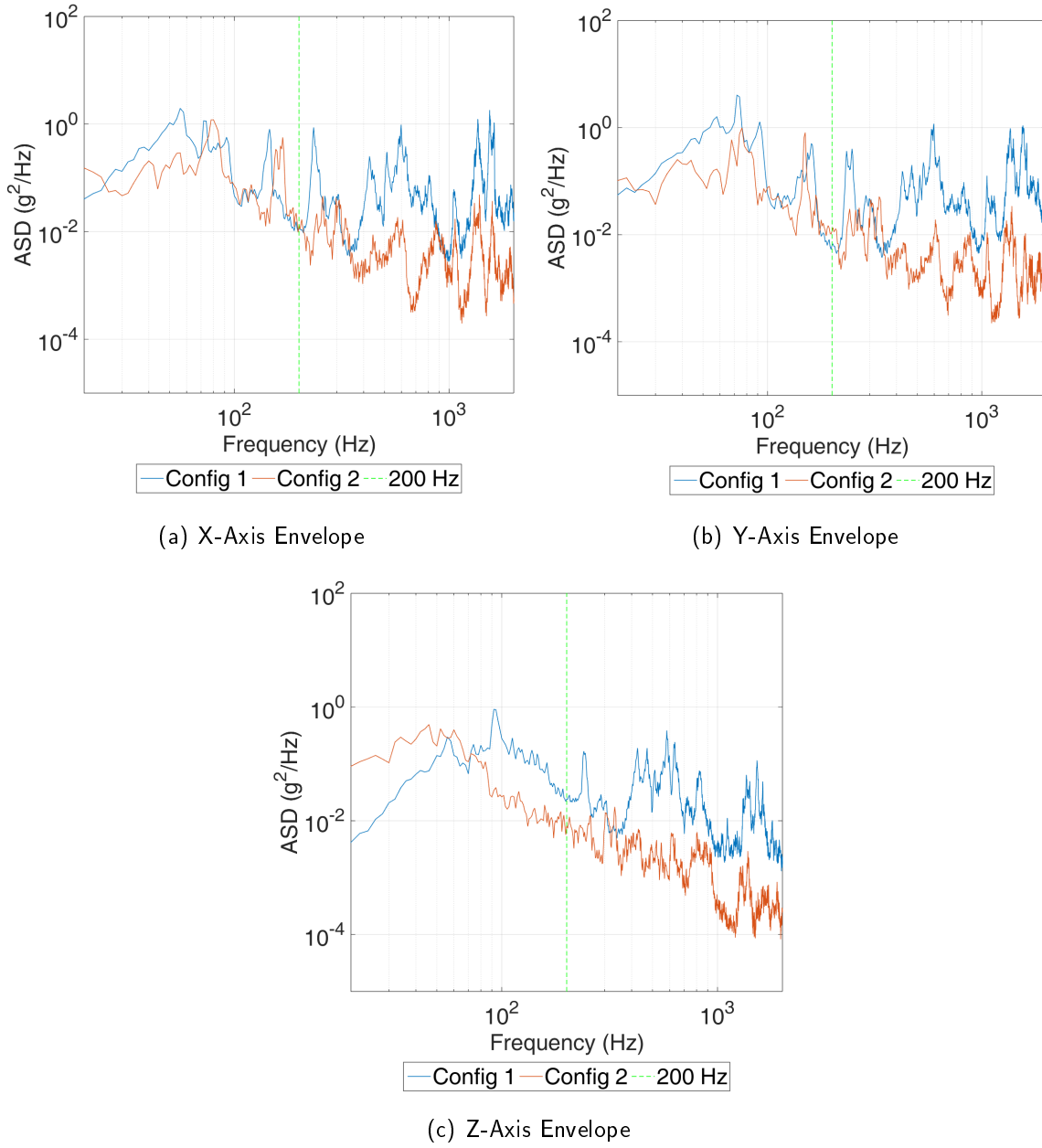


Figure 4.2: Acceleration Responses at P-POD Interface Due to ABC Input with FLVT, Baseline NPSCuL with Conical Isolators

The G_{RMS} from 20 to 2000 Hz and from 500 to 2000 Hz for both configurations, shown in Table 4.2 and Table 4.3, confirm that the high-frequency content (above 500 Hz) is

reduced by up to 98% when isolators are used. These values correspond to the data shown in Figure 4.2. As shown in Figure 4.3, the high-frequency content accounts for up to 50% of the G_{RMS} on the baseline NPSCuL; however, the high-frequency content is no more than 10% of the total G_{RMS} when conical isolators are incorporated.

Table 4.2: G_{RMS} Reduction at P-POD Interface, 20–2000 Hz — Conical Isolators

Test Axis	G_{RMS}		Percent Difference, %
	Configuration 1	Configuration 2	
X	15.9	6.15	61.2
Y	16.7	5.47	67.3
Z	8.41	4.36	48.1

Table 4.3: G_{RMS} Reduction at P-POD Interface, 500–2000 Hz — Conical Isolators

Test Axis	G_{RMS}		Percent Difference, %
	Configuration 1	Configuration 2	
X	7.73	0.601	92.2
Y	7.46	0.487	93.5
Z	2.33	0.169	92.7

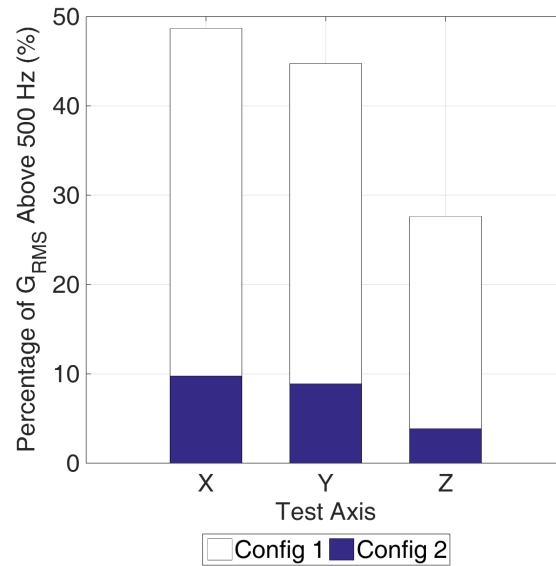


Figure 4.3: Reduction in High Frequency Content at P-POD Interface, Conical Isolators

4.1.1.1 Effect of Fully Constrained Conical Isolators on NPSCuL

Initially, the conical isolators were mistakenly installed as shown in Figure 4.4; these results were presented in [1]. In this configuration, the elastomer was fully constrained (in compression, tension, and shear) because the fastener that joins the supporting unit (base-plate) to the isolator was also threaded into the supporting member (adapter ring). This prevented the elastomer from deflecting as intended by the manufacturer, resulting in little reduction in joint stiffness at each isolator location.

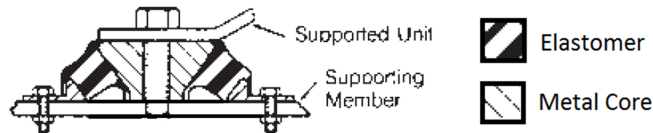


Figure 4.4: Apparent Mass, Conical Isolators on Baseline NPSCuL

Figure 4.5 shows the apparent mass plots of this configuration with fully-constrained conical isolators in comparison with those of the baseline NPSCuL. Although the first funda-

mental frequency in the X and Y axes dropped by approximately 15 Hz, there is no significant reduction in overall amplitude. The reduction in overall joint stiffness at the ring-to-baseplate interface, not the properties of the isolators, are attributed to these changes. Because only eight of the original 24 fasteners of the LV interface are used, and the contact surface area between the baseplate and the adapter ring is significantly less, the overall joint stiffness at this interface is lower than that of the baseline NPSCuL. In the Z-axis, both the apparent mass amplitude and the fundamental frequency are lower, which indicates that the reduction in overall joint stiffness may also be a result of the isolator properties in this direction. The apparent mass plots indicate that the conical isolators are not effective in the lateral directions when fully constrained. However, this constraint method is a possible alternative in the event that an all-attitude isolator cannot be used in a static tension application and the significant reduction in isolation performance is acceptable.

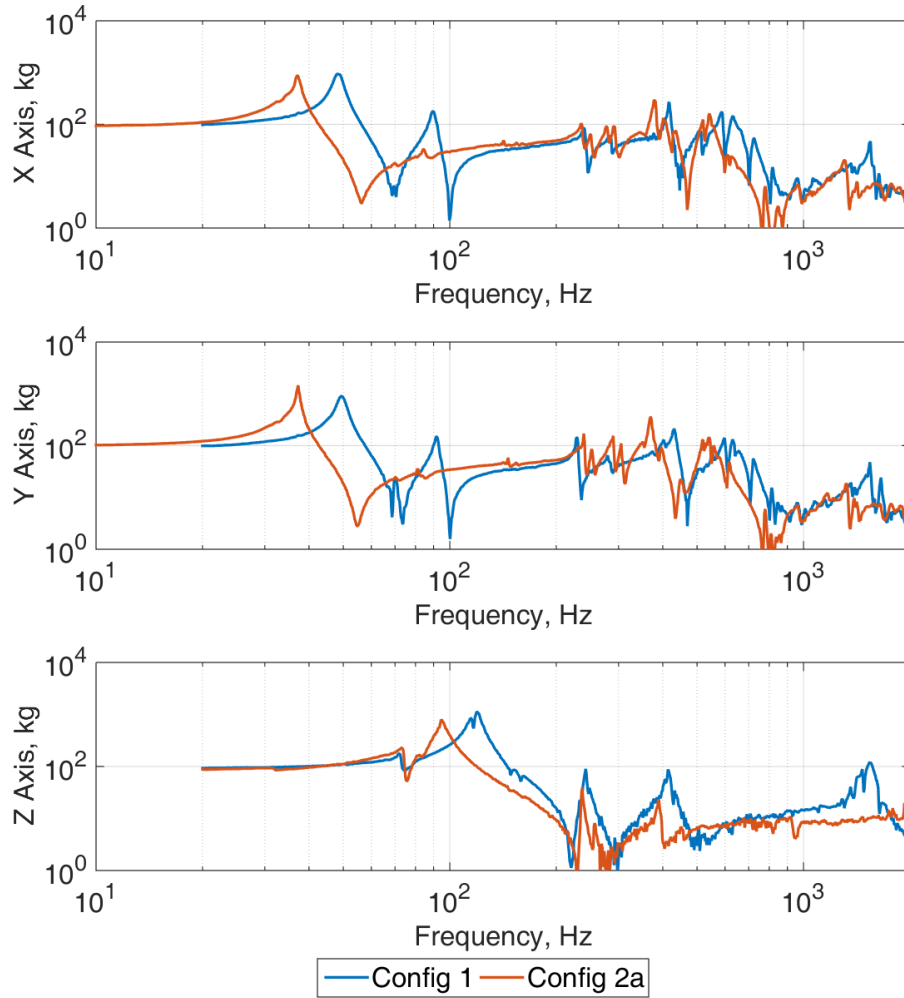


Figure 4.5: Apparent Mass, Fully Constrained Conical Isolators on Baseline NPSCuL

4.1.2 Conical Isolators on Isogrid NPSCuL

The apparent mass plots shown in Figure 4.6 exhibit very similar responses between the baseline and isogrid NPSCuL when isolators are incorporated. The mass and CG of NPSCuL are designed to be the same with both designs, so it is likely that there are similar responses because the unibase on the isogrid NPSCuL was replaced with a separate ring and baseplate that is in the same configuration as the baseline NPSCuL.

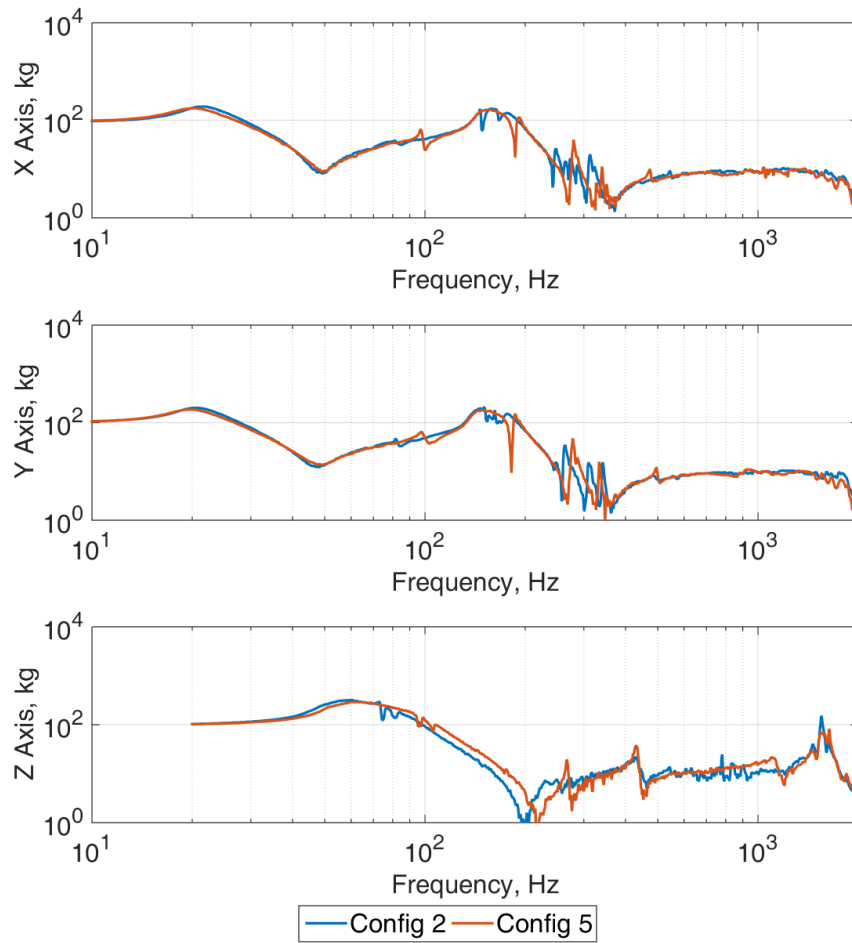


Figure 4.6: Apparent Mass, Conical Isolators on Baseline and Isogrid NPSCuL

Due to the comparable performance between the two configurations and the additional work that would be required to use the isogrid structure for a future flight (i.e. accommodating the structure for ground support equipment (GSE), additional load and environmental testing), no further testing was performed on the isogrid NPSCuL, and it was not considered for future missions.

4.2 Cupmount Isolator Results

The apparent mass comparison plots for the baseline NPSCuL with and without the cupmount isolators (Configurations 1 and 3) are shown in Figure 4.7, and the corresponding fundamental frequencies measured from the sine sweeps are shown in Table 4.4, along with the frequencies measured for the baseline NPSCuL with conical isolators. Similar to the results with the conical isolators, there are two distinct modes in each lateral axis (X and Y) that are much lower in amplitude compared to the fundamental mode in the baseline NPSCuL, and the apparent mass in the isolation region (above $\sqrt{2}\omega_n$) is greatly reduced in all axes.

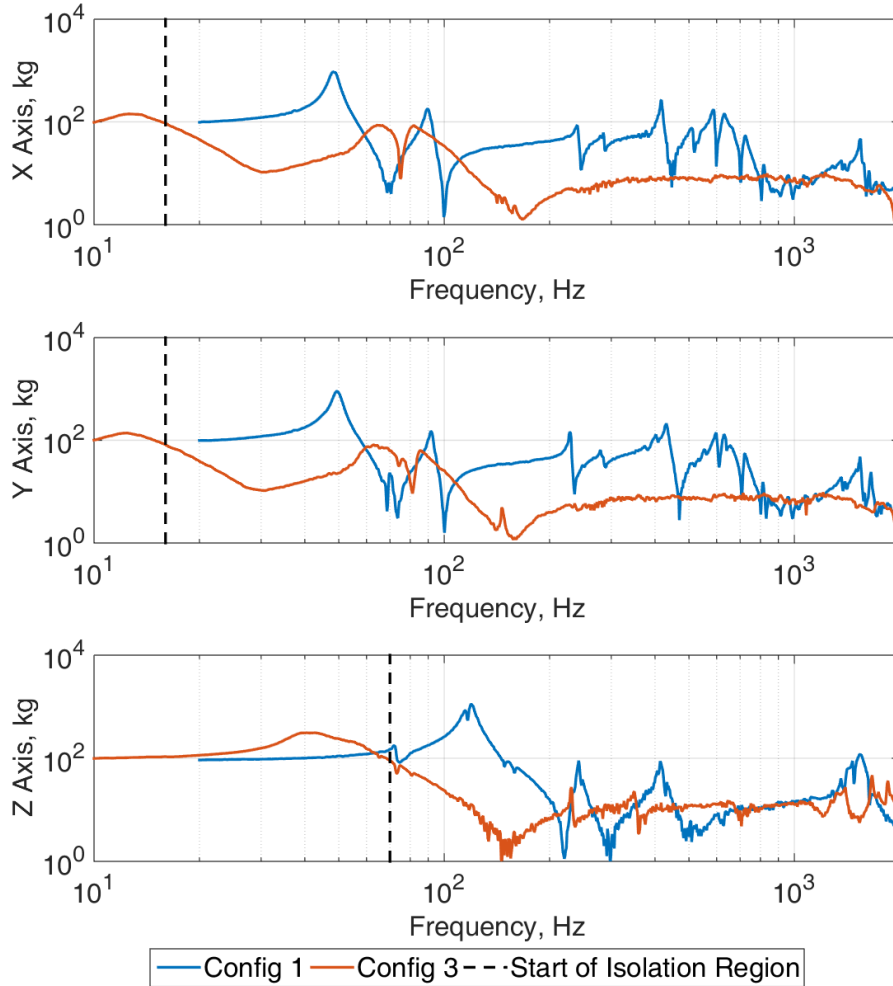


Figure 4.7: Apparent Mass, Cupmount Isolators on Baseline NPSCuL

The fundamental frequencies in the lateral directions are also below 20 Hz, where the ABC random input starts. The ASD values are not defined below 20 Hz, so the roll-off frequency for the testing performed on Configuration 3 with force-limiting is 20 Hz instead of the fundamental frequencies shown in Table 4.4.

Table 4.4: Measured Frequencies from Apparent Mass, Cupmount Isolators on NPSCuL

Mode	Measured Frequencies (Hz)		
	Configuration 1	Configuration 2	Configuration 3
1 (Rocking, Y)	49.7	19.8	12.4
2 (Rocking, X)	48.5	20.4	12.5
3 (Axial, Z)	117.0	56.3	39.5

Compared to the results of the conical isolators, the cupmount isolators are more effective due to the lower fundamental frequencies, as shown in Figure 4.8. Although the performance is similar above 500 Hz in the X- and Y-axes and 300 Hz in the Z-axis, the isolation region of the cupmount isolators starts at a lower frequency in the lateral directions, thus indicating a reduction in response over a broader frequency range.

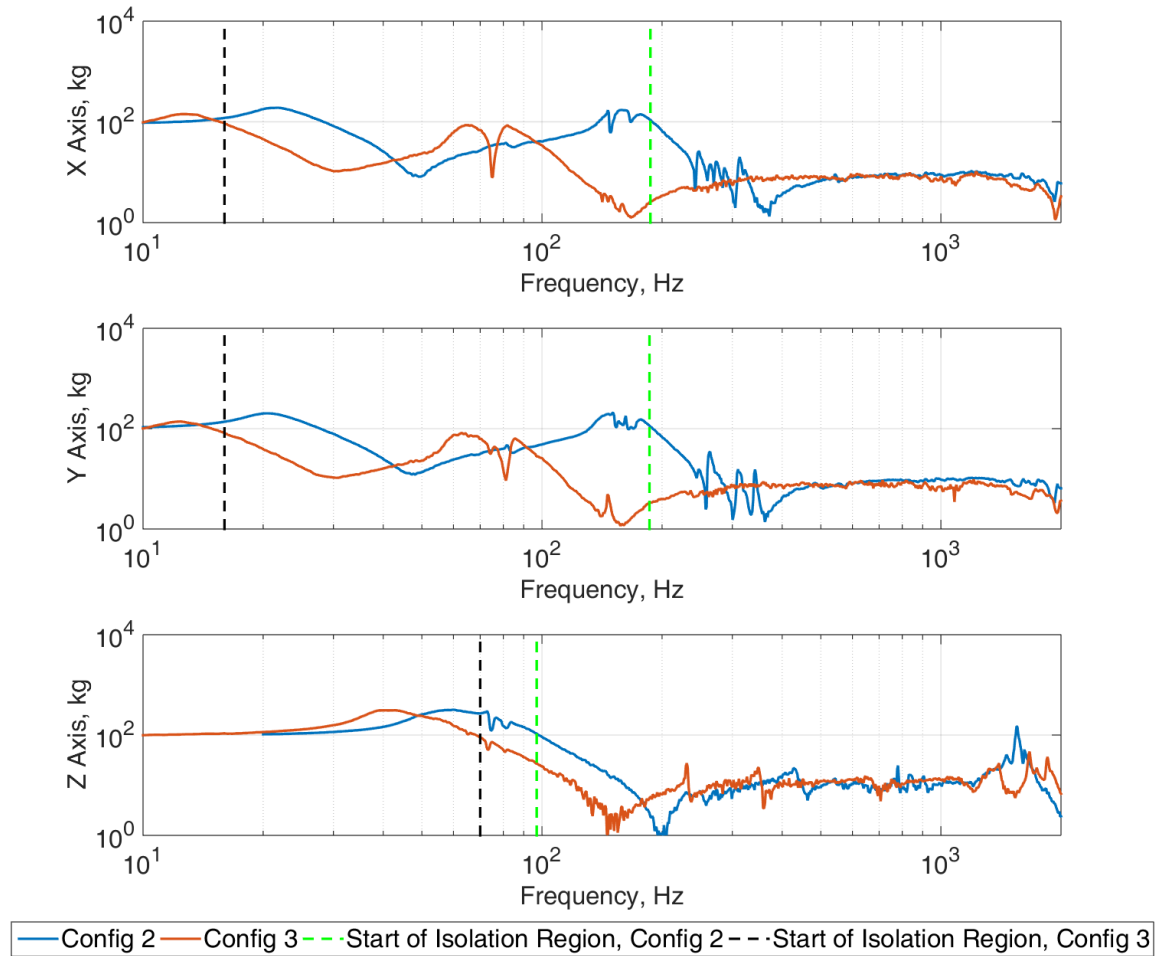
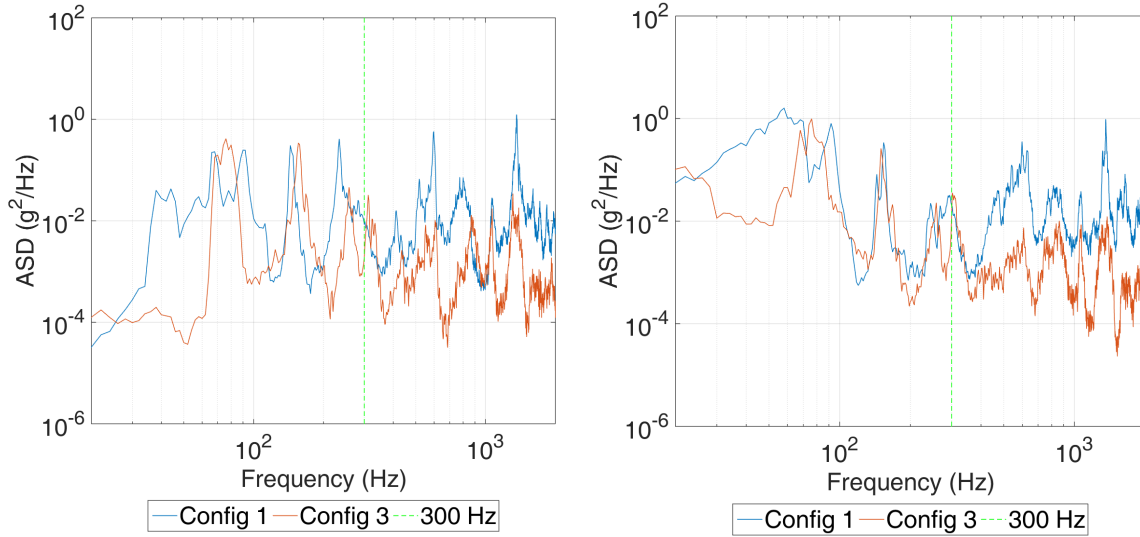


Figure 4.8: Apparent Mass, Conical and Cupmount Isolators on Baseline NPSCuL

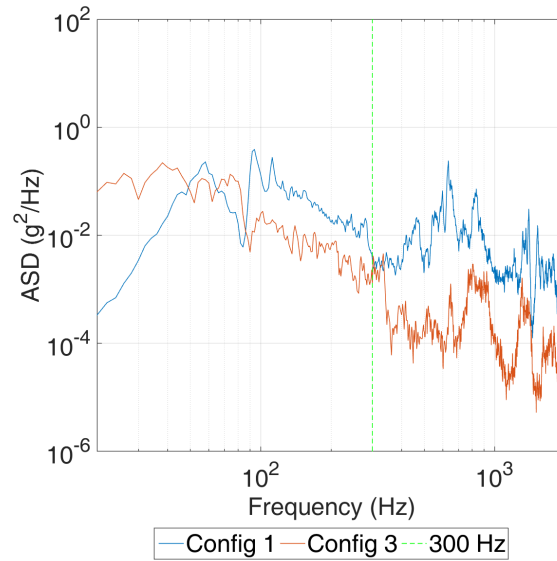
The enveloped acceleration responses at the P-POD interface in each test axis for the baseline NPSCuL with and without cupmount isolators are shown in Figure 4.9; these responses were measured during the random vibration test for the ABC profile with force limiting. The responses at the peak frequencies up to 300 Hz are comparable to the baseline NPSCuL in all axes, and the response consistently drops by two orders of magnitude (20 dB) in all axes above 300 Hz in the X- and Y-axes and 70 Hz in the Z-axis. It is noted that the responses are lower below 300 Hz as well, except at the peaks. This is most likely due to the significant apparent mass of the second mode, so there is some reduction in amplitude in

the lower frequencies, but full isolation does not occur until after this second mode. Similar to the conical isolators, the cupmount isolators also effectively reduce the response above 500 Hz.



(a) X-Axis Envelope

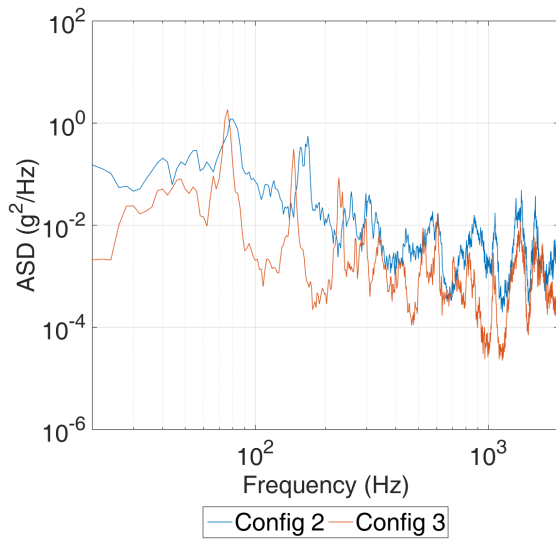
(b) Y-Axis Envelope



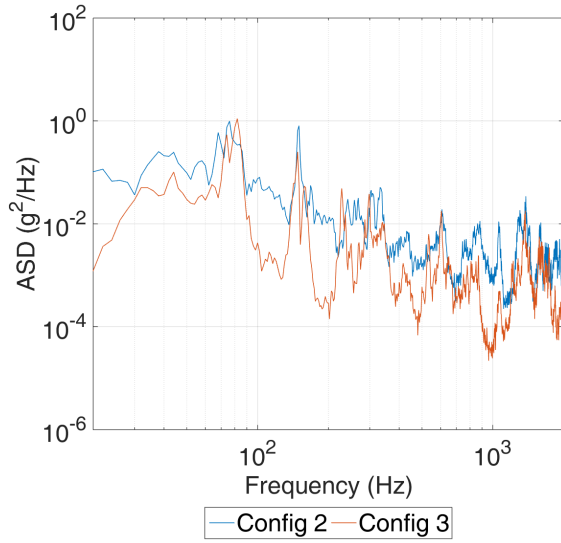
(c) Z-Axis Envelope

Figure 4.9: Acceleration Responses at P-POD Interface Due to ABC Input with FLVT, Baseline NPSCuL with Cupmount Isolators

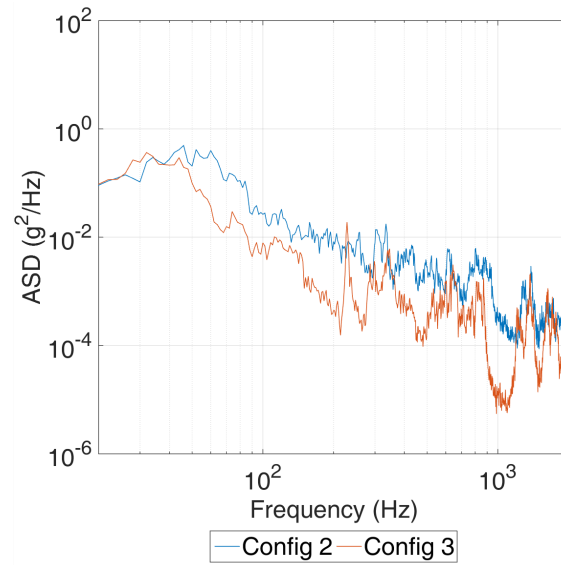
The P-POD interface responses with the cupmount isolators (Configuration 3) were also compared to those with the conical isolators (Configuration 2); these plots are shown in Figure 4.10. Although the apparent mass above 300 Hz is the same with both isolators, the cupmount isolators reduce the response at the P-POD interface even further over the entire frequency range from 20 to 2000 Hz. The resulting G_{RMS} is also lower by an additional 32% overall and 57% above 500 Hz, as shown in Table 4.5 and Table 4.6. Figure 4.11 highlights the reduction in high-frequency content. These results confirm that when the isolation region starts at a lower frequency, the isolator is more effective. This ultimately results in a better vibration environment at the P-POD interface.



(a) X-Axis Envelope



(b) Y-Axis Envelope



(c) Z-Axis Envelope

Figure 4.10: Acceleration Responses at P-POD Interface Due to ABC Input with FLVT, Baseline NPSCuL with Conical and Cupmount Isolators

Table 4.5: G_{RMS} Reduction at P-POD Interface, 20–2000 Hz — Cupmount Isolators

Test Axis	G_{RMS}			Percent Difference, %	
	Configuration 1	Configuration 2	Configuration 3	Config. 1 vs 3	Config. 2 vs 3
X	15.9	6.15	3.76	76.3	38.8
Y	16.7	5.47	3.72	77.7	32.0
Z	8.41	4.36	2.96	64.9	32.3

Table 4.6: G_{RMS} Reduction at P-POD Interface, 500–2000 Hz - Cupmount Isolators

Test Axis	G_{RMS}			Percent Difference, %	
	Configuration 1	Configuration 2	Configuration 3	Config. 1 vs 3	Config. 2 vs 3
X	7.73	0.601	0.257	96.7	57.3
Y	7.46	0.487	0.240	96.8	50.6
Z	2.33	0.169	0.077	96.7	54.7

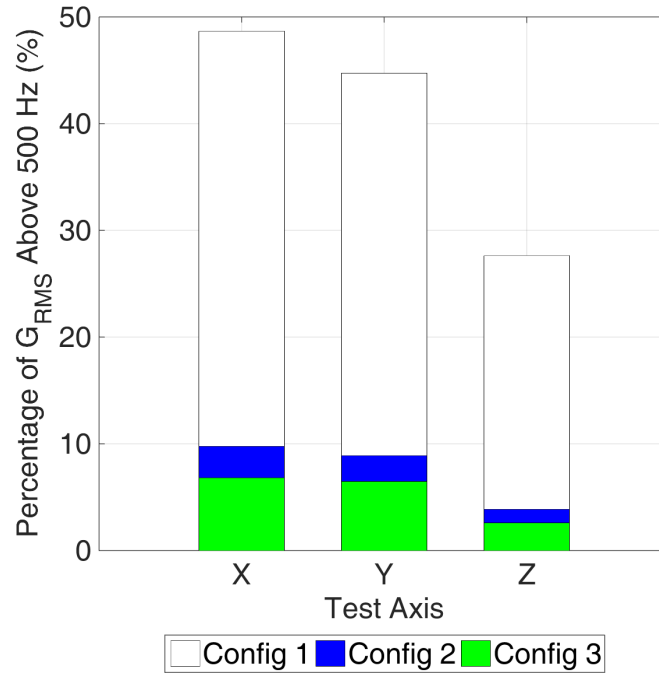


Figure 4.11: Reduction in High Frequency Content at P-POD Interface, Cupmount Isolators

4.2.1 Isolator Characterization - Test Like You Fly

Due to the orientation of NPSCuL on the ABC plate, the driving static loading condition is in tension; this is not a typical loading condition for spacecraft. The practice of testing in a flight-like condition, or "test like you fly," is a primary concern in the aerospace industry because it is often difficult to replicate flight conditions on the ground for various environments. The vibration tests performed on the ground are usually done in a compressive static loading condition, but it was not practical to replicate the tension loading condition for NPSCuL. Although the cupmount isolators are all-attitude, a separate characterization test was performed to verify that the isolator performance was comparable in both compression and tension, thus alleviating the concern that the typical vibration test set-up may not be valid for NPSCuL on the ABC.

The test set-up for the tension and compression cases in the axial (Z) direction are shown in Figure 4.12 and Figure 4.13, in which a P2M2 is supported by four cupmount isolators.

The tension and compression configurations were tested in the axial (Z-axis) and worst-case lateral (Y-axis) directions. The isolators and mass model were mounted at the same height for both cases to maintain a consistent boundary condition at the isolator input location. The input accelerometer for the Z-axis test was located in the middle of the isolator mounting plate, and the input accelerometer for the lateral test was located on the shaker adapter plate for better control. The test set-ups for the lateral direction are shown in Figure 4.14 and Figure 4.15. In both set-ups, the accelerometers were located on both the isolator mounting plate and the mass model interface plate to measure the response across the isolators. Following the test flow in Figure 3.12, sine sweeps and a 3-minute random vibration test at MPE +0 dB of the ABC input levels were performed for all set-ups shown.

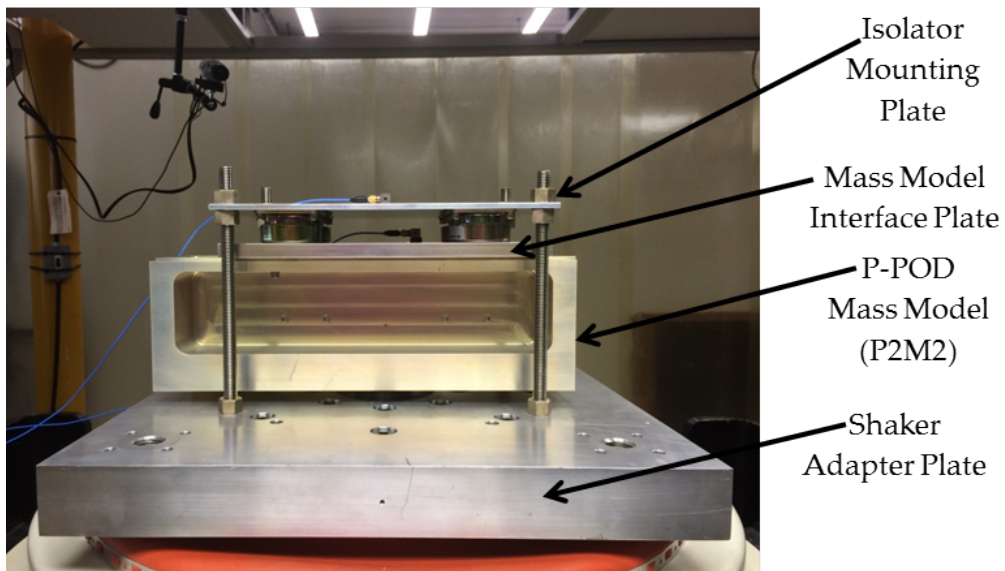


Figure 4.12: Z-Axis Test, Tension

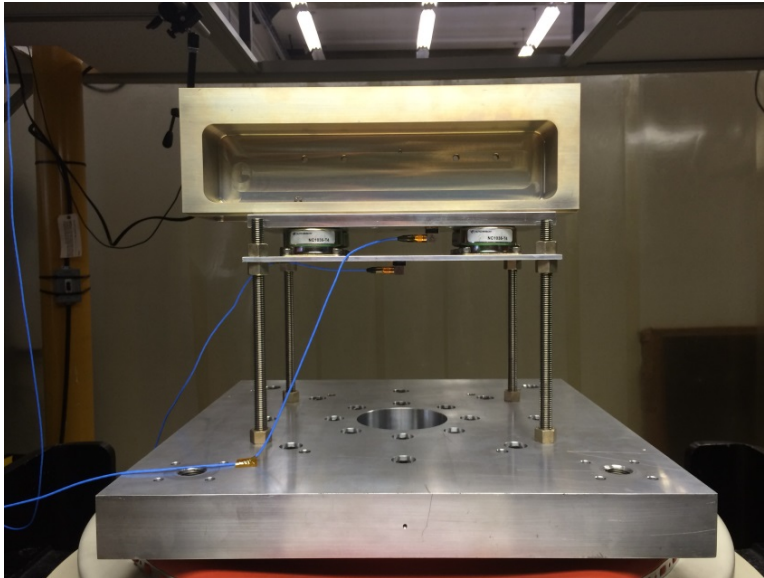


Figure 4.13: Z-Axis Test, Compression

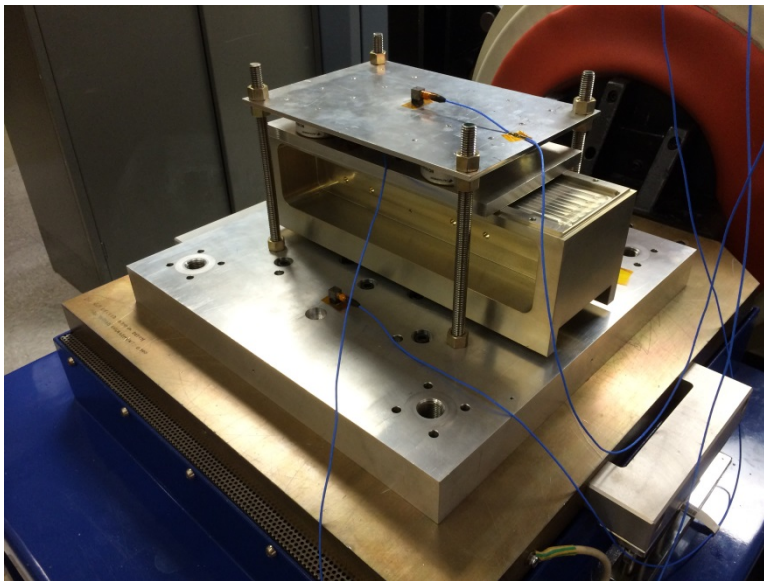


Figure 4.14: Lateral Test, Tension

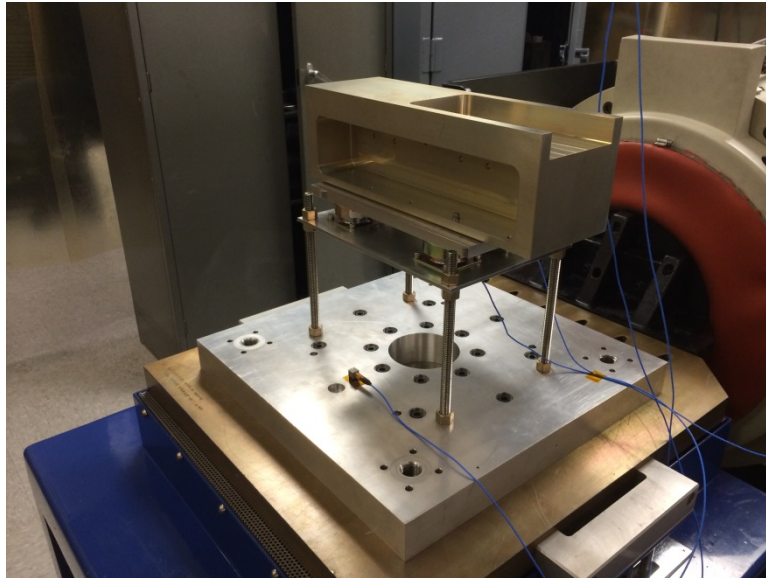


Figure 4.15: Lateral Test, Compression

As shown in Figure 4.16 and Figure 4.17, the acceleration responses measured on the mass model interface plate in both compression and tension tests are nearly identical for both axial and lateral test configurations. This indicates that the test configuration for NPSCuL represents a test-like-you-fly configuration with respect to dynamic loads, despite the difference in static the static loading conditions between the flight and test configurations.

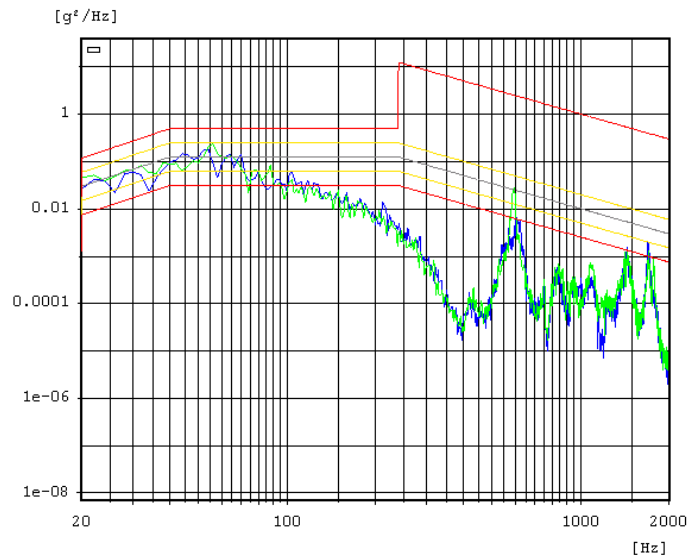


Figure 4.16: Lateral Random Vibe Test, Compression and Tension at MPE +0 dB

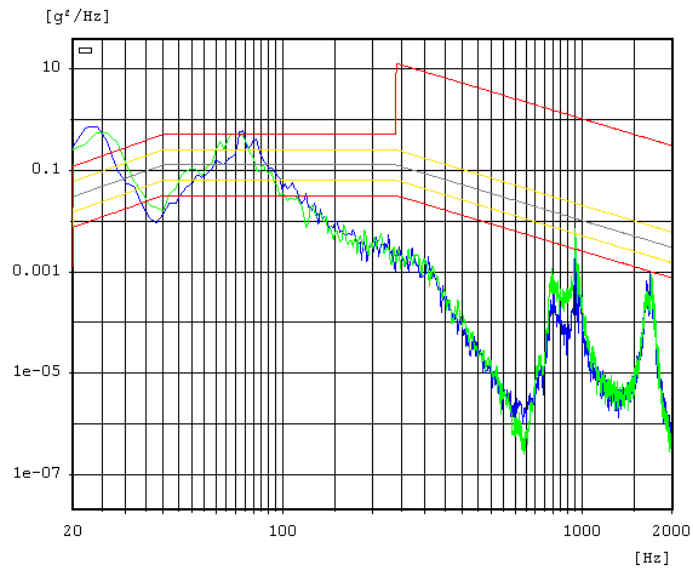


Figure 4.17: Lateral Random Vibe Test, Compression and Tension at MPE +0 dB

4.2.2 Break-In Testing

As recommended by the vendor, the cupmount isolators were subjected to a "break-in" test to relieve the molded-in stresses in the elastomer. Unlike the conical isolators, the elastomer is not bonded to the metal inner core or outer cup; therefore, there is some residual stress from molding the elastomer in the cupmount isolator. The break-in test can be performed by deflecting the isolator in the axial direction to at least three times the published deflection limits; this can be done by using a hand-operated arbor press instrumented with a load cell and deflection gage. Alternatively, the break-in test can also be performed by running an extra operational-level vibration test prior to testing [36]. The break-in test performed for the cupmount isolators on NPSCuL was a 20-second duration qualification-level (MPE +6 dB) random vibration test in the Z-axis. The pre- and post-random sine sweeps, plotted in Figure 4.18, show a shift in fundamental frequency of 20 Hz. The subsequent sine sweeps did not exhibit any additional shifts, thus indicating that the isolators were properly broken in.

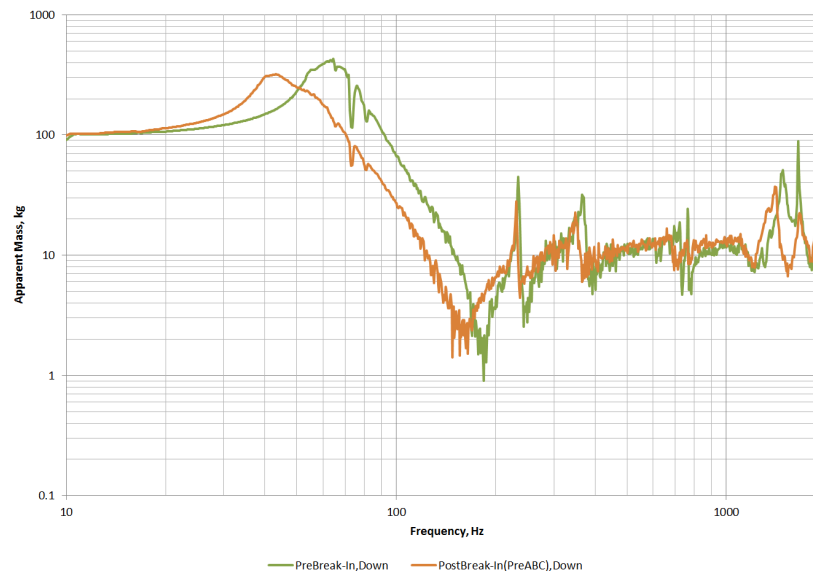


Figure 4.18: Pre- and Post-random Sine Sweep Comparison, Z-Axis Break-In Test

4.2.3 Qualification Testing

Based on the favorable results of this configuration during feasibility testing and the cup-mount isolator's all-attitude, fail-safe features, the baseline NPSCuL with cupmount isolators was subjected to a qualification-level test in which the random vibration test was performed to MPE +6 dB of the ABC profile for a duration of 3 minutes. Performing the qualification test provided confidence that incorporating these isolators on NPSCuL would be a viable option for future flights. The fasteners that go through the baseplate and into the threaded core of the isolators (see Figure 3.5) must be torqued appropriately for the expected dynamic loading condition. It was determined that a torque of 125 in-lbs was required, but this was not achievable without a means of restraining the threaded core; anything higher than approximately 60 in-lbs caused the threaded core to spin. The vendor-recommended torque value of 50 in-lbs was based on a lower grade bolt (Grade 2 instead of A286 stainless steel) and was designed to prevent the threaded core from spinning. Due to a lack of experience with these isolators, the vendor-recommended torque value was applied without any secondary back-out prevention in the initial qualification test, and six of the eight isolators were damaged due to insufficient torque and subsequent gapping; the damage is shown in Figure 4.19.

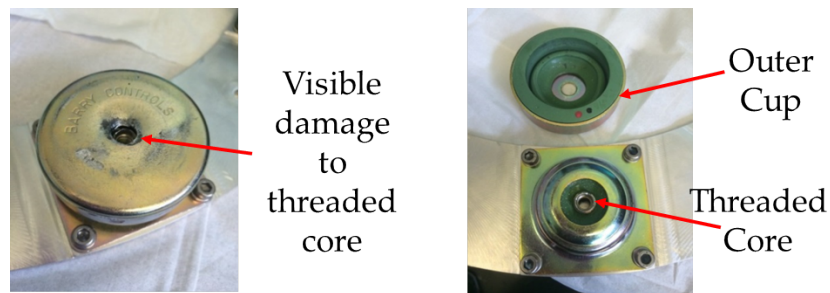


Figure 4.19: Damaged Isolators Due to Insufficient Torque

No foreign-object-debris (FOD) resulted from the damage. The post-test disassembly was performed after the structure had been qualification tested in all three axes; at this point, it was discovered that the fasteners had backed out of, but were not able to full disengage from, the core due to the low clearance between the P2M2s and the baseplate. Two of the isolators were still intact, and there was enough thread engagement to keep the structure together. Additionally, there was no clear indication in the test data that indicated a failure

had occurred. The initial drop in fundamental frequency was attributed only to the break-in process, not any loss in pre-load, and the subsequent shifts in fundamental frequency were within the typical 10% range. It is noted that time histories were not saved due to the limitations of the data acquisition system; all data captured was in the frequency domain. The availability of the time histories might have aided in determining when the damage occurred.

The qualification test was successfully repeated with a new set of isolators; the fasteners were torqued to 14.1 N-m (125 in-lbf) and thread-lock was applied to each of the eight fasteners for secondary backout prevention. To achieve the proper torque value, the threaded core was restrained with another fastener on the underside of the isolator; this allowed equal and opposite moments to be applied on both sides.

4.2.4 Temperature Effects

The isolator temperatures were measured to alleviate the concern that the frequencies would shift significantly due to a large change in temperature, induce coupling, and cause failures to the launch vehicle or primary payload. Thermocouples were attached to six of the eight isolators during the qualification test; the isolator designations are shown in Figure 4.20, and the thermocouple taped to Isolator 1 is shown in Figure 4.21.

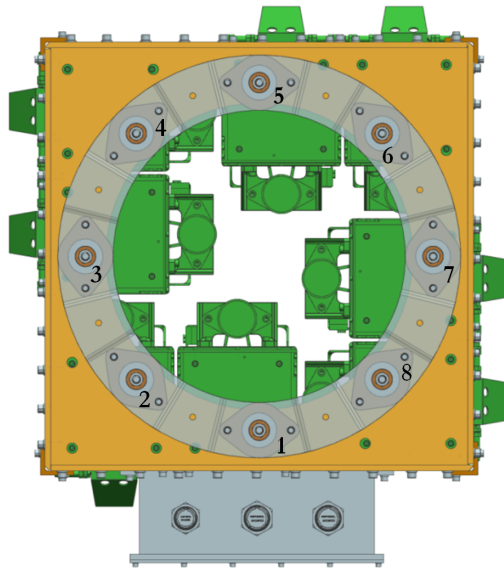


Figure 4.20: Isolator Designation

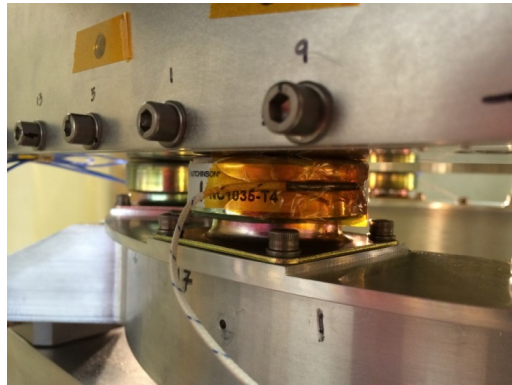


Figure 4.21: Thermocouple on Isolator 1

Temperatures were recorded for all three axes at five-second intervals, as shown in Figure 4.22 through Figure 4.24. It is noted that no temperature data was captured during the Y-axis sine-sweep. The maximum temperature difference observed was 12 °C (22 °F) during the Y-axis qual test, from the beginning of MPE -18 dB through the end of MPE +0 dB of target level. However, the maximum temperature difference observed through the 20-second-duration acceptance level (ABC MPE +0 dB) was only 0.56 °C (1 °F). The

temperature difference may have been larger for a full 60-second-duration acceptance test, but the data indicates that it likely would not be more than 2.2 °C (5 °F). Also, there was no appreciable difference in peak frequencies and amplitudes during the 3-minute qualification test despite the temperature increase. The measured fundamental frequencies in each axis are shown in Table 4.7; all shifts are within 10%.

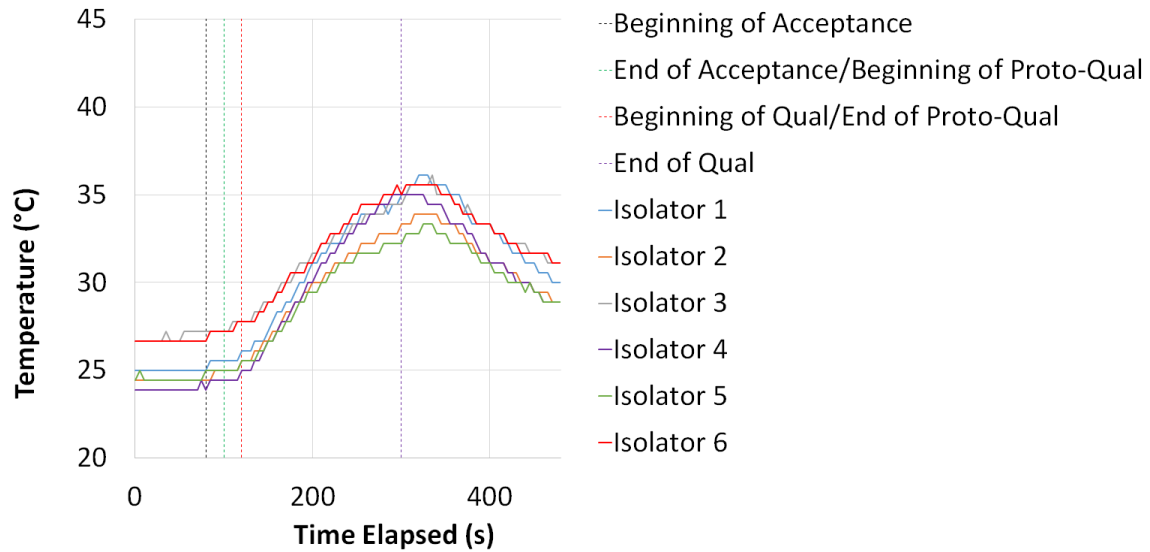


Figure 4.22: Isolator Temperatures — MPE +6 dB, Z

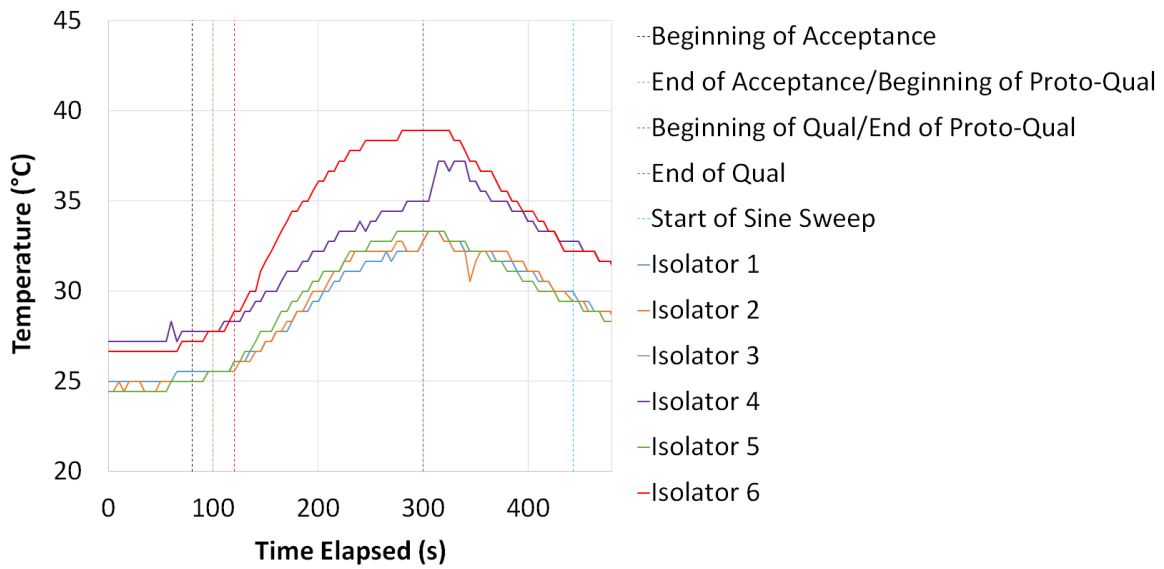


Figure 4.23: Isolator Temperatures — MPE +6 dB, X

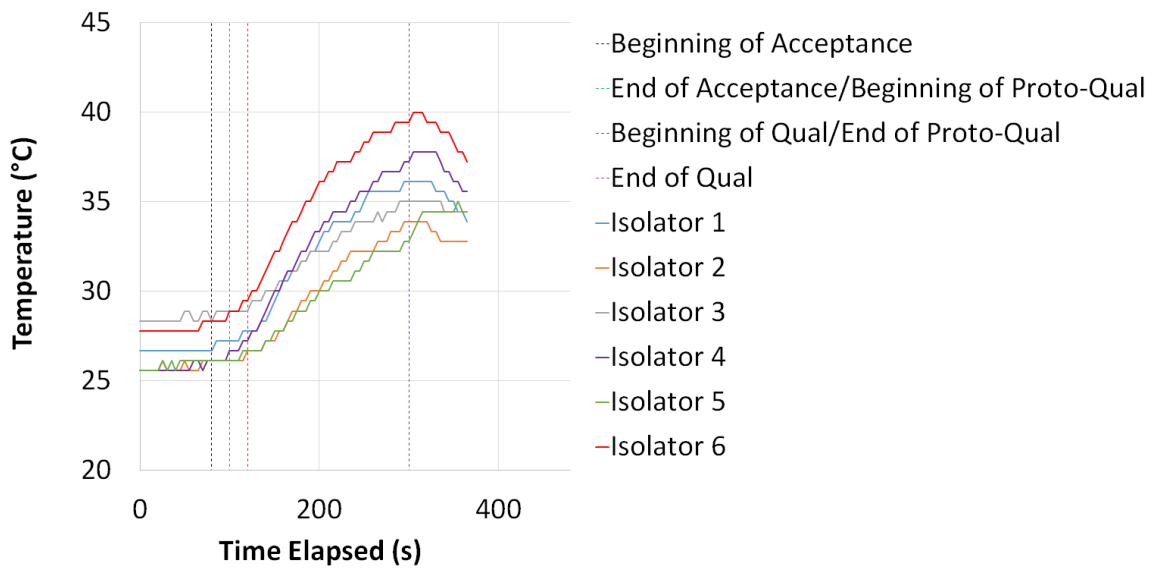


Figure 4.24: Isolator Temperatures — MPE +6 dB, Y

Table 4.7: Measured Fundamental Frequencies, Pre- and Post-random Sine Sweeps

Axis		Mode 1	Mode 2	Mode 3
X	Pre-Qual Frequency (Hz)	12.3	63.5	79.8
	Post-qual Frequency (Hz)	12.5	65.4	82.2
	Percent Difference (%)	1.63	2.99	3.01
Y	Pre-Qual Frequency (Hz)	11.4	60.3	84.6
	Post-qual Frequency (Hz)	12.4	62.8	85.6
	Percent Difference (%)	8.77	4.15	1.18
Z	Pre-Qual Frequency (Hz)	43.3	N/A	
	Post-qual Frequency (Hz)	43.3		
	Percent Difference (%)	0.00		

The effects of the ambient temperature are also a common concern for elastomeric isolators; depending on the material used, the dynamic stiffness can increase by up to nine times at cold temperatures. Cold temperatures can also cause the elastomer to be brittle and fail under load. However, the cupmount isolators selected for NPSCuL use silicone, which does not vary significantly with ambient temperature, especially for the typical ABC thermal environment. The stiffening ratio is shown in Figure 4.25.

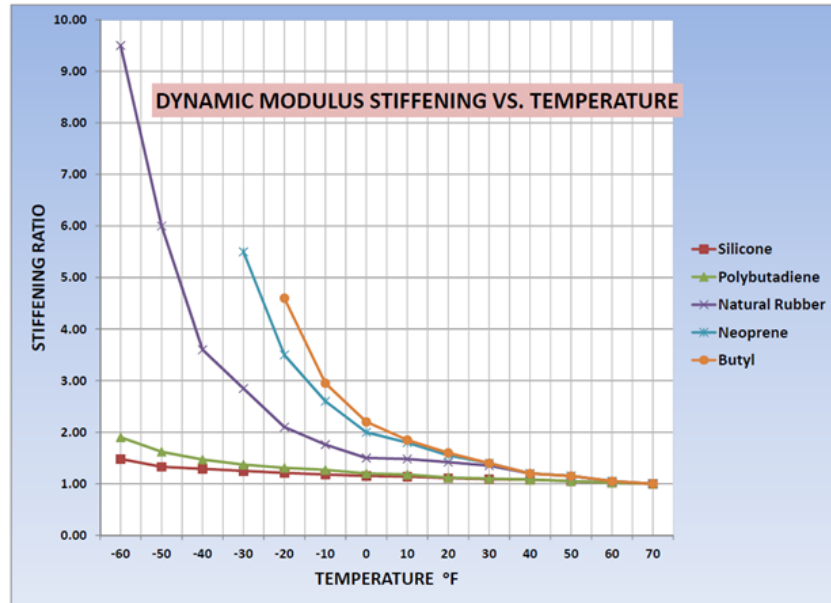


Figure 4.25: Dynamic Modulus Variation of Silicone Due to Temperature.
Source: "Elastomer dynamic modulus stiffening vs temperature," Oct. 2015. [Online]. Available: http://www.hutchinsonai.com/uploads/tech/Elastomer_Temp_Range.pdf

4.3 Combined Effects of FLVT and Isolation

The isolators are effective in reducing the response at the P-POD interface on NPSCuL, but comparing the results between the tests performed with and without FLVT show that the test conservatism is further reduced when FLVT is employed. The envelopes of the acceleration responses at the P-POD interface in each test axis for Configurations 1 through 3 with and without FLVT are shown in Appendix B; these responses were measured during the random vibration test for the ABC profile without force limiting. As expected, the high-frequency response for the isolated configurations are comparable, similar to the force-limited data. The force-limited set-up was not intended or expected to affect the response in this frequency range. The corresponding G_{RMS} values calculated over the entire test frequency range for the unnotched tests are shown in Table 4.8.

Table 4.8: X-Axis G_{RMS} Envelope of P-POD Interface at MPE +0 dB, ABC Profile, Unnotched

Test Axis	G_{RMS}		
	Configuration 1	Configuration 2	Configuration 3
X	29.6	9.66	3.43
Y	29.9	10.9	4.62
Z	25.1	7.35	3.36

The G_{RMS} values from Table 4.5 and Table 4.8 are plotted in Figure 4.26 to show the significant reduction in response due to the combined use of isolators and FLVT. If the fundamental modes of the system lie within the random vibration acceleration input frequency range of 20–2000 Hz, force limiting is still beneficial in reducing the response at the P-POD interface; this is exhibited in the significant reductions for Configurations 1 and 2 when FLVT is employed. However, FLVT is not as beneficial as the isolators become more effective due the shift in fundamental frequency outside of the test frequency range. This is most evident in the X and Y axes for Configuration 3, where the fundamental frequency is 12 Hz instead of 20 or 50 Hz.

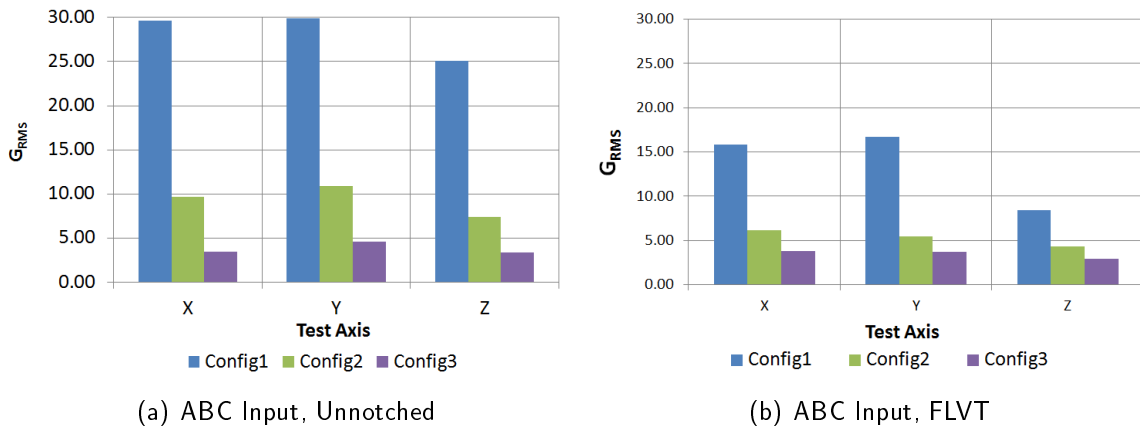


Figure 4.26: Overall G_{RMS} Envelope at P-POD Interface, MPE +0 dB

4.4 Effects of Varying Random Vibration Inputs

The baseline NPSCuL with and without cupmount isolators were also subjected to the ORS random vibration profile without force limiting; only the baseline NPSCuL with cupmount isolators was subjected to the force-limited ORS random vibration profile. The G_{RMS} values calculated over 20 to 2000 Hz corresponding to the tests without force limiting are shown in Table 4.9; the G_{RMS} values calculated over 20 to 2000 Hz corresponding to the test with force limiting are shown in Table 4.10. The envelopes of the acceleration responses at the P-POD interface in each test axis due to the ORS random input without FLVT are shown in Figure 4.27.

Table 4.9: G_{RMS} Reduction at P-POD Interface, 20–2000 Hz — MPE -6 dB of ORS Input without Force Limiting

Test Axis	Configuration 1, G_{RMS}	Configuration 3, G_{RMS}	Percent Difference (%)
X	30.3	3.90	87.2
Y	27.3	3.68	86.5
Z	12.1	1.66	86.2

Table 4.10: G_{RMS} Reduction at P-POD Interface on Configuration 3, 20–2000 Hz — MPE -6 dB of ORS Input

Test Axis	Configuration 3, Unnotched G_{RMS}	Configuration 3, FLVT G_{RMS}	Percent Difference (%)
X	3.90	3.88	0.513
Y	3.68	3.73	1.36
Z	1.66	1.69	1.81

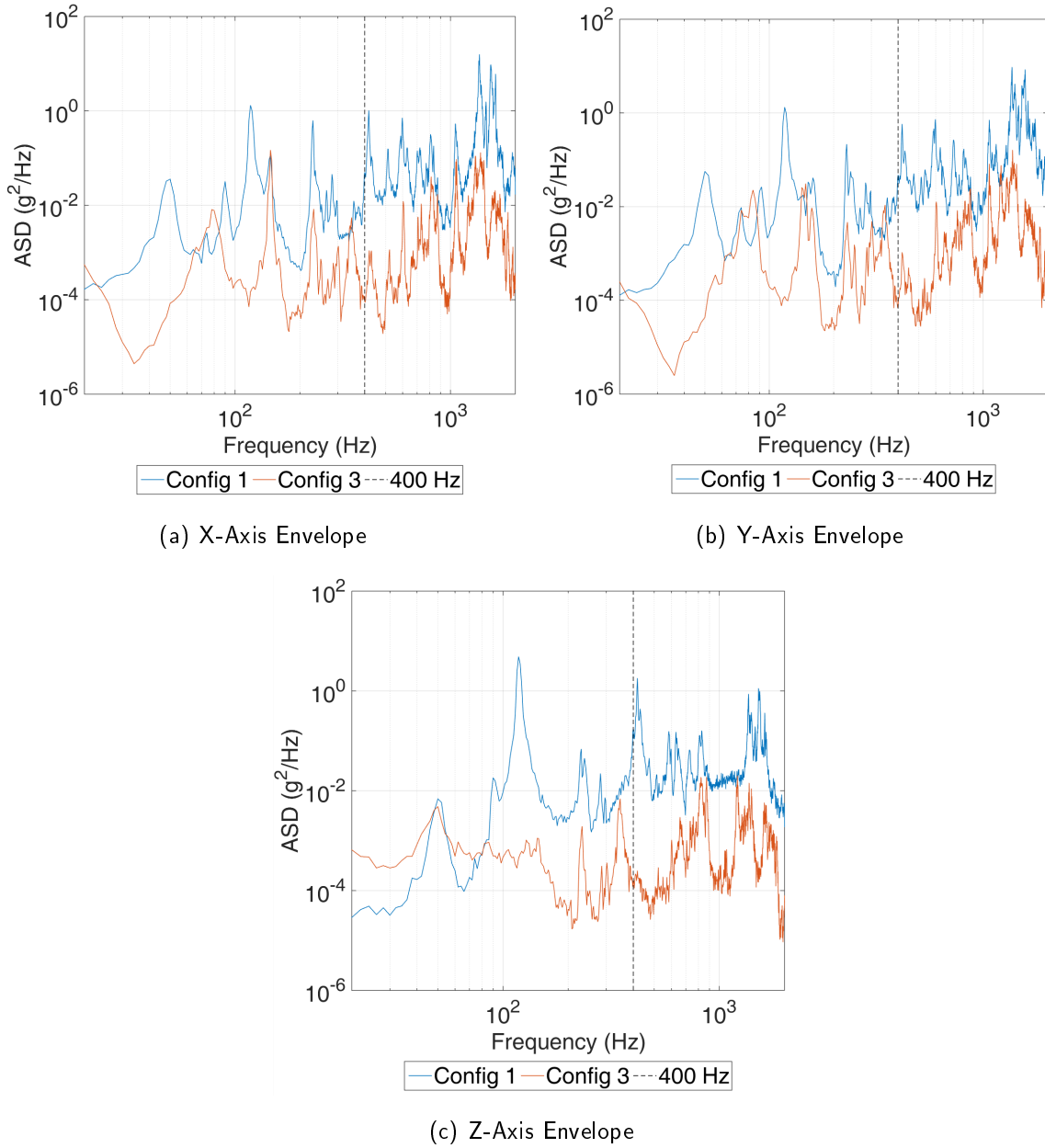


Figure 4.27: Acceleration Response at P-POD Interface Due to ORS Input without FLVT, Baseline NPSCuL with and without Cupmount Isolators

Due to the large amount of energy above 400 Hz in the ORS profile compared to the ABC profile, the isolators are very effective in reducing the response at the P-POD interface.

However, there is very little energy in the ORS profile below 400 Hz, especially in the frequency range of the fundamental modes of the system. Therefore, force limiting is not beneficial for this type of input. The G_{RMS} values from Table 4.9 and Table 4.10 are plotted in Figure 4.28 and Figure 4.29 to illustrate this finding - there is a large reduction in G_{RMS} between the isolated and baseline configurations, but there is no significant change with and without FLVT.

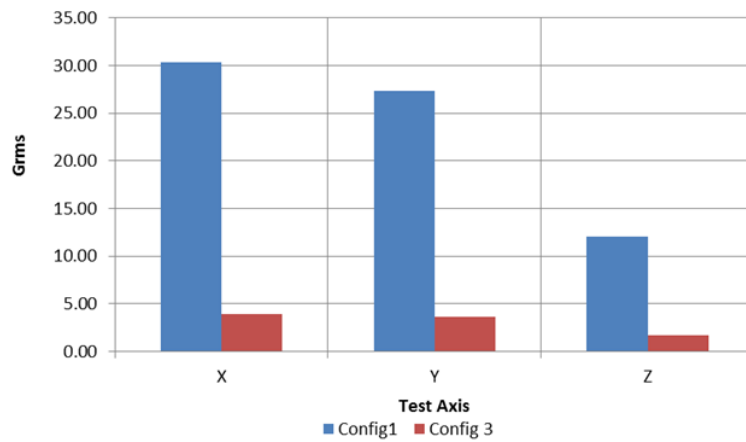


Figure 4.28: Overall G_{RMS} Envelope at P-POD Interface, MPE -6 dB of ORS Vibration Profile, Unnotched

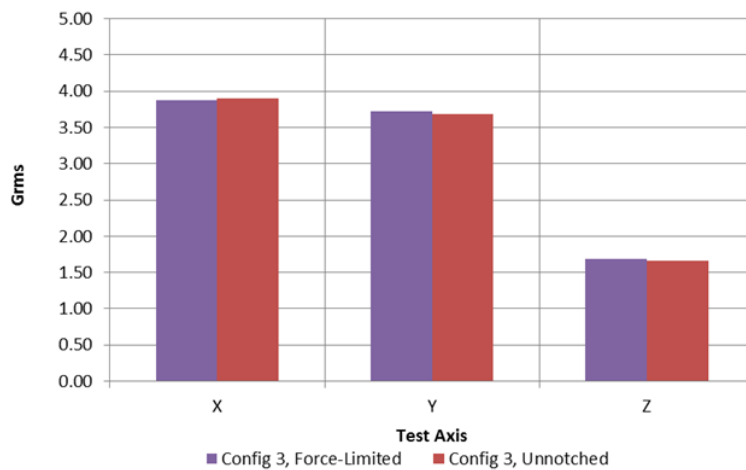


Figure 4.29: Overall G_{RMS} Envelope at P-POD Interface, MPE -6 dB of ORS Vibration Profile, FLVT

4.5 Force Limit Example of Isolated NPSCuL

The plots shown in Figure 2.6 and Figure 2.7 are repeated for the isolated NPSCuL to show that the 2DOF assumption in justifying the notched acceleration input is still valid for an isolated spacecraft. In the model, the fundamental frequency of the isolated NPSCuL was set to 50 Hz, which corresponds to the measured fundamental frequency during the Z-axis sine sweep for the baseline NPSCuL with cupmount isolators. The difference between the baseline and isolated NPSCuL models is the fundamental frequency, both of which are below 240 Hz. In this frequency range, the ASD values of the unnotched acceleration input are still relatively high. To properly compare the acceleration response of the ABC plate with the force limit used in test, the damping of the isolated NPSCuL model was set to 0.22, which was measured from the sine sweep data. The large increase in damping from 0.02 to 0.22 causes the anti-resonance of the ABC plate in Figure 4.30 to be muted. However, Figure 4.31 shows that the 2DOF model is still adequate for predicting the magnitude of the notched input near the fundamental frequency of the fixed-base spacecraft.

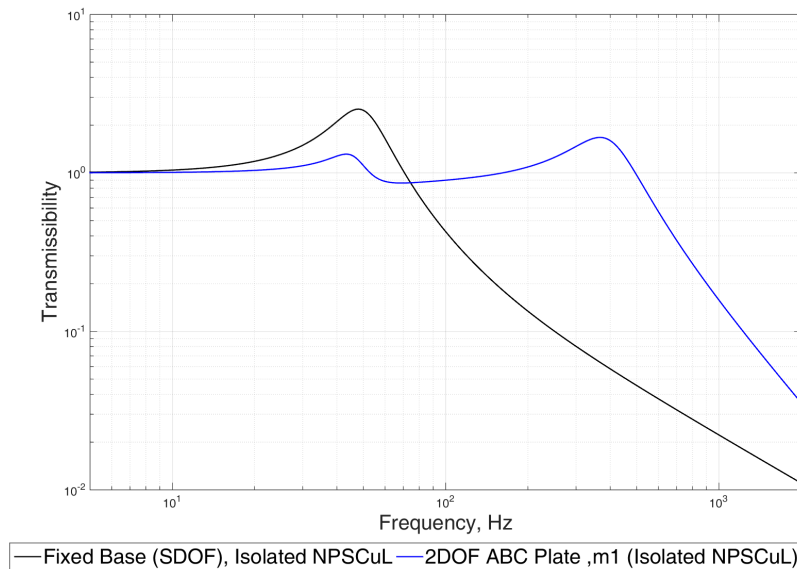


Figure 4.30: Transmissibility of Isolated NPSCuL (SDOF Model) and ABC Plate (2DOF Model)

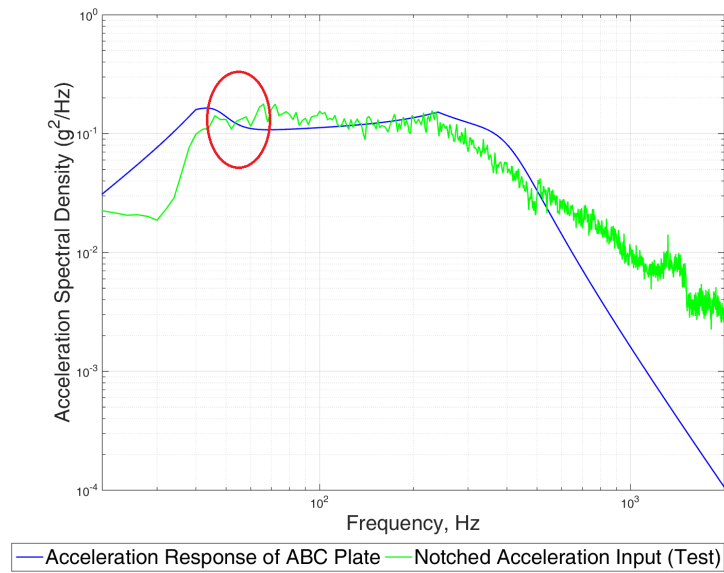


Figure 4.31: Predicted and Actual Force-Limited Acceleration Input, Isolated NPSCuL

CHAPTER 5:

Finite Element Model and Analyses

The finite element models (FEMs) were constructed and used for analysis in NX and NAS-TRAN. The baseline NPSCuL FEM that has been delivered for all launch vehicle mission-specific CLAs was modified for each isolator configuration. All of the FEMs were correlated with the modal properties measured during testing and provided a sanity check for these modal properties. However, only the FEM for the baseline NPSCuL with cupmount isolators was used for loads analyses and was delivered to ULA for CLA purposes because it is the most likely configuration to fly on a future ABC mission. All analyses were performed with the model fixed at rigid-body element used to tie the nodes representing the bolted interface to the ABC plate together.

5.1 Baseline NPSCuL FEM

The baseline NPSCuL FEM is shown in Figure 5.1. The primary structure consists of thin-shell elements, and the P-POD/P2M2, SAD, and harness mass properties are represented as concentrated mass elements that are rigidly connected to the primary structure. All fasteners are modeled as beam elements to facilitate adjusting the joint stiffness for correlation purposes and to extract fastener loads from the static load analyses. The modal properties for this model were correlated to the measured fundamental frequencies from the sine sweeps.

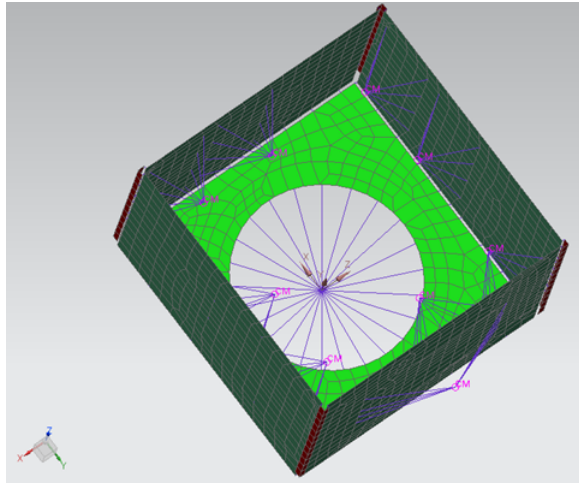


Figure 5.1: Baseline NPSCuL FEM

The material properties, joint stiffnesses, and element physical properties used in this model are shown in Table 5.1 and Table 5.2. The entire primary structure is made of aluminum 7075, and all fasteners are A286 stainless steel. The masses associated with the concentrated mass elements are listed in Table 5.3, and the overall FEM mass properties are shown in Table 5.4.

Table 5.1: Material Properties

Material	Density, kg/m^3 $[lbm/in^3]$	Poisson's Ratio	Modulus of Elasticity (E), GPa [psi]
Aluminum 7075	2.85E+03 [0.103]	0.33	68.9 [1.04E+07]
A286 Stainless Steel	7.92E+02 [0.286]	0.33	27.6 [4.00E+06]

Table 5.2: Element Physical Properties

Element Property Type	Element Description	Thickness, cm.[in.]	Non-Structural Mass (NSM), kg/m^2 [lbm/in²]
Shell	Angle Brackets	0.476 [0.1875]	0
	Side Wall	0.635 [0.250]	2.55 [3.63E-03]
	Baseplate	1.27 [0.500]	0
	Ring (Upper)	0.343 [0.135]	0
	Ring (Wall)	0.635 [0.250]	0
	Ring (Bottom)	0.432 [0.170]	0
Bar	Baseplate-to-Wall Fasteners	0.635 (dia.) [0.250]	20.7 [2.94E-02]

Table 5.3: Concentrated Mass Element Properties

Element Description	Mass, kg [lbm]
P-POD 1	8.12 [17.9]
P-POD 2	8.12 [17.9]
P-POD 3	8.07 [17.8]
P-POD 4	8.12 [17.9]
P-POD 5	8.12 [17.9]
P-POD 6	8.12 [17.9]
P-POD 7	8.12 [17.9]
P-POD 8	7.94 [17.5]
SAD	2.04 [4.50]
Harnessing	2.89 [6.37]

Table 5.4: FEM Mass Properties Summary

Property	Value
Mass, kg [lbm]	85.7 [189]
X_{ABC} , cm [in]	-9.96E-03 [-3.92E-03]
Y_{ABC} , cm [in]	6.68E-03 [2.63E-01]
Z_{ABC} , cm [in]	26.2 [10.3]

5.1.1 Fundamental Modes — Frequencies and Mode Shapes

The fundamental frequencies of the baseline NPSCuL FEM are shown in Table 5.5 along with the measured frequencies from the sine sweep test. There is good correlation for the rocking modes, but the axial mode of the FEM is not as stiff as the measured frequency. This discrepancy was acceptable for the CLAs because the lower fundamental frequency in the FEM produces more conservative results when used in the static load analyses. Additionally, the frequency range of concern in the CLAs is often cut off around 50 Hz, so the large discrepancy was not considered a risk for the LV. The corresponding mode shapes are shown in Figure 5.2.

Table 5.5: Baseline NPSCuL — Fundamental Frequencies

Mode	Frequencies (Hz)		Percent Difference (%)
	FEM	Test	
1 (Rocking, X)	50.5	48.5	4.12
2 (Rocking, Y)	50.9	49.7	2.41
3 (Axial, Z)	90.3	117.0	22.8

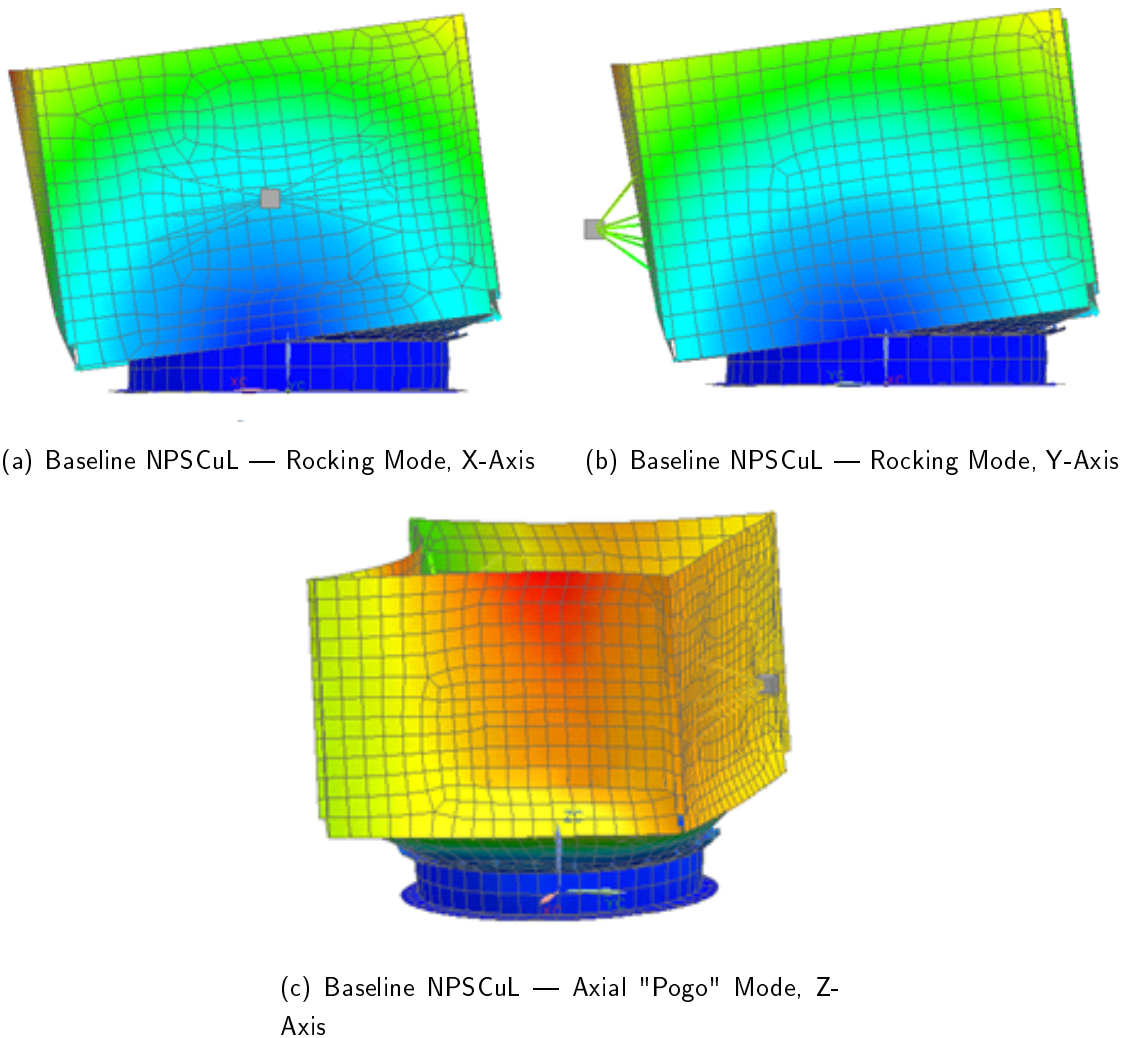


Figure 5.2: Baseline NPSCuL Fundamental Modes — Mode Shapes

5.2 Baseline NPSCuL FEM with Conical Isolators

The baseline NPSCuL FEM was modified to reflect the test configuration with conical isolators. As shown in Figure 5.3, the baseline adapter ring was replaced with a flat ring and the isolators, which are modeled using thin-shell and spring elements (CBUSH elements in Nastran), respectively. The thickness of the raised portions of the ring that accommodate the isolators is 1.17 cm (0.460"), and the thickness of the thinner portions of the ring that

interface with the ABC plate is 0.432 cm (0.170"); these are accounted for in the shell properties of the model. The spring stiffness value in all degrees of freedom was 525 kN/m (3000 lbf/in) to correlate the model with the test frequencies. The remaining NPSCuL structure and components were not modified.

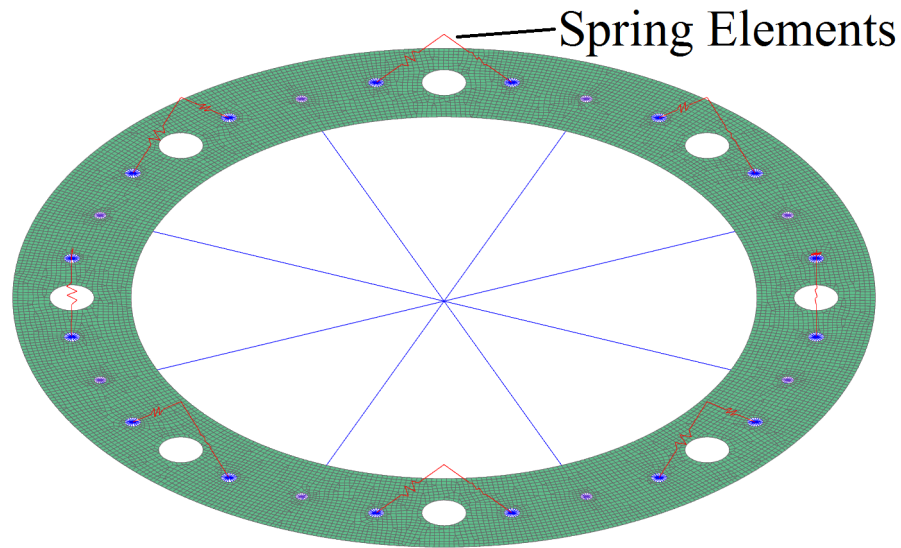


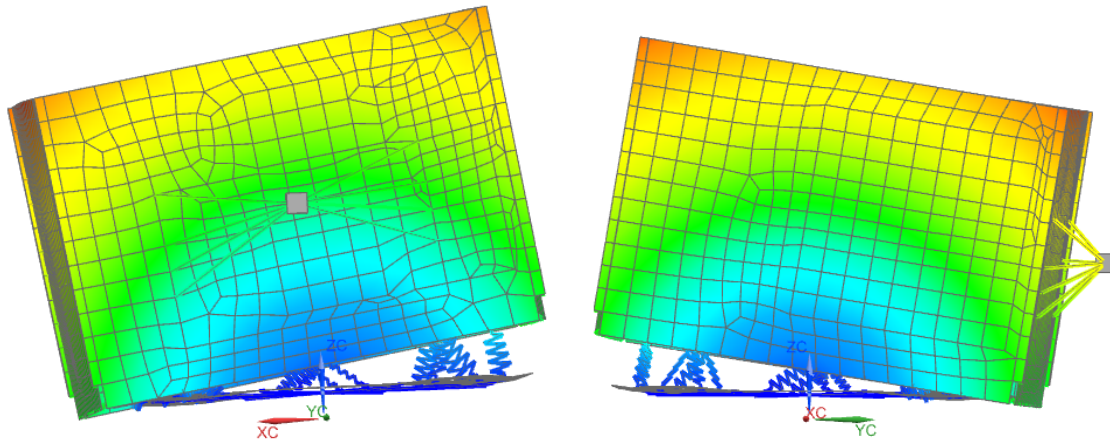
Figure 5.3: Flat Ring and Conical Isolator FEM

5.2.1 Fundamental Modes — Frequencies and Mode Shapes

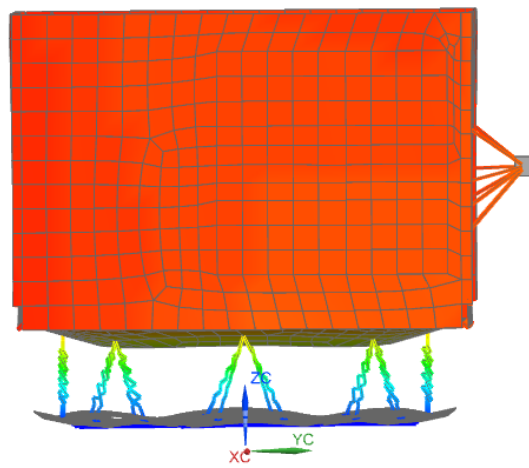
The fundamental frequencies of the baseline NPSCuL FEM with conical isolators are shown in Table 5.6 along with the measured frequencies from the sine sweep test. The corresponding mode shapes are shown in Figure 5.4 and Figure 5.5. Similar to the baseline NPSCuL FEM, there is good correlation for the first two rocking modes, but the axial mode of the FEM is not as stiff as the measured frequency. However, this discrepancy was expected due to the poor correlation in the baseline NPSCuL FEM. Frequency correlation was not expected near and above 100 Hz, either, but it was not a concern because the higher modes do not typically affect the CLA results.

Table 5.6: Baseline NPSCuL with Conical Isolators — Fundamental Frequencies [1]

Mode	Frequencies (Hz)		Percent Difference (%)
	FEM	Test	
1 (Rocking, Y)	20.3	19.8	2.42
2 (Rocking, X)	20.5	20.4	0.490
3 (Axial, Z)	42.7	56.3	24.2
4 (Rocking/Bending, X)	73.0	77.8	6.14
5 (Rocking/Bending, Y)	71.4	81.5	12.4
6 (Shear/Rocking, Y)	105	144	27.1
7 (Shear/Rocking, X)	103	154	33.1

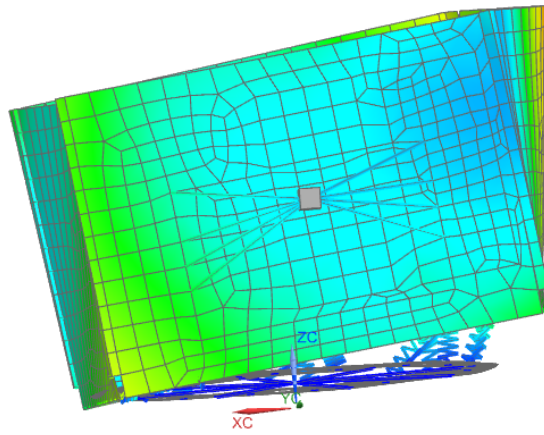


(a) Baseline NPSCuL with Conical Isolators — Rocking Mode, X-Axis
 (b) Baseline NPSCuL with Conical Isolators — Rocking Mode, Y-Axis

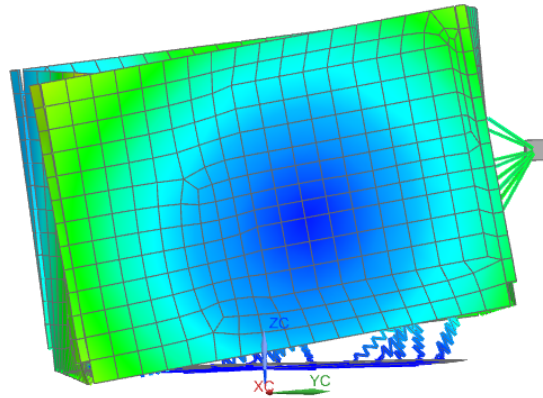


(c) Baseline NPSCuL with Conical Isolators — Axial "Pogo" Mode, Z-Axis

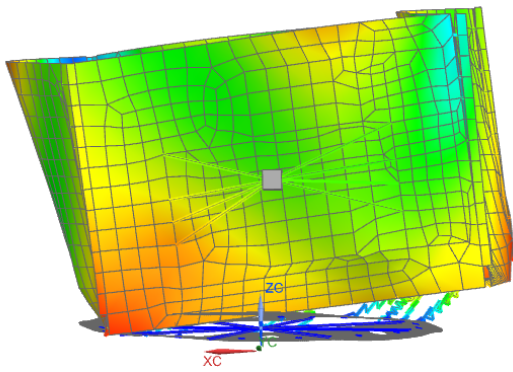
Figure 5.4: Baseline NPSCuL with Conical Isolators — Fundamental Mode Shapes



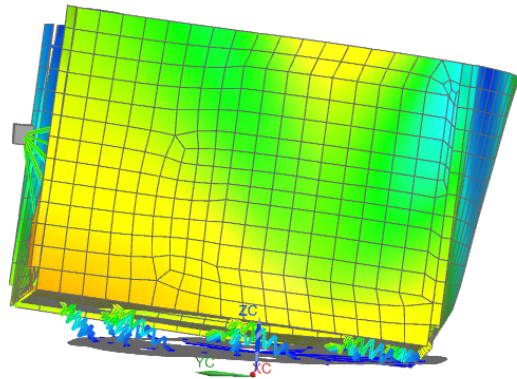
(a) Baseline NPSCuL with Conical Isolators — 2nd Rocking Mode, X-Axis



(b) Baseline NPSCuL with Conical Isolators — 2nd Rocking Mode, Y-Axis



(c) Baseline NPSCuL with Conical Isolators — Shear Mode, X-Axis



(d) Baseline NPSCuL with Conical Isolators — Shear Mode, Y-Axis

Figure 5.5: Baseline NPSCuL with Conical Isolators — Secondary Mode Shapes

5.3 Isogrid NPSCuL FEM with Conical Isolators

The isogrid NPSCuL FEM, which consists of shell elements for the face sheets and beam elements for the stringers and fasteners [19], was modified to reflect the test configuration with conical isolators; this model is shown in Figure 5.6. The baseplate, the flat ring, and the conical isolator portions of the FEM from the baseline NPSCuL FEM replaced the

unibase in the isogrid NPSCuL FEM. The fundamental frequencies of the isogrid NPSCuL FEM with conical isolators in each axis are shown in Table 5.7 along with the measured frequencies from the sine sweep test.

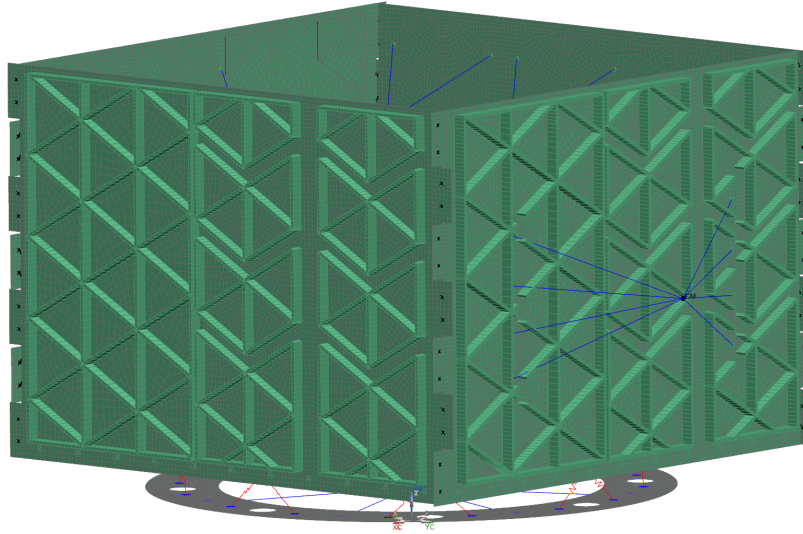


Figure 5.6: Isogrid NPSCuL FEM with Conical Isolators

Table 5.7: Isogrid NPSCuL with Conical Isolators — Fundamental Frequencies

Mode	Frequencies (Hz)		Percent Difference (%)
	FEM	Test	
1 (Rocking, Y)	19.4	19.5	0.564
2 (Rocking, X)	19.6	19.1	2.56
3 (Axial, Z)	44.0	58.4	24.6

The frequencies of the baseline and isogrid FEMs with conical isolators, shown in Table 5.8, confirm that the isogrid and baseline NPSCuL designs have the same fundamental modes in each axis (see Figure 4.6). The discrepancies for the higher modes are attributed to the stiffer walls and baseplate on the isogrid NPSCuL; however, the mode shapes are the same despite the differences in frequencies.

Table 5.8: Frequencies of Baseline and Isogrid NPSCuL FEMs with Conical Isolators

Mode	Frequencies (Hz)		Percent Difference (%)
	Baseline FEM	Isogrid FEM	
1 (Rocking, Y)	20.3	19.4	4.43
2 (Rocking, X)	20.5	19.6	4.59
3 (Axial, Z)	42.7	44.0	3.0
4 (Rocking/Bending, X)	73.0	83.8	12.9
5 (Rocking/Bending, Y)	71.4	86.5	17.4
6 (Shear/Rocking, Y)	105	133	21.2
7 (Shear/Rocking, X)	103	133	22.9

5.4 Baseline NPSCuL FEM with Cupmount Isolators

The baseline NPSCuL FEM was also modified to reflect the test configuration with cupmount isolators. Similar to the FEMs with the conical isolators, the baseline adapter ring was replaced with a flat ring and the isolators, which are modeled using thin-shell, concentrated mass, beam, and spring elements (CBUSH elements in Nastran), respectively. The thinner sections of the ring that interface with the ABC plate are kept the same as the baseline adapter ring flange at 0.432 cm (0.17"), but the thicker sections of the ring that accommodate the isolators are 0.635 cm (0.25"); these thicknesses are modeled in the shell properties. The spring stiffness value in all degrees of freedom was 947 kN/m (5400 lbf/in), as specified by the vendor's isolator sizing analysis [37], which is performed by the vendor as a rough estimate of the isolator performance by modeling the isolated component as a single DOF at the CG of the component. The beam elements represent the base of each isolator, which does not contribute to the spring stiffness but provides a load path between the isolator and the adapter ring. The modulus of elasticity of these beam elements was adjusted to 5.52 GPa (8.0×10^5 psi) to represent the joint stiffness for correlation with the test frequencies. The non-structural mass of the isolators are accounted for in the concentrated mass elements located at the interface node between the beam and spring elements. The remaining NPSCuL structure and components were not modified. The FEM for the adapter

ring and isolators is shown in Figure 5.7.

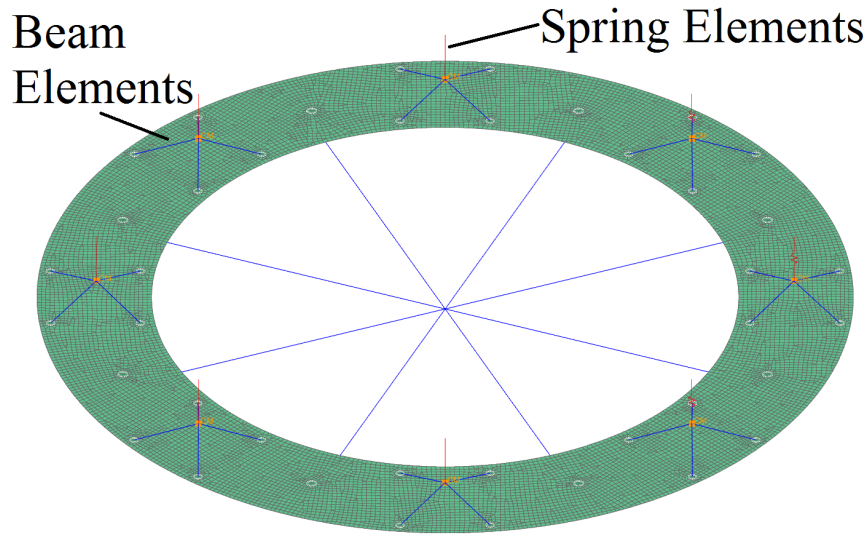


Figure 5.7: Flat Ring and Conical Isolator FEM

5.4.1 Fundamental Modes — Frequencies

The fundamental frequencies of the baseline NPSCuL FEM with cupmount isolators are shown in Table 5.9 along with the measured frequencies from the sine sweep test. Similar to the baseline NPSCuL FEMs with and without conical isolators, there is good correlation for the rocking modes, but the axial mode of the FEM is not as stiff as the measured frequency. The corresponding mode shapes are similar to those shown in Figure 5.4 and Figure 5.5.

Table 5.9: Baseline NPSCuL with Cupmount Isolators — Fundamental Frequencies

Mode	Frequencies (Hz)		Percent Difference (%)
	FEM	Test	
1 (Rocking, Y)	13.5	12.4	9.20
2 (Rocking, X)	13.7	12.5	8.93
3 (Axial, Z)	30.2	39.5	23.6
4 (Rocking/Bending, X)	53.9	62.8	14.2
5 (Rocking/Bending, Y)	54.3	65.4	17.0
6 (Shear/Rocking, Y)	80.3	82.2	2.28
7 (Shear/Rocking, X)	81.0	85.6	5.36

5.5 Loads Analyses

Loads analyses were only performed on the baseline NPSCuL with cupmount isolators because it is the most likely configuration to fly on a future ABC mission. In all axial load cases, the loads were applied to NPSCuL in tension (+Z direction). The structural integrity of the structure was also demonstrated during the qualification test.

5.5.1 Fastener Analysis

Similar to previous ABC missions, the static loads of 5 Gs lateral (X and Y) and 7 Gs axial (Z), as described in 3.1.1.4.2, were applied simultaneously to the FEM. The loads were extracted from the beam elements that were used to represent the fasteners. The maximum root-sum-square (RSS) shear and maximum axial loads at each joint type were used to calculate the margins of safety (MS); the NPSCuL fastener analysis tool was used to perform these calculations [19]. The margins of safety are shown in Table 5.10 and are positive at all joints, indicating that there will be no structural failures if the appropriate torque values are used. The torque values shown in Table 5.11, except for the ring/baseplate and ring/isolator joints, are calculated using the fastener analysis tool as well. The torque values for these two joints are instead based on experience with those bolt sizes and engineering judgment because the torques predicted by the analysis tool were higher than the typical range. The

values shown do not include running torque, but the final installation torques were used during the qualification test with no issues.

Table 5.10: Margins of Safety, Fastener Analysis — Cupmount Isolators on NPSCuL

Failure Mode	Joint							
	Ring/ ABC Plate	Baseplate/ Wall	Bracket/ Wall	PPOD/ Wall	SAD/ Wall	SAD Plate/ SAD Frame	Ring/ Baseplate	Ring/ Isolator
Yield	0.10	0.10	0.11	0.12	0.11	0.13	0.75	1.15
Ultimate	0.69	0.72	0.73	0.73	0.74	0.76	1.70	2.29
Shear	3.2	13	4.4	10	18	14.3	7.2	46.6
Gapping	1.20	9.5	4.4	1.5	21.5	13.7	1.9	0.8
Tear-Out	1.9	1.9	0.52	0.52	0.53	1.2	0.1	0.1

Table 5.11: Torque Values For Baseline NPSCuL with Cupmount Isolators

Joint	Ring/ ABC Plate	Baseplate/ Wall	Bracket/ Wall	PPOD/ Wall	SAD/ Wall	SAD Plate/ SAD Frame	Ring/ Baseplate	Ring/ Isolator
Torque, in-lbs	94	101	41	39	42	12	125	50

5.5.2 Stress Analysis

Similar to the fastener loads analysis, the static loads requirement detailed in 3.1.1.4.2 was applied to the FEM. However, the adapter ring was modeled using solid brick elements for more accurate stress prediction. This model is shown in Figure 5.8.

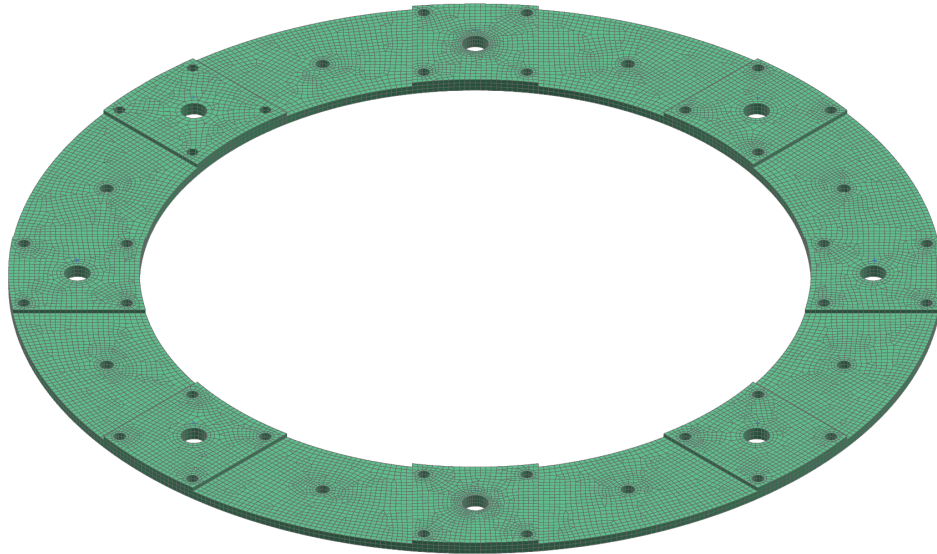


Figure 5.8: Flat Ring FEM — Solid Brick Elements

Factors of safety (FS) of 1.25 and 1.4 were applied to the resulting stresses; these are the most conservative factors amongst the common aerospace industry testing standards [21]. Yield and ultimate stress allowables of 393 kPa (57 ksi) and 469 kPa (68 ksi), respectively, were used to evaluate the margins [38]. The MS is calculated as follows:

$$MS = \frac{\sigma_{allowable}}{\sigma_{FEM}} - 1 \quad (5.1)$$

where $\sigma_{allowable}$ is the allowable stress and σ_{FEM} is the maximum elemental Von Mises stress obtained from the FEM. As shown in Table 5.12, there are positive margins throughout the structure. The maximum stress is in the adapter ring at the ABC interface; this is shown in Figure 5.9.

Table 5.12: Margins of Safety, Stress Analysis — Cupmount Isolators on NPSCuL

Load Case Description	Max Stress kPa [ksi]	Yield MS	Ultimate MS
5 Gs Lateral (X,Y), 7 Gs Axial (Z)	182 [26.5]	0.72	0.83

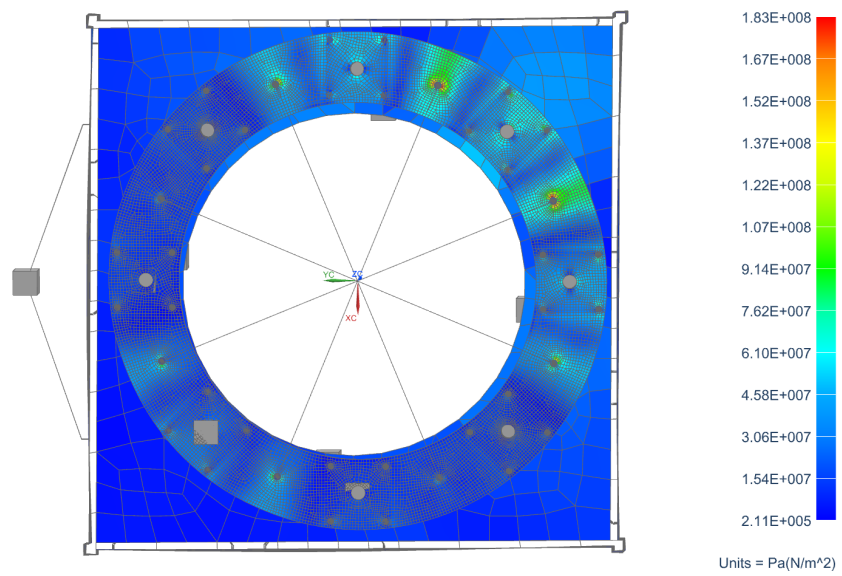


Figure 5.9: Von Mises Stress Distribution Due to ABC Static Loads

CHAPTER 6:

Conclusion

The combined use of FLVT and COTS isolators effectively reduces vibration levels for small satellites. This method, with the cupmount isolators on NPSCuL subjected to the ABC profile in particular, resulted in lowering the vibration G_{RMS} levels by 64 to 78% over the entire test frequency range. In the high-frequency range, the G_{RMS} responses were 97% lower, and the magnitude of the P-POD acceleration response at the P-POD interface was 20 dB lower (2 orders of magnitude). Additionally, the cost of this modification at approximately \$1,000 is about 2% of existing whole-spacecraft isolation systems.

The incorporation of COTS isolators on to NPSCuL and using an FLVT set-up has also been demonstrated to be effective for a worst-case environment such as NPSCuL. It was shown that various COTS isolators can be used depending on the LV mounting configuration; the cupmount isolators are appropriate for any static loading condition, and the conical isolators are appropriate for mainly compressive static loading conditions. Table 6.1 summarizes how the design requirements have been met in modifying NPSCuL to incorporate cupmount isolators; this includes the completion of a successful qualification test.

It was found that FLVT is more effective with vibration profiles that have high ASD values near the fundamental frequencies of the system, such as the ABC profile and other common vibration environments that are applicable to spacecraft that are similar in size to NPSCuL. It was also shown that COTS isolators are beneficial to small satellites, independent of a FLVT set-up.

Table 6.1: Launch Vehicle Requirements Summary

Requirement	Isolator/Re-Designed NPSCuL Feature
AP static envelope must be within the auxiliary payload (AP) volume	AP static envelope is the same in X and Y, 1.78 cm (0.7 in) reduction in Z
AP mechanical interface must be compatible with the ABC plate	Uses 8 of 24 available fasteners
AP mass properties must be within the interface control document (ICD) range	Increases NPSCuL mass by 1.13 kg (2.5 lbs); no significant impact to AP mass properties
AP must be able to withstand thermal environment	Thermal environment is enveloped by operating range of elastomers
AP must be able to withstand static loads environment	Positive margins infastener and strength analysis
AP must be able to withstand random vibration environment	Baseline NPSCuL withcupmount isolators have been qualified to ABC levels
AP fundamental frequency must be above 35 Hz or have no negative impacts to the LV or primary spacecraft	Isolated NPSCuL fundamental frequenciesare below 35 Hz, but CLA results indicate no negative impacts to LV or primary spacecraft

6.1 Summary of Contributions

A novel, practical method of combining the use of COTS isolators and FLVT to reduce the vibration levels for small satellites has been developed. This method has not been previously used on small satellites, and it is compatible with the ESPA interface. The design can also be easily modified for different spacecraft interfaces and masses. The application of FLVT has also been extended to include the use of the semi-empirical method with isolated small spacecraft, which has now been validated.

The reduction in vibration levels allows more sensitive and complex payloads to gain access

to space, which consequently improves the government's infrastructure for launching small satellites because NPSCuL is the only government-owned launch vehicle interface that is also capable of launching multiple satellites from one auxiliary payload. Additionally, the reduction in cost by approximately 98% of existing whole-spacecraft isolation systems allows this method to be used on low-budget missions.

6.2 Recommendations for Future Work

Several topics may be investigated in the future to improve the isolator selection process and installation. An optimization program can be developed to determine the ideal isolator stiffness from a spacecraft's mass, CG, and fundamental frequency requirements. Using cupmount isolators with non-threaded cores would improve the installation process by allowing a large torque value to be applied to the fastener without spinning the threaded core. Other types of secondary backout prevention would also be available, such as staking compound, instead of just a thread-lock adhesive. Capturing time histories during random vibration testing would also be beneficial for interpreting results.

To further reduce the vibration test environment, the roll-off slope and C^2 value can be adjusted when flight data becomes available over the entire test frequency range. The data would allow for efforts to verify if a less conservative force limit would still provide adequate margin to actual flight levels.

THIS PAGE INTENTIONALLY LEFT BLANK

APPENDIX A:

Shock and Acoustic Testing No-Test Rationale

Shock and acoustic environments were not driving requirements in re-designing NPSCuL, and no-test rationale was provided for the baseline NPSCuL configuration. As mentioned in [1], these environments and the analyses for the no-test rationales were performed to take the significant vibration reduction into account. It is noted that these will require formal approval from ULA in the event that the isolated NPSCuL is manifested for an auxiliary payload mission on the ABC.

A.1 Shock No-Test Rationale

The ABC shock and vibration profiles are defined at the ABC-to-NPSCuL interface [2], the shock level is below the 50 in/sec velocity no-test line as specified in SMC-S-016 [12]. The shock profile is not intended to change for future missions; therefore, shock testing is still not required by ULA.

A.2 Acoustic No-Test Rationale

Similarly, acoustic analysis was performed assuming the ABC acoustic environment [2], shown in Figure A.1 and defined at the ABC-to-NPSCuL interface, will not change for future missions.

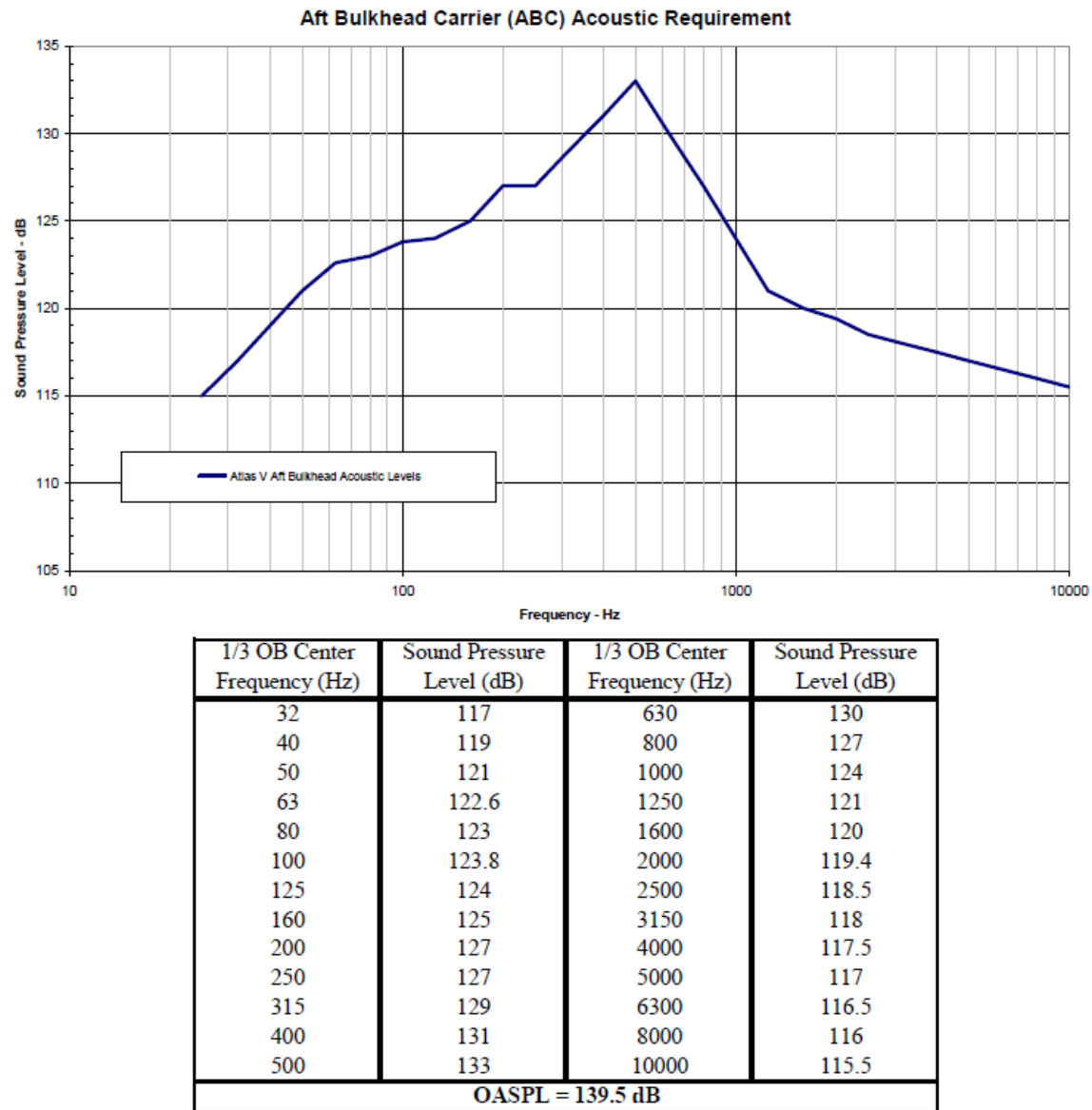


Figure A.1: Atlas V Maximum Predicted Acoustic Levels [2]

The method described in a study performed by JPL [39] was used to determine that acoustic testing was not required because the random vibration environment encompassed the acoustic levels; if the break-even surface area is higher than the component surface area, then the random vibration test will be more effective. Additionally, the study showed that

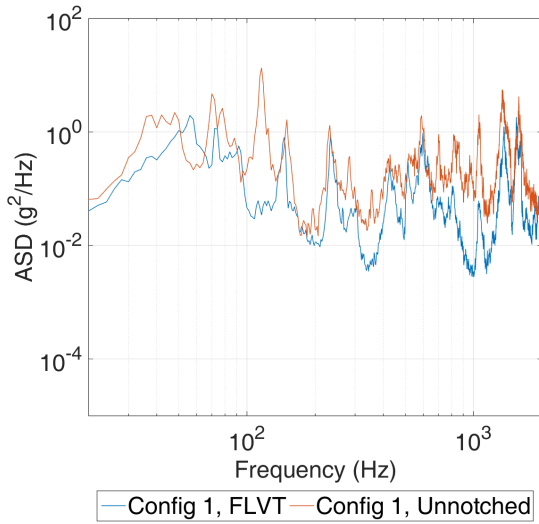
if the area/mass ratio of an object is less than $0.213 \text{ m}^2/\text{kg}$ ($150 \text{ in}^2/\text{lbm}$), the random vibration environment usually encompasses the acoustic profile.

This analysis has been performed for all previous missions, and it was redone for 2 P-PODs or 1 6U dispenser mounted to the wall of NPSCuL using the isolated P-POD response level. The surface area calculated for both configurations was 0.152 m^2 (236 in^2); this includes the conservative assumption that the entire NPSCuL wall is susceptible to acoustic loading. The total mass of the 6U configuration used in this analysis was 11.3 kg (25 lbm), and the total mass of the two P-PODs was assumed to be 15.9 kg (35 lbs); both are conservatively low estimates. Although the sound pressure level (SPL) at 100 Hz, the estimated frequency of the panel mode, is 123.8 dB, the overall SPL (OASPL) of 139.5 dB was used for this analysis. The resulting break-even surface areas are 0.155 and 0.217 m^2 (240 and 337 in^2) for the P-POD and 6U configurations, respectively. Although the break-even surface area is now lower for the isolated NPSCuL when compared to the baseline NPSCuL, it is still greater than the component surface area. Also, the break-even surface area/mass ratio of an NPSCuL wall with two P-PODs (using the lowest PSD value of $0.003 \text{ G}^2/\text{Hz}$ in the X-axis) is approximately $0.0137 \text{ m}^2/\text{kg}$ ($9.6 \text{ in}^2/\text{lb}$), which also indicates that acoustic testing is not required. The Matlab code used to perform this analysis is included in Appendix G.

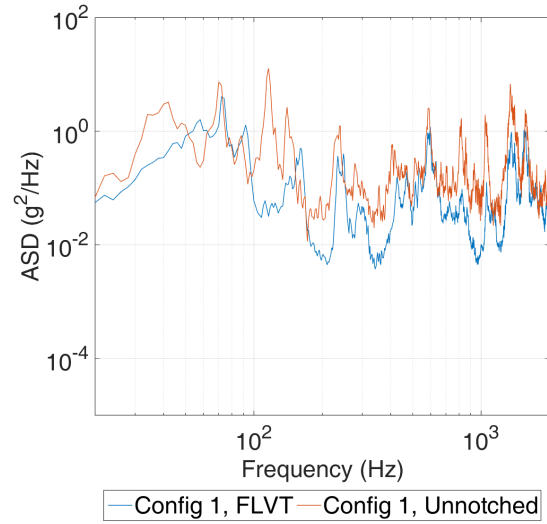
THIS PAGE INTENTIONALLY LEFT BLANK

APPENDIX B:

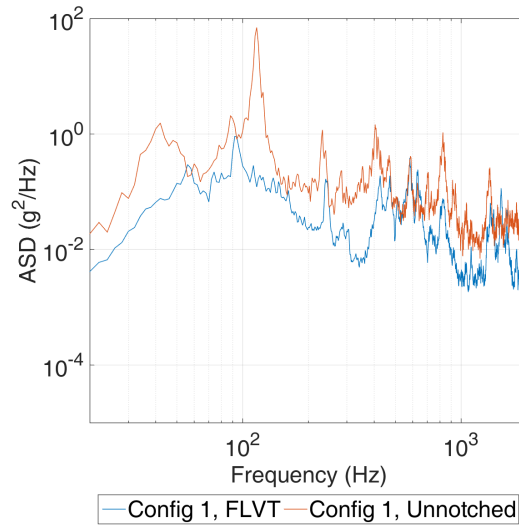
P-POD Response Comparison Plots



(a) X-Axis Envelope

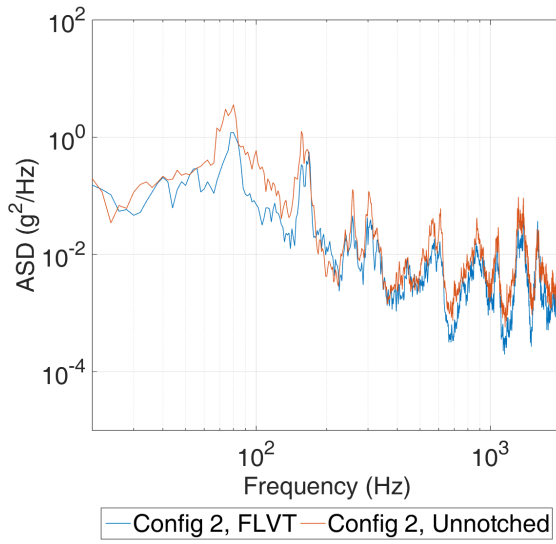


(b) Y-Axis Envelope

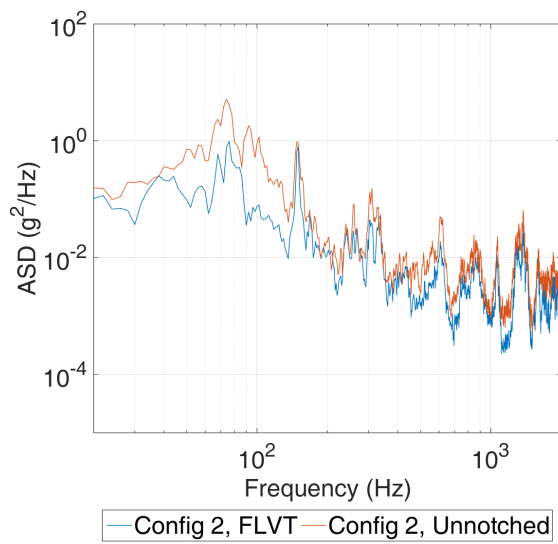


(c) Z-Axis Envelope

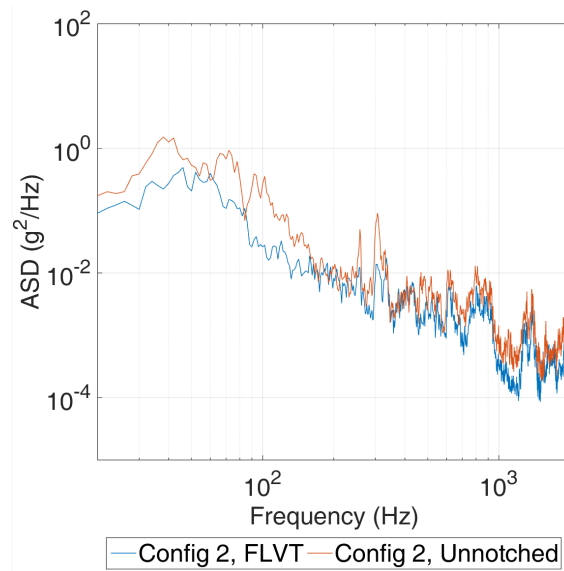
Figure B.1: Acceleration Response at P-POD Interface Due to ABC Profile, Configuration 1, with and without FLVT



(a) X-Axis Envelope

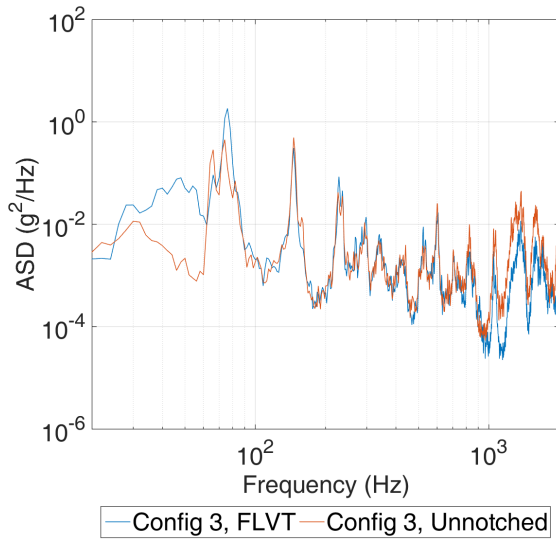


(b) Y-Axis Envelope

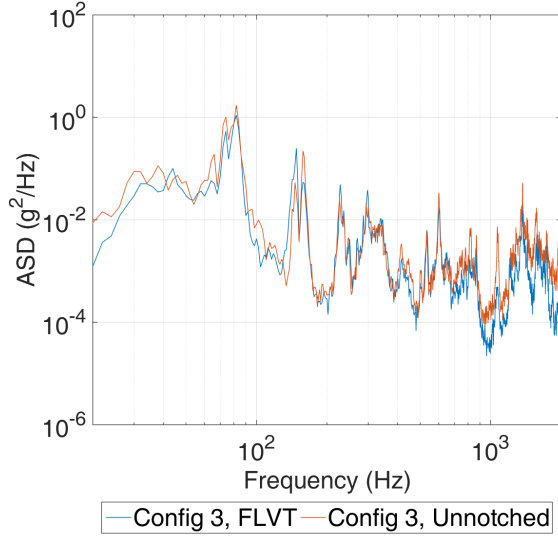


(c) Z-Axis Envelope

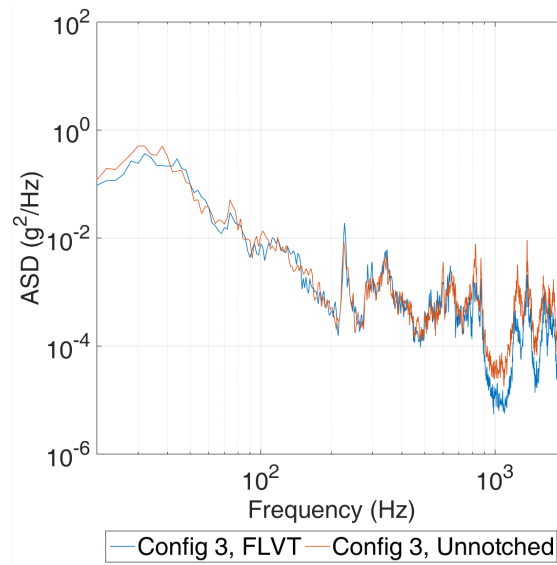
Figure B.2: Acceleration Response at P-POD Interface Due to ABC Profile, Configuration 2, with and without FLVT



(a) X-Axis Envelope



(b) Y-Axis Envelope



(c) Z-Axis Envelope

Figure B.3: Acceleration Response at P-POD Interface Due to ABC Profile, Configuration 3, with and without FLVT

THIS PAGE INTENTIONALLY LEFT BLANK

APPENDIX C:

Individual P-POD Responses, G_{RMS}

This appendix contains all the G_{RMS} data for each P-POD by test axis for reference. Not all P-PODs were instrumented for every test configuration and input, but at a minimum, P-PODs 1 through 4 were instrumented to capture any trends due to differences in P-POD location. Only the data obtained for Configurations 1 through 3 due to the ABC input with and without FLVT are presented here.

Table C.1: Configuration 1 P-POD Responses Due to ABC Input with FLVT

P-POD	G_{RMS} By Axis (Includes Cross-Axis Response)		
	X	Y	Z
1	9.56	6.51	6.29
2	11.85	8.12	6.86
3	6.36	10.79	6.11
4	7.73	12.58	6.73
5	10.27	6.14	6.23
6	12.10	7.36	6.98
7	5.98	7.75	6.32
8	6.60	10.53	6.58

Table C.2: Configuration 1 P-POD Responses Due to ABC Input without FLVT

P-POD	G_{RMS} By Axis (Includes Cross-Axis Response)		
	X	Y	Z
1	17.82	9.94	22.33
2	26.72	11.87	22.81
3	10.16	17.50	23.21
4	13.21	28.20	24.09

Table C.3: Configuration 2 P-POD Responses Due to ABC Input with FLVT

P-POD	G_{RMS} By Axis (Includes Cross-Axis Response)		
	X	Y	Z
1	3.11	2.04	3.72
2	4.46	2.25	3.78
3	2.24	3.05	3.79
4	2.34	4.63	3.91
5	3.38	2.15	3.90
6	5.05	2.30	3.83

Table C.4: Configuration 2 P-POD Responses Due to ABC Input without FLVT

P-POD	G_{RMS} By Axis (Includes Cross-Axis Response)		
	X	Y	Z
1	5.15	4.18	5.71
2	7.66	4.31	5.69
3	3.64	5.77	6.68
4	3.66	9.17	6.93
5	5.32	4.22	5.95
6	8.06	4.37	5.84

Table C.5: Configuration 3 P-POD Responses Due to ABC Input with FLVT

P-POD	G_{RMS} By Axis (Includes Cross-Axis Response)		
	X	Y	Z
1	2.08	1.18	2.54
2	3.10	1.29	2.57
3	1.49	1.86	2.70
4	1.56	2.72	2.74
5	3.40	1.48	2.59
6	2.76	1.60	2.58
7	1.25	2.20	2.56
8	1.28	3.11	2.58

Table C.6: Configuration 3 P-POD Responses Due to ABC Input without FLVT

P-POD	G_{RMS} By Axis (Includes Cross-Axis Response)		
	X	Y	Z
1	1.98	1.39	2.80
2	2.97	1.57	2.84
3	0.89	2.19	3.15
4	1.09	3.30	3.25
5	1.86	1.82	2.84
6	2.85	1.92	2.82
7	1.02	2.75	3.06
8	0.990	3.85	3.09

APPENDIX D:

MATLAB Code — Force Limit Validation

This appendix contains the MATLAB scripts for calculating the transmissibility of the base-line and isolated NPSCuL in a fixed-base and FLVT set-up; NPSCuL is modeled as a single degree-of-freedom in both cases. However, in the FLVT set-up, a second degree-of-freedom is introduced to explain the theory behind the notched input.

```
%FLVT Illustration
%Calculate accleration of mass and force in spring vs frequency
%FLVT and standard random vibe set up
%Using relative support motion equations
%
%W. Lan

clc; clear all; close all;

%SYSTEM PROPERTIES
mass_sc = 200; %lbs
mass_ABC = 20; %lbs

k_LV = 2587221;
% k_LV = 2737800; %axial K

zheta = 0.02;

%INPUT PARAMETERS
omega = 0:2:3200; %Hz
ABC_interface_MPE = [20 40 240 2000; 0.03 0.125 0.125 0.003];
ABC_MPE_full = 10.^interp1(log10(ABC_interface_MPE(1,:)),log10(...
    ABC_interface_MPE(2,:)),log10(omega)); %ASD, g^2/Hz

%CASE 1 - "FIXED BASE" CONFIGURATION
%ASSUME SUPPORT MOTION USING ABSOLUTE COORDINATES
```

```

%natural frequencies, rad/s
wn = sqrt(k_LV/mass_sc);
disp('Fixed Base Model Damped Frequencies, Hz')
wd1 = wn*sqrt(1-zheta^2)

Y = 1; %sine sweep, g's
for i = 1:length(omega)
    %Displacement
    X(i) = Y*sqrt(1+(2*zheta*(omega(i)/wn))^2)/sqrt((1-(omega(i)/wn)^2)^2+(2*zheta*omega(i)/wn)^2);
    %Acceleration
    % Xdoubledot(i) = X(i)*omega(i)^2/386.4;
end
%Acceleration of mass due to 7.6 Grms input

accel = X.*ABC_MPE_full;
%Force in Spring
k_LV_force = accel*mass_sc;

%CASE 2 - FLVT CONFIGURATION
%ASSUME VIBRATION ABSORBER MODEL%ABC PLATE IS THE ABSORBER (CONTRARY ...
    TO BC
%SETUP)
%"2" refers to NPSCuL
%"1" refers to ABC plate
m1 = mass_ABC;
m2 = mass_sc;
k1 = k_LV; %assume fixed base stiffness
k2 = 2737800; %axial K

disp('FLVT Model Damped Frequencies, Hz')
w1 = sqrt(k1/m1)
w2 = sqrt(k2/m2)

mu = m2/m1;
q = w2/w1;

toggle = 2; %1 for undamped, 2 for damped

```

```

if toggle == 1

    %FROM KELLY, EQN 8.42 AND 8.43 - UNDAMPED VIBRATION ABSORBER
    for i = 1:length(omega)
        r1 = omega(i)/w1;
        r2 = omega(i)/w2;
        Am1(i) = abs((1-r2^2)/(r1^2*r2^2-r2^2-(1+mu)*r1^2+1));
        Am2(i) = abs(1/(r1^2*r2^2-r2^2-(1+mu)*r1^2+1));
        if Am1(i) == 0
            Am1(i) = 1E-4;
        end
        if Am2(i) == 0
            Am2(i) = 1E-4;
        end
    end

else

    %FROM KELLY, EQN 8.54 AND 8.55 - DAMPED VIBRATION ABSORBER
    for i = 1:length(omega)
        r1 = omega(i)/w1;
        r2 = omega(i)/w2;
        Am1(i) = sqrt(((2*zeta*r1*q)^2+(r1^2-q^2)^2)/((r1^4-(1+(1+mu)*q^2)*r1^2+q^2)*(r1^2+q^2)^2+(2*zeta*r1*q)^2*(1-r1^2*(1+mu))^2));
        Am2(i) = sqrt((q^4+(2*zeta*q)^2)/((r1^4-(1+(1+mu)*q^2)*r1^2+q^2)^2+(2*zeta*r1*q)^2*(1-r1^2*(1+mu))^2));
        if Am1(i) == 0
            Am1(i) = 1E-4;
        end
        if Am2(i) == 0
            Am2(i) = 1E-4;
        end
    end

end

%Acceleration of S/C
accel2 = Am2.*ABC_MPE_full;

```

```

%Force in Spring, S/C to LV
kforce2 = accel2*mass_sc;
%Acceleration of ABC plate
accel1 = Am1.*ABC_MPE_full;
%Force in Spring, S/C to LV
kforce1 = accel1*mass_ABC;

%TRANSMISSIBILITY PLOT
figure('Color',[1 1 1])
loglog(omega,X)
hold on
xlim([20 2000])
grid on
ylabel('Transmissibility','FontSize',24)
loglog(omega,Am1)
plot([117,117],[1E-4,1E3],'k--')
xlim([20 2000])
grid on
xlabel('Frequency, Hz','FontSize',24)
legend1=legend('SDOF,NPSCuL','2DOF,ABC Plate (m_1)','Location','...
    SouthOutside','Orientation','Horizontal');
set(legend1,'FontSize',24)
% title('Vibration Absorber Effect in a 2DOF Model','FontSize',24)

%2DOF (FLVT) PLOT - % Acceleration of ABC plate and test control
load testdata.mat
figure('Color',[1 1 1])
loglog(omega,accel1,'-b','LineWidth',1.5)
hold on
loglog(freq,config1.ABC.control.Z,'-g','LineWidth',1.5)
xlim([20 2000])
grid on
xlabel('Frequency, Hz','FontSize',24)
% title('2DOF Model Comparison with Force Limited Test Control','...
    FontSize',24)
ylabel('Acceleration Spectral Density (g^2/Hz)','FontSize',24)
% legend('Fixed Base (NPSCuL)','FLVT,m1 (ABC Plate)','FLVT,m2 (NPSCuL)...
    ','Location','SouthOutside','Orientation','Horizontal')

```

```

legend2=legend('Acceleration Response of ABC Plate','Notched ...
    Acceleration Input (Test)','Location','SouthOutside','Orientation...
    ','Horizontal');
set(legend2,'FontSize',24)

%SIMPLE TDFS METHOD
Q=1/(2*zeta);
c=2*zeta;
beta1 = 1+1/2*mu+sqrt(mu+1/4*mu^2);
beta2 = 1+1/2*mu-sqrt(mu+1/4*mu^2);
for i = 1:251
%     H2(i)=-(k2 + c*omega(i)*j)/(k1*m2*omega(i)^2 - k1*k2 + k2*m1*...
    omega(i)^2 + k2*m2*omega(i)^2 - m1*m2*omega(i)^4 - c*k1*omega(i)*...
    j + c*m1*omega(i)^3*j + c*m2*omega(i)^3*j);
%     Sff(i)=(1+(omega(i)/w2/Q)^2)/((1-(omega(i)/w2)^2)^2+(omega(i)/...
    w2/Q)^2)*ABC_MPE_full(i)*abs(H2(i))^2;
    Sff(i) = ABC_MPE_full(i)*m2^2*(1+(omega(i)/w2)^2/Q^2)/((1-(omega(...
    i)/w2)^2)^2+(omega(i)/w2)^2/Q^2)*4.448221628254617;
%
end
Sff1 = (1+beta1/Q^2)/((1-beta1)^2+beta1/Q^2)*ABC_MPE_full*m2^2;
Sff2 = (1+beta2/Q^2)/((1-beta2)^2+beta2/Q^2)*ABC_MPE_full(1:251)*m2...
    ^2;
Sff3 = [1.52E+03,2.60E+03,6.31E+03,5.57E+03,2.95E+03,2.95E+03,2.59E...
    +03,1.15E+03,7.06E+01]*4.448221628254617;

%COMPLEX TDFS METHOD
%from Excel spreadsheet
f_center = [20,25,40,64,102,162,258,410,500];
Sff_complex = [1.07E+03,1.84E+03,4.46E+03,1.58E+04,1.48E+04,4.46E...
    +03,3.93E+03,1.74E+03,1.07E+02]*4.448221628254617;

%MAX OF BOTH
Sff_max = max([Sff_complex;Sff3]);

%SEMI-EMPIRICAL METHOD
[F,T,dataout] = forcelimitcalc(ABC_interface_MPE',w2,500,0,m2);

%COMPARISON PLOT, FORCE LIMIT METHODS

```

```

figure('Color',[1 1 1])
% loglog(omega(1:251),abs(Sff2),omega(1:251),abs(Sff),dataout(:,1),...
    dataout(:,2),f_center,Sff_complex,f_center,Sff3)
% loglog(dataout(:,1),dataout(:,2),f_center,Sff_complex,f_center,Sff3...
    )
% loglog(dataout(:,1),dataout(:,2),f_center,Sff_max)
loglog(dataout(:,1),dataout(:,2)*4.448221628254617,'k-','LineWidth'...
    ,2)
hold on
scatter(f_center,Sff_complex,40,'r','filled')
scatter(f_center,Sff3,40,'b','filled')
loglog(f_center,Sff_max,'g-','LineWidth',2)
xlim([20 2000])
grid on
xlabel('Frequency, Hz','FontSize',24)
ylabel('Force Spectral Density (N^2/Hz)','FontSize',24)
% ylabel('Force Spectral Density (lb^2/Hz)','FontSize',24)
set(gca,'FontSize',24)
% legend2=legend('Semi-Empirical','TDFS','Location','SouthOutside','...
    Orientation','Horizontal');
legend2=legend('Semi-Empirical','Complex TDFS','Simple TDFS','TDFS ...
    Max','Location','SouthOutside','Orientation','Horizontal');
set(legend2,'FontSize',24)

%FLVT Illustration, Isolated NPSCuL
%Calculate accleration of mass and force in spring vs frequency
%FLVT and standard random vibe set up
%Using relative support motion equations
%
%W. Lan

clc; clear all; close all;

%SYSTEM PROPERTIES
mass_sc = 189; %lbs
mass_ABC = 20; %lbs

```

```

% k_LV = 605000; %lb/in, lateral
k_LV = 2737800; %axial K

zheta = 0.02;

%INPUT PARAMETERS
omega = 0:1:2000; %Hz
ABC_interface_MPE = [20 40 240 2000; 0.03 0.125 0.125 0.003];
%"ABC_MPE_full" is really just 0.5 G sine sweep to compare with ...
    apparent
%mass #'s
% ABC_MPE_full = 0.5;
ABC_MPE_full = 10.^interp1(log10(ABC_interface_MPE(1,:)),log10(...
    ABC_interface_MPE(2,:)),log10(omega)); %ASD, g^2/Hz
%plot ABC_MPE_full to check
% figure
% loglog(omega, (ABC_MPE_full))
% xlim([20 2000])
% grid on

%CASE 1 - FIXED BASE CONFIGURATION - NO ISOLATORS
%ASSUME SUPPORT MOTION USING ABSOLUTE COORDINATES

%natural frequencies, rad/s
wn = sqrt(k_LV/mass_sc);
disp('Fixed Base Model Damped Frequencies, Hz')
wd1 = wn*sqrt(1-zheta^2)

Y = 1; %sine sweep, g's
for i = 1:length(omega)
    %Displacement
    X(i) = Y*sqrt(1+(2*zheta*(omega(i)/wn))^2)/sqrt((1-(omega(i)/wn)...
        ^2)^2+(2*zheta*omega(i)/wn)^2);
    %Acceleration
    % Xdoubledot(i) = X(i)*omega(i)^2/386.4;
end
%Acceleration of mass due to 7.6 Grms input

accel = X.*ABC_MPE_full;

```

```

%Force in Spring
% k_LV_force = accel*mass_sc;

%CASE 2 - FLVT CONFIGURATION - NO ISOLATORS
%ASSUME VIBRATION ABSORBER MODEL
%USING EQN 3.15 FROM HARTOG, P. 89
%"2" refers to NPSCuL
%"1" refers to ABC plate
m1 = mass_ABC;
m2 = mass_sc;
k1 = k_LV; %assume fixed base stiffness
% k2 = 460800; %lateral K
k2 = 2737800; %axial K

disp('FLVT Model Damped Frequencies, Hz')
w1 = sqrt(k1/m1)
w2 = sqrt(k2/m2)

mu = m2/m1;
q = w2/w1;

toggle = 2; %1 for undamped, 2 for damped

if toggle == 1

    %FROM KELLY, EQN 8.42 AND 8.43 - UNDAMPED VIBRATION ABSORBER
    for i = 1:length(omega)
        r1 = omega(i)/w1;
        r2 = omega(i)/w2;
        Am1(i) = abs((1-r2^2)/(r1^2*r2^2-r2^2-(1+mu)*r1^2+1));
        Am2(i) = abs(1/(r1^2*r2^2-r2^2-(1+mu)*r1^2+1));
        if Am1(i) == 0
            Am1(i) = 1E-4;
        end
        if Am2(i) == 0
            Am2(i) = 1E-4;
        end
    end
end

```

```

else
    %FROM KELLY, EQN 8.54 AND 8.55 - DAMPED VIBRATION ABSORBER
    for i = 1:length(omega)
        r1 = omega(i)/w1;
        r2 = omega(i)/w2;
        Am1(i) = sqrt(((2*zeta*r1*q)^2+(r1^2-q^2)^2)/((r1^4-(1+(1+mu...
            )*q^2)*r1^2+q^2)^2+(2*zeta*r1*q)^2*(1-r1^2*(1+mu))^2));
        Am2(i) = sqrt((q^4+(2*zeta*q)^2)/((r1^4-(1+(1+mu)*q^2)*r1^2+...
            q^2)^2+(2*zeta*r1*q)^2*(1-r1^2*(1+mu))^2));
        if Am1(i) == 0
            Am1(i) = 1E-4;
        end
        if Am2(i) == 0
            Am2(i) = 1E-4;
        end
    end
end

%CASE 3 - FLVT CONFIGURATION - WITH ISOLATORS
% k3 = 302400; %lateral K
k3 = 2.9489e+05; %axial K to match sine sweep data
k3 = 472500; %axial K to match random test data
zeta = 0.22;
%k3 = 99981; %isolator stiffness

% w1 = sqrt(k1/m1)
w3 = sqrt(k3/m2)
disp('FLVT Isolated Model Damped Frequencies, Hz')
w1
wd3 = w3*sqrt(1-zeta^2)

q3 = w3/w1;

if toggle == 1

    %FROM KELLY, EQN 8.42 AND 8.43 - UNDAMPED VIBRATION ABSORBER
    for i = 1:length(omega)
        r1 = omega(i)/w1;

```

```

    r3 = omega(i)/w3;
    Am13(i) = abs((1-r3^2)/(r1^2*r3^2-r3^2-(1+mu)*r1^2+1));
    Am23(i) = abs(1/(r1^2*r3^2-r3^2-(1+mu)*r1^2+1));
    if Am13(i) == 0
        Am13(i) = 1E-4;
    end
    if Am23(i) == 0
        Am23(i) = 1E-4;
    end
end

else
    %FROM KELLY, EQN 8.54 AND 8.55 - DAMPED VIBRATION ABSORBER
    for i = 1:length(omega)
        r1 = omega(i)/w1;
        Am13(i) = sqrt(((2*zeta*r1*q3)^2+(r1^2-q3^2)^2)/((r1...
            ^4-(1+(1+mu)*q3^2)*r1^2+q3^2)^2+(2*zeta*r1*q3)^2*(1-r1...
            ^2*(1+mu))^2));
        Am23(i) = sqrt((q3^4+(2*zeta*q3)^2)/((r1^4-(1+(1+mu)*q3^2)*...
            r1^2+q3^2)^2+(2*zeta*r1*q3)^2*(1-r1^2*(1+mu))^2));
        if Am13(i) == 0
            Am13(i) = 1E-4;
        end
        if Am23(i) == 0
            Am23(i) = 1E-4;
        end
    end
end

end

%FIXED BASE MODEL - WITH ISOLATORS
Y = 1; %sine sweep, g's
for i = 1:length(omega)
    %Displacement -if Y = 1, then same as amplitude ratio, X/Y
    X3(i) = Y*sqrt(1+(2*zeta*(omega(i)/w3))^2)/sqrt((1-(omega(i)/w3)...
        ^2)^2+(2*zeta*omega(i)/w3)^2);
    %Acceleration
    % Xdoubledot(i) = X(i)*omega(i)^2/386.4;
end

```

```

%2DOF (FLVT) PLOT - % Acceleration of ABC plate and test control
load testdata.mat
figure('Color',[1 1 1])
loglog(omega,Aml3.*ABC_MPE_full,'-b','LineWidth',1.5)
hold on
loglog(freq,config2d.ABC.control.Z,'-g','LineWidth',1.5)
xlim([20 2000])
grid on
xlabel('Frequency, Hz','FontSize',24)
% title('2DOF Model Comparison with Force Limited Test Control, ...
    Isolated NPSCuL','FontSize',24)
ylabel('Acceleration Spectral Density (g^2/Hz)','FontSize',24)
% legend('Fixed Base (NPSCuL)','FLVT,m1(ABC Plate)','FLVT,m2(NPSCuL)...
    ','Location','SouthOutside','Orientation','Horizontal')
legend2=legend('Acceleration Response of ABC Plate','Notched ...
    Acceleration Input (Test)','Location','SouthOutside','Orientation...
    ','Horizontal');
set(legend2,'FontSize',24)

%TRANSMISSIBILITY PLOT
%M1, FLVT PLATE
figure('Color',[1 1 1])
loglog(omega,X3,'-k','LineWidth',1.5)
hold on
loglog(omega,Aml3,'-b','LineWidth',1.5)
xlim([5 2000])
grid on
xlabel('Frequency, Hz','FontSize',24)
ylabel('Transmissibility','FontSize',24)
% title('Vibration Absorber Effect in a 2DOF Model - Isolated NPSCuL...
    ')
legend1=legend('Fixed Base (SDOF), Isolated NPSCuL','2DOF ABC Plate ,...
    m1 (Isolated NPSCuL)','Location','SouthOutside','Orientation','...
    Horizontal')
set(legend1,'FontSize',24)
% bigtitle = sprintf('Effect of FLVT (2DOF Damped TMD Model) on ...
    Baseline and Isolated NPSCuL Fundamental Frequencies wrt ABC ...
    Plate');

```

```
%      suptitle(bigtitle)
```

APPENDIX E:

MATLAB Code — Force Limit Calculation

This appendix contains the MATLAB script and associated functions for calculating the force limit using the semi-empirical method. The inputs are the unnotched ASD values, the roll-off frequency, and the mass of the test article. The force limit is plotted and exported as a text file.

```
clc; clear all; close all;

%calculate force limit using the semi-empirical method

load randomvibeinputs

%input at MPE
MPE = input('Enter desired input name (see available inputs in ...
            workspace): ');

%scaled MPE
scale = input('Enter desired scale of MPE (dB): ');
MPE(:,2) = 10.^(scale./10).*MPE(:,2);

%roll-off frequency and ASD value
freq_rolloff = input('Enter roll-off frequency (Hz): ');
ASD_rolloff = logslope(MPE,freq_rolloff);

%cut-off frequency and ASD value
freq_cutoff = 500;
ASD_cutoff = logslope(MPE,freq_cutoff);

%new sorted MPE data
ASD_forcelimit_all = sortrows([MPE;[freq_rolloff,ASD_rolloff];[...
    freq_cutoff,ASD_cutoff]]);
ASD_forcelimit = ASD_forcelimit_all((find(ASD_forcelimit_all(:,1) ≤ ...
    freq_cutoff)),:);
```

```

%C value
C = sqrt(2);

%Mass of test article
M0 = input('Enter mass of test article(lbs): ');

[F,T,dataout] = forcelimitcalc(MPE,freq_rolloff,freq_cutoff,scale,M0) ...
;
format longg
csvwrite('Force Limit.dat',dataout)

for i = 1:length(ASD_forcelimit)-1
    y2 = dataout(i+1,2);
    y1 = dataout(i,2);
    x2 = dataout(i+1,1);
    x1 = dataout(i,1);
    dB = 10*log10(y2/y1);
    Oct = log(x2/x1)/log(2);
    slope(i) = dB/Oct;
end

function y = logslope(MPE,freq_rolloff);

%interpolate y value of log scale

%find slope at roll-off frequency
%find x1,y1
temp = MPE((find(MPE(:,1) ≤ freq_rolloff)),:);
[dump,idx1] = min(abs(freq_rolloff-temp(:,1)));
x1 = temp(idx1,1);
y1 = temp(idx1,2);
%find x2,y2
temp = MPE((find(MPE(:,1) > freq_rolloff)),:);
[dump,idx2] = min(abs(freq_rolloff-temp(:,1)));
x2 = temp(idx2,1);
y2 = temp(idx2,2);
%calculate slope

```

```

dB = 10*log10(y2/y1);
Oct = log(x2/x1)/log(2);
slope = dB/Oct;

%ASD value at roll-off frequency
y = y1*(freq_rolloff/x1)^(slope/(10*log10(2)));

function [F,T,dataout] = forcelimitcalc(MPE,freq_rolloff,freq_cutoff,...
    scale,M0);
%function to calculate force limit using the semi-empirical method

%scaled MPE
% MPE(:,2) = 10.^(scale./10).*MPE(:,2);

%roll-off frequency ASD value
ASD_rolloff = logslope(MPE,freq_rolloff);

%cut-off frequency ASD value
ASD_cutoff = logslope(MPE,freq_cutoff);

%new sorted MPE data
ASD_forcelimit_all = sortrows([MPE;[freq_rolloff,ASD_rolloff];[...
    freq_cutoff,ASD_cutoff]]);
ASD_forcelimit = ASD_forcelimit_all((find(ASD_forcelimit_all(:,1) ≤ ...
    freq_cutoff)),:);

%C value
C = sqrt(2);

%calculate force limit
for i = 1:length(ASD_forcelimit);
    if ASD_forcelimit(i,1) < freq_rolloff
        force_limit(i,1) = C^2*M0^2*ASD_forcelimit(i,2);
    else % ASD_forcelimit(i,1) ≥freq_rolloff
        force_limit(i,1) = C^2*M0^2*ASD_forcelimit(i,2)*(freq_rolloff...
            /ASD_forcelimit(i,1))^2;
    end
end
end

```

```

freq = ASD_forcelimit(:,1);

F = figure;
% plotyy(ASD_forcelimit(:,1),force_limit,ASD_forcelimit(:,1),...
    ASD_forcelimit(:,2),'loglog','plot');
loglog(freq,force_limit,'ks-')
grid on
hold on
loglog(ASD_forcelimit_all(:,1),ASD_forcelimit_all(:,2),'bs-')
xlabel('Frequency, Hz')
axis([20 2000 0.1*min(ASD_forcelimit(:,2)) 1.1*max(force_limit)])

format short
T = table(freq,force_limit)

dataout = [freq,force_limit];
% dataout = [freq;force_limit];

```

APPENDIX F:

MATLAB Code — Data Processing

This appendix contains the MATLAB scripts and associated functions for reading in data from an Excel spreadsheet, finding the max ASD values for a specified P-POD position or test axis, and calculating the G_{RMS} over a specified frequency range. This appendix also contains the MATLAB scripts for generating figures from the measured data.

```
clc; clear all; close all;

global freq Δf

%Run vibedataread and plot data

%cutoff frequency for low/high freq content, Hz
cutoff = 500;

ABCfilename = 'NPSCuL_8P2M2s_ABCMPE+0dB';
ABCUfilename = '131107_NPSCuL_8P2M2s_ABCMPE+0dB_Unnotched';
ORS3filename = 'NPSCuL_8P2M2s_ORS3MPE-6dB';
ORS3Ufilename = 'NPSCuL_8P2M2s_ORS3MPE-6dB_Unnotched';

%%%%%%%%%%%%%%%%%%%%%%%%%%%%%%%%%%%%%%%%%%%%%%%%%%%%%%%%%%%%%%%%%%%%%%%% ABC MPE ...
%%%%%%%%%%%%%%%%%%%%%%%%%%%%%%%%%%%%%%%%%%%%%%%%%%%%%%%%%%%%%%%%%%%%%%%%
[freq,Δf,config.ABC.ppod.X,config.ABC.force.X,config.ABC.control.X] =...
    vibedataread(ABCfilename,'X+0dB');
[~,~,config.ABC.ppod.Y,config.ABC.force.Y,config.ABC.control.Y] = ...
    vibedataread(ABCfilename,'Y+0dB');
[~,~,config.ABC.ppod.Z,config.ABC.force.Z,config.ABC.control.Z] = ...
    vibedataread(ABCfilename,'Z+0dB');

%calculate Grms for each P-POD in every axis for every test axis
config.ABC.grms.X.all = grmscalc(20,2000,'p',config.ABC.ppod.X,8);
config.ABC.grms.X.low = grmscalc(20,cutoff,'p',config.ABC.ppod.X,8);
config.ABC.grms.X.high = config.ABC.grms.X.all-config.ABC.grms.X.low;
```

```

config.ABC.grms.Y.all = grmscalc(20,2000,'p',config.ABC.ppod.Y,8);
config.ABC.grms.Y.low = grmscalc(20,cutoff,'p',config.ABC.ppod.Y,8);
config.ABC.grms.Y.high = config.ABC.grms.Y.all-config.ABC.grms.Y.low;

config.ABC.grms.Z.all = grmscalc(20,2000,'p',config.ABC.ppod.Z,8);
config.ABC.grms.Z.low = grmscalc(20,cutoff,'p',config.ABC.ppod.Z,8);
config.ABC.grms.Z.high = config.ABC.grms.Z.all-config.ABC.grms.Z.low;

%calculate Grms for envelope of each P-POD
ppodnum = size(config.ABC.ppod.X.x,2); % # of P-PODs in data set - ...
    should be 8 unless it is unnotched ABC of baseline (old data)
config.ABC.max.PPOD = maxASD(config.ABC.ppod,ppodnum); % max ASD ...
    values of each P-POD in each axis
config.ABC.grmsall.all = grmscalc(20,2000,'p',config.ABC.max.PPOD,8);
config.ABC.grmsall.low = grmscalc(20,cutoff,'p',config.ABC.max.PPOD...
    ,8);
config.ABC.grmsall.high = config.ABC.grmsall.all-...
    config.ABC.grmsall.low;

%calculate Grms for envelope of each axis
config.ABC.max.Axis = maxAxis(config.ABC.max.PPOD); %max ASD values ...
    of all P-PODs in each axis
config.ABC.grmsAxis.all = grmscalc(20,2000,'d',config.ABC.max.Axis,8) ...
    ;
config.ABC.grmsAxis.low = grmscalc(20,cutoff,'d',config.ABC.max.Axis...
    ,8);
config.ABC.grmsAxis.high = config.ABC.grmsAxis.all-...
    config.ABC.grmsAxis.low;

%%%%%%%%%%%%%%%%%%%%%%%%%%%%%%%%%%%%%%%%%%%%%%%%%%%%%%%%%%%%%%%%%%%%%%%%%%%%%ORS3 MPE-6dB ...
UNNOTCHED %%%%%%%%%%%%%%%%%%%%%%%%%%%%%%%%%%%%%%%%%%%%%%%%%%%%%%%%%%%%%%%%%%%%%%%%%%%%%%
[~,~,config.ORS3Unnotched.ppod.X,config.ORS3Unnotched.force.X,...
    config.ORS3Unnotched.control.X] = vibedataread(ORS3Ufilename,'X-6...
    dB');
[~,~,config.ORS3Unnotched.ppod.Y,config.ORS3Unnotched.force.Y,...
    config.ORS3Unnotched.control.Y] = vibedataread(ORS3Ufilename,'Y-6...
    dB');
[~,~,config.ORS3Unnotched.ppod.Z,config.ORS3Unnotched.force.Z,...
    config.ORS3Unnotched.control.Z] = vibedataread(ORS3Ufilename,'Z-6...

```

```

dB');

%calculate Grms for each P-POD in every axis for every test axis
config.ORS3Unnotched.grms.X.all = grmscalc(20,2000,'p',...
    config.ORS3Unnotched.ppod.X,8);
config.ORS3Unnotched.grms.X.low = grmscalc(20,cutoff,'p',...
    config.ORS3Unnotched.ppod.X,8);
config.ORS3Unnotched.grms.X.high = config.ORS3Unnotched.grms.X.all-...
    config.ORS3Unnotched.grms.X.low;

config.ORS3Unnotched.grms.Y.all = grmscalc(20,2000,'p',...
    config.ORS3Unnotched.ppod.Y,8);
config.ORS3Unnotched.grms.Y.low = grmscalc(20,cutoff,'p',...
    config.ORS3Unnotched.ppod.Y,8);
config.ORS3Unnotched.grms.Y.high = config.ORS3Unnotched.grms.Y.all-...
    config.ORS3Unnotched.grms.Y.low;

config.ORS3Unnotched.grms.Z.all = grmscalc(20,2000,'p',...
    config.ORS3Unnotched.ppod.Z,8);
config.ORS3Unnotched.grms.Z.low = grmscalc(20,cutoff,'p',...
    config.ORS3Unnotched.ppod.Z,8);
config.ORS3Unnotched.grms.Z.high = config.ORS3Unnotched.grms.Z.all-...
    config.ORS3Unnotched.grms.Z.low;

%calculate Grms for envelope of each P-POD
ppodnum = size(config.ORS3Unnotched.ppod.X.x,2); % # of P-PODs in ...
    data set - should be 8 unless it is unnotched ABC of baseline (...
    old data)
config.ORS3Unnotched.max.PPOD = maxASD(config.ORS3Unnotched.ppod,...
    ppodnum); % max ASD values of each P-POD in each axis
config.ORS3Unnotched.grmsall.all = grmscalc(20,2000,'p',...
    config.ORS3Unnotched.max.PPOD,8);
config.ORS3Unnotched.grmsall.low = grmscalc(20,cutoff,'p',...
    config.ORS3Unnotched.max.PPOD,8);
config.ORS3Unnotched.grmsall.high = config.ORS3Unnotched.grmsall.all-...
    config.ORS3Unnotched.grmsall.low;

%calculate Grms for envelope of each axis

```

```

config.ORS3Unnotched.max.Axis = maxAxis(config.ORS3Unnotched.max.PPOD...
    ); %max ASD values of all P-PODs in each axis
config.ORS3Unnotched.grmsAxis.all = grmscalc(20,2000,'d',...
    config.ORS3Unnotched.max.Axis,8);
config.ORS3Unnotched.grmsAxis.low = grmscalc(20,cutoff,'d',...
    config.ORS3Unnotched.max.Axis,8);
config.ORS3Unnotched.grmsAxis.high = ...
    config.ORS3Unnotched.grmsAxis.all-...
    config.ORS3Unnotched.grmsAxis.low;

%%%%%%%%%%%%%%%%%%%%%%%%%%%%%%%%%%%%%%%%%%%%%%%%%%%%%%%%%%%%%%%%%%%%%%%% ORS3 MPE-6dB ...
%%%%%%%%%%%%%%%%%%%%%%%%%%%%%%%%%%%%%%%%%%%%%%%%%%%%%%%%%%%%%%%%%%%%%%%%
[~,~,config.ORS3.ppod.X,config.ORS3.force.X,config.ORS3.control.X] = ...
    vibdataread(ORS3filename,'X-6dB');
[~,~,config.ORS3.ppod.Y,config.ORS3.force.Y,config.ORS3.control.Y] = ...
    vibdataread(ORS3filename,'Y-6dB');
[~,~,config.ORS3.ppod.Z,config.ORS3.force.Z,config.ORS3.control.Z] = ...
    vibdataread(ORS3filename,'Z-6dB');

%calculate Grms for each P-POD in every axis for every test axis
config.ORS3.grms.X.all = grmscalc(20,2000,'p',config.ORS3.ppod.X,8);
config.ORS3.grms.X.low = grmscalc(20,cutoff,'p',config.ORS3.ppod.X,8) ...
    ;
config.ORS3.grms.X.high = config.ORS3.grms.X.all-...
    config.ORS3.grms.X.low;

config.ORS3.grms.Y.all = grmscalc(20,2000,'p',config.ORS3.ppod.Y,8);
config.ORS3.grms.Y.low = grmscalc(20,cutoff,'p',config.ORS3.ppod.Y,8) ...
    ;
config.ORS3.grms.Y.high = config.ORS3.grms.Y.all-...
    config.ORS3.grms.Y.low;

config.ORS3.grms.Z.all = grmscalc(20,2000,'p',config.ORS3.ppod.Z,8);
config.ORS3.grms.Z.low = grmscalc(20,cutoff,'p',config.ORS3.ppod.Z,8) ...
    ;
config.ORS3.grms.Z.high = config.ORS3.grms.Z.all-...
    config.ORS3.grms.Z.low;

%calculate Grms for envelope of each P-POD

```

```

ppodnum = size(config.ORS3.ppod.X.x,2); % # of P-PODs in data set - ...
    should be 8 unless it is unnotched ABC of baseline (old data)
config.ORS3.max.PPOD = maxASD(config.ORS3.ppod,ppodnum); % max ASD ...
    values of each P-POD in each axis
config.ORS3.grmsall.all = grmscalc(20,2000,'p',config.ORS3.max.PPOD...
    ,8);
config.ORS3.grmsall.low = grmscalc(20,cutoff,'p',config.ORS3.max.PPOD...
    ,8);
config.ORS3.grmsall.high = config.ORS3.grmsall.all-...
    config.ORS3.grmsall.low;

%calculate Grms for envelope of each axis
config.ORS3.max.Axis = maxAxis(config.ORS3.max.PPOD); %max ASD values...
    of all P-PODs in each axis
config.ORS3.grmsAxis.all = grmscalc(20,2000,'d',config.ORS3.max.Axis...
    ,8);
config.ORS3.grmsAxis.low = grmscalc(20,cutoff,'d',...
    config.ORS3.max.Axis,8);
config.ORS3.grmsAxis.high = config.ORS3.grmsAxis.all-...
    config.ORS3.grmsAxis.low;
%%%%%%%%%%%%%%%%%%%%%%%%%%%%%%%%%%%%%%%%%%%%%%%%%%%%%%%%%%%%%%%%%%%%%%%% ABC MPE UNNOTCHED ...
%%%%%%%%%%%%%%%%%%%%%%%%%%%%%%%%%%%%%%%%%%%%%%%%%%%%%%%%%%%%%%%%%%%%%%%%
[~,~,config.ABCUnnotched.ppod.X,config.ABCUnnotched.force.X,...
    config.ABCUnnotched.control.X] = vibedataread(ABCUfilename,'X+0dB...
    ');
[~,~,config.ABCUnnotched.ppod.Y,config.ABCUnnotched.force.Y,...
    config.ABCUnnotched.control.Y] = vibedataread(ABCUfilename,'Y+0dB...
    ');
[~,~,config.ABCUnnotched.ppod.Z,config.ABCUnnotched.force.Z,...
    config.ABCUnnotched.control.Z] = vibedataread(ABCUfilename,'Z-3dB...
    ');
axis = ['xyz'];
for k = 1:length(axis)
    config.ABCUnnotched.ppod.Z.(axis(k)) = config.ABCUnnotched.ppod.Z.(...
        axis(k))*2;
end
config.ABCUnnotched.force.Z = config.ABCUnnotched.force.Z*2;
config.ABCUnnotched.control.Z = config.ABCUnnotched.control.Z*2;

```

```

%calculate Grms for each P-POD in every axis for every test axis
config.ABCUnnotched.grms.X.all = grmscalc(20,2000,'p',...
    config.ABCUnnotched.ppod.X,4);
config.ABCUnnotched.grms.X.low = grmscalc(20,cutoff,'p',...
    config.ABCUnnotched.ppod.X,4);
config.ABCUnnotched.grms.X.high = config.ABCUnnotched.grms.X.all-...
    config.ABCUnnotched.grms.X.low;

config.ABCUnnotched.grms.Y.all = grmscalc(20,2000,'p',...
    config.ABCUnnotched.ppod.Y,4);
config.ABCUnnotched.grms.Y.low = grmscalc(20,cutoff,'p',...
    config.ABCUnnotched.ppod.Y,4);
config.ABCUnnotched.grms.Y.high = config.ABCUnnotched.grms.Y.all-...
    config.ABCUnnotched.grms.Y.low;

config.ABCUnnotched.grms.Z.all = grmscalc(20,2000,'p',...
    config.ABCUnnotched.ppod.Z,4);
config.ABCUnnotched.grms.Z.low = grmscalc(20,cutoff,'p',...
    config.ABCUnnotched.ppod.Z,4);
config.ABCUnnotched.grms.Z.high = config.ABCUnnotched.grms.Z.all-...
    config.ABCUnnotched.grms.Z.low;

%calculate Grms for envelope of each P-POD
ppodnum = 4; % # of P-PODs in data set - should be 8 unless it is ...
    unnotched ABC
config.ABCUnnotched.max.PPOD = maxASD(config.ABCUnnotched.ppod,...
    ppodnum); % max ASD values of each P-POD in each axis
config.ABCUnnotched.grmsall.all = grmscalc(20,2000,'p',...
    config.ABCUnnotched.max.PPOD,4);
config.ABCUnnotched.grmsall.low = grmscalc(20,cutoff,'p',...
    config.ABCUnnotched.max.PPOD,4);
config.ABCUnnotched.grmsall.high = config.ABCUnnotched.grmsall.all-...
    config.ABCUnnotched.grmsall.low;

%calculate Grms for envelope of each axis
config.ABCUnnotched.max.Axis = maxAxis(config.ABCUnnotched.max.PPOD);...
    %max ASD values of all P-PODs in each axis
config.ABCUnnotched.grmsAxis.all = grmscalc(20,2000,'d',...
    config.ABCUnnotched.max.Axis,4);

```

```

config.ABCUnnotched.grmsAxis.low = grmscalc(20,cutoff,'d',...
    config.ABCUnnotched.max.Axis,4);
config.ABCUnnotched.grmsAxis.high = config.ABCUnnotched.grmsAxis.all-...
    config.ABCUnnotched.grmsAxis.low;

config1 = config;

save('testdata','config1','freq','-append') %

function grms = grmscalc(freq_start,freq_end,toggle,ppod,num)
% function grms = grmscalc(freq_start,freq_end,toggle,ppod)
%calculate Grms for a specified frequency range for all P-PODs
%toggle is for # of P-PODs ('p') or a single ASD

global freq

% freq_start = 20;
% freq_end = 2000;

index_start = find(freq==freq_start);
index_end = find(freq==freq_end);

axis = ['xyz'];

if toggle == 'p'
for k = 1:length(axis)
    for j = 1:num;
%        for j = 1:size(ppod.(axis(k)),2);
            for i = index_start+1:1:index_end
                asdminus1 = ppod.(axis(k))(i-1,j);
                asd = ppod.(axis(k))(i,j);
                db = 10*log(asd/asdminus1);
                oct = log(freq(i)/freq(i-1))/log(2);
                slope = db/oct;
                if i == index_start+1
                    if slope == -3.010299957
                        psdarea(j,k) = asdminus1*freq(i-1)*log10(freq(i)/...
                            freq(i-1));

```

```

        else
            psdarea(j,k) = (10*log(2)*asd/(10*log(2)+slope))...
                *(freq(i)-(freq(i-1)/freq(i))^(slope/(10*log...
                (2)))*freq(i-1));
        end
    else
        if slope == -10*log(2)
            psdarea(j,k) = psdareaminus1(j,k)+asdminus1*freq(...
                i-1)*log10(freq(i)/freq(i-1));
        else
            psdarea(j,k) = psdareaminus1(j,k)+(10*log(2)*asd...
                /(10*log(2)+slope))*(freq(i)-(freq(i-1)/freq(...
                i))^(slope/(10*log(2)))*freq(i-1));
        end
    end
    psdareaminus1(j,k)=psdarea(j,k);
end
% Grms(j,k) = (grms(end,j));
    grms(j,k) = sqrt(psdarea(j,k));
end
end

else
    for k = 1:length(axis)
        for i = index_start+1:1:index_end
            asdminus1 = ppod(i-1,k);
            asd = ppod(i,k);
            db = 10*log(asd/asdminus1);
            oct = log(freq(i)/freq(i-1))/log(2);
            slope = db/oct;
            if i == index_start+1
                if slope == -3.010299957
                    psdarea = asdminus1*freq(i-1)*log10(freq(i)/freq(...
                        i-1));
                else
                    psdarea = (10*log(2)*asd/(10*log(2)+slope))*(freq...
                        (i)-(freq(i-1)/freq(i))^(slope/(10*log(2)))*...
                        freq(i-1));
                end
            end
        end
    end
end

```

```

        else
            if slope == -10*log(2)
                psdarea = psdareaminus1+asdminus1*freq(i-1)*log10...
                    (freq(i)/freq(i-1));
            else
                psdarea = psdareaminus1+(10*log(2)*asd/(10*log(2) ...
                    +slope))*(freq(i)-(freq(i-1)/freq(i))^(slope...
                    /(10*log(2)))*freq(i-1));
            end
        end
        psdareaminus1 = psdarea;
    end
    % Grms(j,k) = (grms(end,j));
    grms(k) = sqrt(psdarea);
end
end

```

```

function maxPPOD = maxASD(config,ppodnum)

```

```

%find max ASD values for each P-POD, including cross-axis responses
testaxis = fieldnames(config); %pull test axis names
axisnames = fieldnames(config.X); %only need one testaxis to grab ...
axisnames

```

```

for k = 1:numel(axisnames) % # of measurement axes
    for j = 1:ppodnum % # of P-PODs
        for i = 1:numel(testaxis) % # of test axes
            dump(:,i,j) = (config.(testaxis{i}).(axisnames{k}))(:,j);
        end
        maxPPOD.(axisnames{k})(:,j) = max(dump(:, :, j), [], 2);
    end
    clear dump
end
end

```

```

function maxAxis = maxAxis(config)

```

```

%find max ASD values for each axis, including cross-axis responses
fields = fieldnames(config);
for k = 1:numel(fields)
    maxAxis(:,k) = max(config.(fields{k}),[],2);
end

function [freq,Δf,ppod,force,control] = vibedataread(filename,sheet)

%W. Lan
%4 DEC 2014
%reads in 1 sheet of data from Excel, force summations, control ...
    channel, and outputs Grms for every P-POD in each
%axis

%read in 1 set of data (1 axis at 1 level)
% [data,headers,all] = xlsread('141118_NPSCuL+Isolators+FlatRing+8...
    P2M2s_WrongFL_Data.xlsx','MPE+6dB,X');
[data,headers,all] = xlsread(filename,sheet);
% testaxis = input('Test axis (enter with single quotation marks, ...
    lower case): ');

%pull out frequency
freq = data(:,find(strcmp(headers(1,:), 'X-Data [Hz]')));
%calculate frequency resolution
Δf = freq(2)-freq(1);

%pull out control
control = data(:,find(~cellfun(@isempty, strfind(headers(1,:), 'Control...
    channel'))));

%find force summations (x=1, etc)
force(:,1) = data(:,find(~cellfun(@isempty, strfind(headers(1,:), '...
    Force Summation'))&~cellfun(@isempty, strfind(headers(1,:), 'X')))...
    );
force(:,2) = data(:,find(~cellfun(@isempty, strfind(headers(1,:), '...
    Force Summation'))&~cellfun(@isempty, strfind(headers(1,:), 'Y')))...
    );

```

```

force(:,3) = data(:,find(~cellfun(@isempty, strfind(headers(1,:), '...
    Force Summation')) & ~cellfun(@isempty, strfind(headers(1,:), 'Z')))...
);

%find P-POD responses
%P-POD DATA MUST BE ORDERED 1 THROUGH 8
ppod.x(:, :) = data(:, find(~cellfun(@isempty, strfind(headers(1,:), 'P-...
    POD')) & ~cellfun(@isempty, strfind(headers(1,:), 'X'))));
ppod.y(:, :) = data(:, find(~cellfun(@isempty, strfind(headers(1,:), 'P-...
    POD')) & ~cellfun(@isempty, strfind(headers(1,:), 'Y'))));
ppod.z(:, :) = data(:, find(~cellfun(@isempty, strfind(headers(1,:), 'P-...
    POD')) & ~cellfun(@isempty, strfind(headers(1,:), 'Z'))));

clc; clear all; close all;

%Post-processing script

load testdata.mat
% load isolator_trans_20Hz.mat

global freq

percentdiff1v2a_ABCFLVT.all = (config1.ABC.grms.all(1:6, :)-...
    config2a.ABC.grms.all(1:6, :))./config1.ABC.grms.all(1:6, :)*100;
percentdiff1v2a_ABCFLVT.X = (config1.ABC.grms.X.all(1:6, :)-...
    config2a.ABC.grms.X.all(1:6, :))./config1.ABC.grms.X.all(1:6, :)*100;
percentdiff1v2a_ABCFLVT.Y = (config1.ABC.grms.Y.all(1:6, :)-...
    config2a.ABC.grms.Y.all(1:6, :))./config1.ABC.grms.Y.all(1:6, :)*100;
percentdiff1v2a_ABCFLVT.Z = (config1.ABC.grms.Z.all(1:6, :)-...
    config2a.ABC.grms.Z.all(1:6, :))./config1.ABC.grms.Z.all(1:6, :)*100;
%

%create overlay bar chart to show relative Grms of envelopes
prettypictures(3)=figure('units','normalized','position',[0.0035 0...
    .0063 0.4930 0.9278], 'Color',[1 1 1]);
highfreqpercent1 = config1.ABC.grmsAxis.high./...
    config1.ABC.grmsAxis.all*100;
width1 = 0.6;

```

```

% width2 = width1/3;
bar(highfreqpercent1,width1,'FaceColor',[1 1 1])
hold on
grid on
highfreqpercent2 = config2a.ABC.grmsAxis.high./...
    config2a.ABC.grmsAxis.all*100;
bar(highfreqpercent2,width1)
ylabel('Percentage of G_{RMS} Above 500 Hz (%)','FontSize',30)
xlabel('Test Axis','FontSize',30)
set(gca,'XTickLabel',{'X','Y','Z'},'FontSize',30)
legend1=legend('Config 1','Config 2','Location','SouthOutside','...
    Orientation','Horizontal')
set(legend1,'FontSize',30)

% %loglog plots of data - max envelope by axis
for j = 1:3
% subplot(1,3,j)
prettypictures(4+j)=figure('units','normalized','position',[0.5035 0...
    .0063 0.4930 0.9278],'Color',[1 1 1]);
% loglog(freq,config1.ABC.ppod.(test(i)).(axis(j))(:,position(j)),...
    freq,config2a.ABC.ppod.(test(i)).(axis(j))(:,position(j)))
loglog(freq,config1.ABC.max.Axis(:,j),freq,config2a.ABC.max.Axis(:,j)...
    )
grid on
hold on
loglog(ones(2,1)*200,[10E-7; 10E1],'g--')
xlabel('Frequency (Hz)','FontSize',30)
dump = sprintf('ASD (g^2/Hz)');
ylabel(dump,'FontSize',30)
xlim([20 2000])
ylim([10E-6 10E1])
set(gca,'FontSize',30)
% str = sprintf('P-POD Response, %s Axis Envelope',test(j));
% supitle(str)
legend1=legend('Config 1','Config 2','200 Hz','Location','...
    SouthOutside','Orientation','Horizontal')
set(legend1,'FontSize',30)
end
% end

```

```

% %loglog plots of data - max envelope by axis, unnotched
for j = 1:3
% subplot(1,3,j)
prettyfigures(4+j)=figure('units','normalized','position',[0.5035 0...
    .0063 0.4930 0.9278],'Color',[1 1 1]);
% loglog(freq,config1.ABC.ppod.(test(i)).(axis(j))(:,position(j)),...
    freq,config2a.ABC.ppod.(test(i)).(axis(j))(:,position(j)))
loglog(freq,config1.ABCUnnotched.max.Axis(:,j),freq,...
    config2a.ABCUnnotched.max.Axis(:,j))
grid on
xlabel('Frequency (Hz)','FontSize',30)
dump = sprintf('ASD (g^2/Hz)');
ylabel(dump,'FontSize',30)
set(gca,'FontSize',30)
xlim([20 2000])
ylim([10E-6 10E1])
% str = sprintf('P-POD Response, %s Axis Envelope',test(j));
% suptitle(str)
legend1=legend('Config 1','Config 2','Location','SouthOutside','...
    Orientation','Horizontal')
set(legend1,'FontSize',30)
end
% end

clc; clear all; close all;

%Post-processing script

load testdata.mat
% load isolator_trans_20Hz.mat

global freq

% %loglog plots of data - max envelope by axis, unnotched
for j = 1:3
% subplot(1,3,j)

```

```

prettypictures(4+j)=figure('units','normalized','position',[0.5035 0...
    .0063 0.4930 0.9278],'Color',[1 1 1]);
% loglog(freq,config1.ABC.ppod.(test(i)).(axis(j))(:,position(j)),...
    freq,config2a.ABC.ppod.(test(i)).(axis(j))(:,position(j)))
loglog(freq,config2d.ABC.max.Axis(:,j),freq,...
    config2d.ABCUnnotched.max.Axis(:,j))
grid on
xlabel('Frequency (Hz)')
dump = sprintf('ASD (g^2/Hz)');
ylabel(dump)
xlim([20 2000])
ylim([10E-7 10E0])

% str = sprintf('P-POD Response, %s Axis Envelope',test(j));
% supitle(str)
legend('Config 3, FLVT','Config 3, Unnotched','Location','...
    SouthOutside','Orientation','Horizontal','FontSize',20)
end
% end

```

APPENDIX G:

MATLAB Code — Acoustic No-Test Rationale

Calculation

This appendix contains the MATLAB script for calculating the break-even surface areas to determine whether or not acoustic testing is required for P-PODs flying on an isolated NPSCuL.

```
clc; clear all; close all;

%Acoustic No-Test Rationale
%W. Lan
%9.30.2015

fn = 100;%Hz - conservative assumption for panel mode
PSD = 0.003; %G^2/Hz - lowest PSD value at 100 Hz from all isolated ...
    envelopes
Q=10; %damping factor

%use Miles Eqn for rms G's
Grms = sqrt(pi/2*PSD*fn*Q);

%response to acoustic noise - used OASPL from ABC User's Guide for
%conservatism. Note: SPL at 100 Hz is 123.8 dB
dB = 139.5;

%Pressure Spectral Density
Ps = 2.9E-9^2*10^(dB/10)/(0.231*fn);

%use Miles Eqn again nfor rms pressure
Prms = sqrt(pi/2*Ps*fn*Q);

%mass of payload - 6U or 2 3Us. Masses are low estimates to be ...
    conservative
m_6U = 25;
```

```

m_3U = 35;

%surface area calc
SA_break_even_3U = Grms*m_3U/Prms
SA_break_even_6U = Grms*m_6U/Prms

SA_NPSCuL = 18.17*13

break_even_ratio = SA_break_even_3U/m_3U %same as Grms/Prms
% Following Eqns are not correct interpretation of "surface area" - ...
    not
% surface area of component...should be surface area with Grms and ...
    Prms
% taken into account
% break_even_ratio_3U = SA_NPSCuL/m_3U
% break_even_ratio_6U = SA_NPSCuL/m_6U

```

APPENDIX H:

Random Vibration Analysis Example Verification

This appendix contains the MATLAB script and associated functions for calculating the frequencies, mode shapes, and response FRFs for a simply supported beam subject to a random vibration input at one end of the beam. The resulting response is compared with the results obtained using NASTRAN. The frequencies and mode shapes are consistent, but the response FRFs diverge after the first mode. This is most likely due to differences in effective modal masses between the two models.

Table H.1: Frequency Comparison — MATLAB and NASTRAN FEMs

Mode	Frequency, Hz		Percent Difference (%)
	MATLAB FEM	NASTRAN FEM	
1	30.9	30.9	0.267
2	124	123	0.941
3	279	273	2.04
4	495	478	3.53
5	774	732	5.36

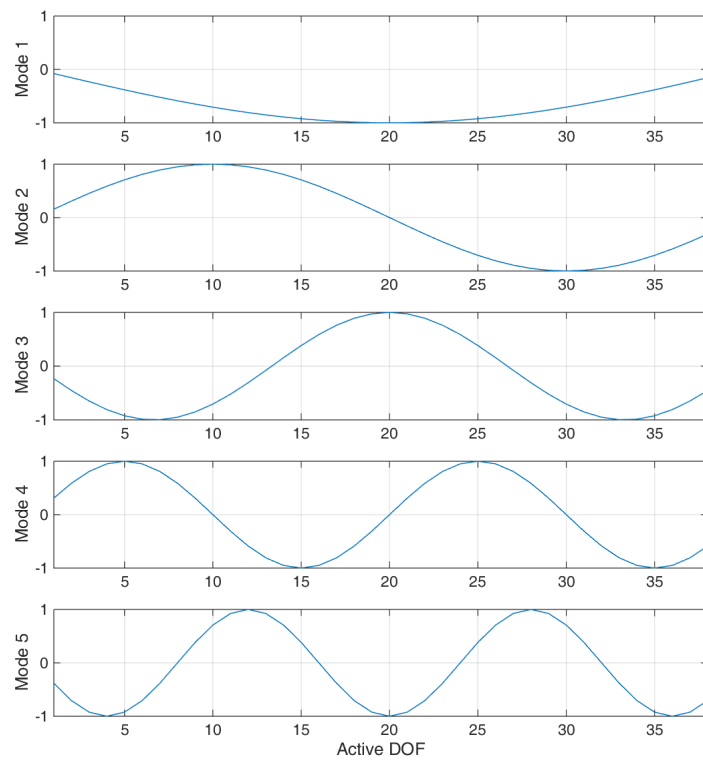


Figure H.1: Mode Shapes of First Five Modes - Normalized Displacement

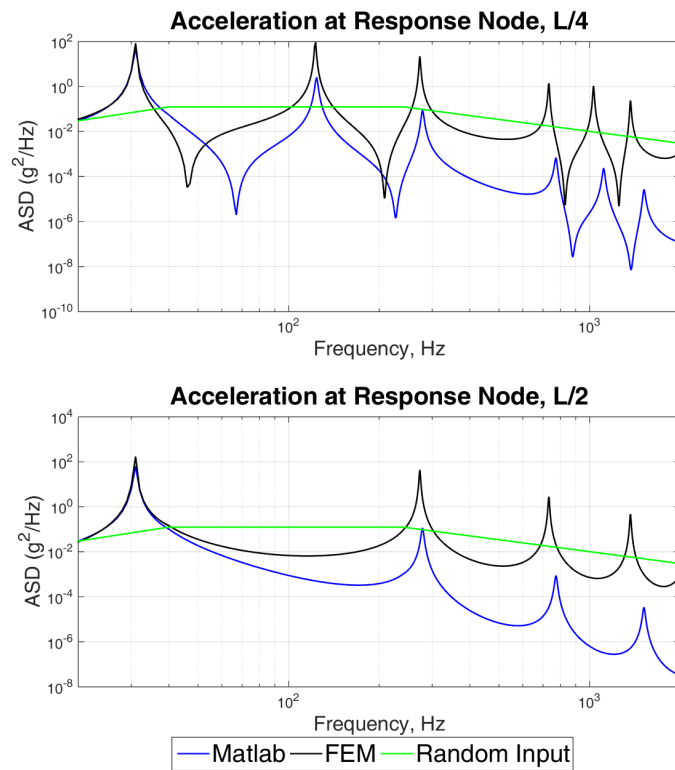


Figure H.2: Acceleration Response at L/4 and L/2

```

clc; clear all; close all;

% Modified from ME4522 PROJECT 3
% W. LAN
% 27 AUG 2015

% global variables
global E rho I A L M K ff x_vector

% a. Definition of Nodal Coordinates
elem=40;
% elem=input('Number of elements: ');
nodes=elem+1;
q=nodes*2;

```

```

% c. Specification of material and geometric beam properties
% material: aluminum
E = 1e7; %lbf/in^2
rho = 0.1; %lbm/in^3
rho=rho/386.4; %lbf-s^2/in^4
% geometry
L=10; %feet
L=L*12; %inches
x_vector=0:L/elem:L;
W=5; %inches
D=5; %inches
% moment of inertia, in^4
I=W*D^3/12;
% cross-sectional area, in^2
A=W*D;

% d. assembly of system stiffness and mass matrices
k_global=zeros(q,q);
m_global=zeros(q,q);
for elem_index = 0:(elem-1)
    for i=1:4
        for j=1:4
            [ke me]=elem_ke(elem);
            k_global(2*elem_index+i,2*elem_index+j)=k_global(2*elem_index+i...
                ,2*elem_index+j)+ke(i,j);
            m_global(2*elem_index+i,2*elem_index+j)=m_global(2*elem_index+i...
                ,2*elem_index+j)+me(i,j);
        end
    end
end

%apply boundary conditions
%For simply supported beam, DOFs 1 and n-1 are zero (left and right ...
    ends of beam)
% new DOF 1 is rotation (old DOF 2)
% keep only DOF 2 through q-2, q
K=[k_global(2:q-2,2:q-2), k_global(2:q-2,q);...
    k_global(q,2:q-2),k_global(q,q)];
M=[m_global(2:q-2,2:q-2), m_global(2:q-2,q);...

```

```

m_global(q,2:q-2),m_global(q,q)];

%number of active DOFs
ff=length(K);

% HAPPENIN' NODES
% node for L/4
L4_node=nodes/4;
L4_node=round(L4_node);
% DOF for L/4
L4_DOF=L4_node*2;

% node for L/2
L2_node=nodes/2-1;
L2_node=round(L2_node);
% DOF for L/2
L2_DOF=L2_node*2;

% g. Calculation of normal modes and natural frequencies
format short g
[v,d]=eig(K,M);

% natural frequencies
lambda=sqrt(nonzeros(d));
freq=lambda/(2*pi); %Hz

omega = 20*2*pi:1*2*pi:2000*2*pi;

% damped frequencies
zeta=0.01;
wd=lambda*sqrt(1-zeta^2);
fd=wd/(2*pi);

modal_M=v'*M*v;
modal_K=v'*K*v;
modal_C=diag(2*zeta*lambda);
C=M*v*modal_C*v'*M;

% DOFs for FRFs

```

```

tf = [L4_DOF, L2_DOF];

for n = 1:length(omega)
    % INVERSE IMPEDANCE
    Z=[K-omega(n)^2*M+1i*omega(n)*C];
    %transfer function
    H(:, :, n)=inv(Z);
end

%normalize H
for m = 1:ff
    for k = 1:ff
        h=abs(H(m,k, :));
        H_norm(m,k, :)=h/(real(h(1,1,1)));
    end
end

figure
subplot(2,1,1)
loglog(omega, squeeze(abs(H(1,1, :))), '-b', 'LineWidth', 1.5)
subplot(2,1,2)
loglog(omega, squeeze(H_norm(1,1, :))), '-k', 'LineWidth', 1.5)

%Random Input, Sx
ABC_interface_MPE = [20*2*pi 40*2*pi 240*2*pi 2000*2*pi; 0.03 0.125 0...
    .125 0.003];
ABC_MPE_full = 10.^interp1(log10(ABC_interface_MPE(1, :)), log10(...
    ABC_interface_MPE(2, :)), log10(omega)); %ASD, g^2/Hz

TF_drive = 2;

%Apply input to left end
Sx_vector=zeros(ff, length(omega));
% Acceleration at left end
Sx=ABC_MPE_full; %g^2/Hz
Sx_vector(TF_drive, :)=Sx_vector(TF_drive, :)+Sx;

% DOFs for FRFs
tf = [L4_DOF, L2_DOF];

```

```

for n = 1:length(omega)
for m=1:length(tf) % number of transfer functions
    Sxy(m,:,n) = abs(H_norm(tf(m),:,n)).^2*Sx_vector(:,n);
end
end

[mode_shape_max,modeplot]=modeshape(v)

%load FEM results
%FEM is constrained in translation and axial DOF at ends (simply ...
    supported)
%FEM is constrained in 1 transverse direction for translation, axial
%rotation and translation at all other nodes
load Sxy_FEM_3.mat
Sxy_FEM=Sxy_FEM_3;

FREQ = omega/(2*pi);

figure('Color',[1 1 1])
subplot(2,1,1)
loglog(FREQ,Sxy(1,:), '-b', 'LineWidth',1.5)
hold on
loglog(FREQ,Sxy_FEM(:,1), '-k', 'LineWidth',1.5)
loglog(FREQ,ABC_MPE_full, '-g', 'LineWidth',1.5)
xlim([20 2000])
grid on
xlabel('Frequency, Hz','FontSize',20)
title('Acceleration at Response Node, L/4','FontSize',24)
ylabel('ASD (g^2/Hz)','FontSize',20)
subplot(2,1,2)
loglog(FREQ,Sxy(2,:), '-b', 'LineWidth',1.5)
hold on
loglog(FREQ,Sxy_FEM(:,2), '-k', 'LineWidth',1.5)
loglog(FREQ,ABC_MPE_full, '-g', 'LineWidth',1.5)
xlim([20 2000])
grid on
xlabel('Frequency, Hz','FontSize',20)
title('Acceleration at Response Node, L/2','FontSize',24)
ylabel('ASD (g^2/Hz)','FontSize',20)

```

```

legend1=legend('Matlab','FEM','Random Input','Location','SouthOutside...
    ', 'Orientation','Horizontal');
set(legend1,'FontSize',24)

function [ke me] = elem_ke(elem)
%output: k and m matrices for element
%input: # of elements
global E I rho A L

l=L/elem;

ke=E*I/l^3*[12, 6*l, -12, 6*l;...
    6*l, 4*l^2, -6*l, 2*l^2;...
    -12, -6*l, 12, -6*l;...
    6*l, 2*l^2, -6*l, 4*l^2];

me=rho*A*l/420*[156, 22*l, 54, -13*l;...
    22*l, 4*l^2, 13*l, -3*l^2;...
    54, 13*l, 156, -22*l;...
    -13*l, -3*l^2, -22*l, 4*l^2];

function [mode_shape_max,modeplot]=modeshape(v)

global ff

% first 5 mode shapes
% separate displacement and rotation
for i=0:(ff/2-3)
    v_x(i+1,1:5)=v(2*i+2,1:5);
%     disp_x(i+1,1)=disp(2*i+1,1);
%     v_r(i+1,1:5)=v(2*i+2,1:5);
end
% v_x=[zeros(1,5);v_x;zeros(1,5)];
% v_r=[zeros(1,5);v_r];

modeplot=1;
figure('Color',[1 1 1]);

```

```

% normalized mode shapes
for i = 1:5
mode_shape_max(:,i)=[v_x(:,i) ./max(abs(v_x(:,i)))];

subplot(5,1,i)
plot(mode_shape_max(:,i))
grid on
str = sprintf('Mode %d',i);
ylabel(str)
% title(str)
axis([1 length(mode_shape_max) -1 1])
end

xlabel('Active DOF')

```

THIS PAGE INTENTIONALLY LEFT BLANK

List of References

- [1] W. D. Lan, V. Kaushish, and J. H. Newman, “Progress in Reducing Vibration Levels on the Naval Postgraduate School CubeSat Launcher,” 2015. [Online]. Available: <http://digitalcommons.usu.edu/cgi/viewcontent.cgi?article=3231&context=smallsat>
- [2] “Aft Bulkhead Carrier Auxiliary Payload User’s Guide,” United Launch Alliance, Centennial, CO, May 2014.
- [3] *General Environments Verification Standard (GEVS)*, NASA Goddard Space Flight Center Std. NASA-GEVS-7000A, Apr. 2013.
- [4] SoftRide brochure. (n.d.). Moog CSA Engineering. [Online]. Available: http://www.csaengineering.com/literature/Space_Defense/Vibration_Control/MoogCSA_SoftRide_brochure.pdf
- [5] P. S. Wilke, C. D. Johnson, P. J. Grosserode, and D. Sciulli, “Whole-spacecraft vibration isolation on small launch vehicles,” in *SPIE’s 7th Annual International Symposium on Smart Structures and Materials*, 2000, pp. 440–451. [Online]. Available: <http://proceedings.spiedigitallibrary.org/proceeding.aspx?articleid=924924>
- [6] C. D. Johnson, P. S. Wilke, and S. C. Pendleton, “Softride vibration and shock isolation systems that protect spacecraft from launch dynamic environments,” in *Proceedings of the 38th Aerospace Mechanisms Symposium, Langley Research Center*, 2006. [Online]. Available: <http://www.esmats.eu/amspapers/pastpapers/pdfs/2006/johnson2.pdf>
- [7] J. R. Maly, S. A. Haskett, P. S. Wilke, E. C. Fowler, D. Sciulli, and T. E. Meink, “ESPA: EELV Secondary Payload Adapter with whole-spacecraft isolation for primary and secondary payloads,” in *SPIE’s 7th Annual International Symposium on Smart Structures and Materials*, 2000, pp. 430–439. [Online]. Available: <http://proceedings.spiedigitallibrary.org/proceeding.aspx?articleid=924917>
- [8] B. Fang, S. Li, and W. Huang, “Performance analysis for a new whole-spacecraft isolation using viscoelastic damping material,” M. N. Ghasemi-Nejhad, Ed., Mar. 2011, pp. 79 772B–79 772B–8. [Online]. Available: <http://proceedings.spiedigitallibrary.org/proceeding.aspx?articleid=729323>
- [9] A. J. Bronowicki and J. W. Innis. (2005). A family of full spacecraft-to-payload isolators. Northrop Grumman Corporation. [Online]. Available: <http://citeseerx.ist.psu.edu/viewdoc/download?doi=10.1.1.434.4617&rep=rep1&type=pdf>

- [10] S. Thampi, D. N. Le, and P. Wilke, "Soft-Ride to Orbit: Viscoelastic Treatments for Launch Load Attenuation," 1993.
- [11] T. Irvine. (2009). Avionics Isolation Design Guidelines. [Online]. Available: <http://citeseerx.ist.psu.edu/viewdoc/download?doi=10.1.1.437.2738&rep=rep1&type=pdf>
- [12] *Test Requirements for Launch, Upper-Stage and Space Vehicles*, Air Force Space Command Std. SMC-S-016, Sep. 2014.
- [13] *CubeSat Design Specification*, CubeSat Program, Cal Poly SLO Std. CDS Rev. 13, Feb. 2014. [Online]. Available: http://www.cubesat.org/images/developers/cds_rev13_final2.pdf
- [14] W. Lan, J. Brown, A. Toorian, R. Coelbo, L. Brooks, J. Puig-Suari, and R. Twigg, "CubeSat Development in Education and into Industry." American Institute of Aeronautics and Astronautics, Sep. 2006. [Online]. Available: <http://arc.aiaa.org/doi/abs/10.2514/6.2006-7296>
- [15] J. H. Newman, D. Sakoda, and R. Panholzer, "CubeSat Launchers, ESPA-rings, and Education at the Naval Postgraduate School," Utah, Aug. 2007.
- [16] C. M. Hicks, "NPS CubeSat Launcher program management," master's thesis, DTIC Document, 2009. [Online]. Available: <http://oai.dtic.mil/oai/oai?verb=getRecord&metadataPrefix=html&identifier=ADA509158>
- [17] F. Rossberg, "Structural design of a NPS CubeSat launcher," master's thesis, DTIC Document, 2008. [Online]. Available: <http://oai.dtic.mil/oai/oai?verb=getRecord&metadataPrefix=html&identifier=ADA476837>
- [18] M. R. Crook, "NPS CubeSat launcher design, process and requirements," master's thesis, Monterey, California. Naval Postgraduate School, 2009. [Online]. Available: <http://calhoun.nps.edu/handle/10945/4752>
- [19] V. Kaushish, "Force limited vibration testing and subsequent redesign of the Naval Postgraduate School CubeSat launcher," master's thesis, Monterey, California: Naval Postgraduate School, 2014. [Online]. Available: <http://calhoun.nps.edu/handle/10945/42656>
- [20] *Tyvak Nanosatellite Launch Adapter System (NLAS) Mk. II User Guide*, Std. TK-NLASUG-Rev1, Jan. 2015.
- [21] T. P. Sarafin, *Spacecraft Structures and Mechanisms - From Concept to launch*. Torrance, CA: Microcosm Press, 1995.

- [22] K. Fitzpatrick and S. I. McNeill, “Methods to specify random vibration acceleration environments that comply with force limit specifications,” in *IMAC-XXV: Conference & Exposition on Structural Dynamics-Smart Structures and Transducers*, 2007. [Online]. Available: http://www.vibrationdata.com/tutorials/methods_rvae.pdf
- [23] *Force Limited Vibration Testing*, NASA Std. NASA-HDBK-7004B, Jan. 2003.
- [24] S. G. Kelly, *Fundamentals of Mechanical Vibrations*, 2nd ed. McGraw-Hill, 2000.
- [25] J. Den Hartog, *Mechanical Vibrations*. Dover Publications, Inc., 1985.
- [26] T. Scharton, “Vibration test force limits derived from frequency shift method.” American Institute of Aeronautics and Astronautics, Apr. 1994. [Online]. Available: <http://arc.aiaa.org/doi/abs/10.2514/6.1994-1569>
- [27] T. Scharton, “Force Limited Vibration Testing Monograph,” May 1997.
- [28] *Force Limited Vibration Testing*, NASA Std. NASA-HDBK-7004C, Nov. 2012.
- [29] A. L. Chan. (2008, Aug.). Spectrum and Octave Band. [Online]. Available: <http://moscow.cityu.edu.hk/~bsapplec/spectrum.htm>
- [30] LORD aero catalog. (2011). LORD Corporation. [Online]. Available: <http://www.lord.com/products-and-solutions/vibration-and-motion-control/aerospace-catalog.xml>
- [31] All attitude. (2015, Apr.). Barry Controls. [Online]. Available: http://www.hutchinsonai.com/uploads/tech/All_Attitude.pdf
- [32] Cupmount Series (1000-4000). (2015, Apr.). Barry Controls. [Online]. Available: <http://www.hutchinsonai.com/products/product.cfm?cid=3&fid=13>
- [33] V. Kaushish, “Flvt Transducer Set-Up SOP,” Sep. 2015.
- [34] T. Irvine. (2009). The Half Power Bandwidth Method for Damping Calculation. [Online]. Available: http://vibrationdata.com/tutorials/half_power_bandwidth.pdf
- [35] F. J. Andrews, “A primer on vibration isolation,” *Sound and Vibration*, vol. 36, no. 1, pp. 42–46, 2002. [Online]. Available: http://cmsstructuralisolation.com/vibrationpapers_pdf/APrimerforVibrationIsolat.pdf
- [36] B. Callender, “RE: Question re: Torque Spec on NC1035-T4,” June 2015.
- [37] “Hutchinson Vibration Isolation Analysis for NPSCuL,” Apr. 2015.

- [38] *Metallic Materials Properties Development and Standardization*, FAA Std. MMPDS-03, Oct. 2006.
- [39] J. C. Forgrave, K. F. Man, and J. M. Newell, “Acoustic and Random Vibration Test Tailoring for Low-Cost Missions,” in *Annual Technical Meeting-Institute of Environmental Sciences and Technology*, vol. 44. Institute of Environmental Sciences and Technology, 1998, pp. 165–171. [Online]. Available: <ftp://128.32.147.81/pub/scponly-cinema/pub/oldsite/02.%20Systems/6.%20Procedures/JPL%20acoustic-vib%20tests.pdf>

Initial Distribution List

1. Defense Technical Information Center
Ft. Belvoir, Virginia
2. Dudley Knox Library
Naval Postgraduate School
Monterey, California